On the Performance Analysis of Free-Space Optical Links under Generalized Turbulence and Misalignment Models

Dissertation by

Hessa AlQuwaiee

In Partial Fulfillment of the Requirements

For the Degree of

Doctor of Philosophy

King Abdullah University of Science and Technology

Thuwal, Kingdom of Saudi Arabia

November, 2016

EXAMINATION COMMITTEE PAGE

The dissertation of Hessa AlQuwaiee is approved by the examination committee.

Committee Chairperson: Professor Mohamed-Slim Alouini.

Committee Members: Professor Boon Ooi, Professor Lajos Hanzo, Professor Taous-Meriem Laleg-Kirati.

ABSTRACT

On the Performance Analysis of Free-Space Optical Links under Generalized Turbulence and Misalignment Models

Hessa AlQuwaiee

One of the potential solutions to the radio frequency (RF) spectrum scarcity problem is optical wireless communications (OWC), which utilizes the unlicensed optical spectrum. Long-range outdoor OWC are usually referred to in the literature as free-space optical (FSO) communications. Unlike RF systems, FSO is immune to interference and multi-path fading. Also, the deployment of FSO systems is flexible and much faster than optical fibers. These attractive features make FSO applicable for broadband wireless transmission such as optical fiber backup, metropolitan area network, and last mile access. Although FSO communication is a promising technology, it is negatively affected by two physical phenomenon, namely, scintillation due to atmospheric turbulence and pointing errors. These two critical issues have prompted intensive research in the last decade. To quantify the effect of these two factors on FSO system performance, we need effective mathematical models. In this work, we propose and study a generalized pointing error model based on the Beckmann distribution. Then, we aim to generalize the FSO channel model to span all turbulence conditions from weak to strong while taking pointing errors into consideration. Since scintillation in FSO is analogous to the fading phenomena in RF, diversity has been proposed too to overcome the effect of irradiance fluctuations. Thus, several combining techniques of not necessarily independent dual-branch free-space optical links were investigated over both weak and strong turbulence channels in the presence of pointing errors. On another front, improving the performance, enhancing the capacity and reducing the delay of the communication link has been the motivation of

any newly developed schemes, especially for backhauling. Recently, there has been a growing interest in practical systems to integrate RF and FSO technologies to solve the last mile bottleneck. As such, we also study in this thesis asymmetric an RF-FSO dual-hop relay transmission system with both fixed and variable gain relay.

ACKNOWLEDGEMENTS

In the name of Allah, the Most Gracious, the Most Merciful.

First of all, I would like to express my deepest and sincerest gratitude to Allah for providing me the blessings and strength to complete this work, Alhamdulillah.

Second, I would like to thank my supervisor, Prof. Mohamed-Slim Alouini for his valuable guidance, mentorship, and constant encouragement during my time at King Abdullah University of Science and Technology (KAUST). I am also very thankful to the committee members for their helpful comments during the oral defense.

My sincere gratitude goes to King Abdullah University of Science and Technology (KAUST) for investing in me and giving me the chance to complete my graduate studies.

I would like also to extend my gratitude to

- My beloved parents, Mohammed Al-Kawaie and Princess Aljawahrah Al-Saud.
- My siblings, Haifa, Turki, Hajer, and Ghadah.
- My sister in-law Nisreen and my niece Aljawahrah.

for their endless love, prayers, and moral support.

I would like to thank my friends for their daily support: Afnan Mashat, Amani Alonazi, Bashayer Aljabri, Bedour Alsabban, Dina Abu Samra, Eman Daas, Emna Zedini, Enas Ahmed, Hanin Alzubaidy, Ikram Boukhedimi, Manar Darwish, Mona Alsomali, Noor Almana, Noura Shehab, Rasha Aljahdali, Rayan Naser, Rewaa Jalal, Shahad Alsaiari and Shamael Al-Shuhail.

TABLE OF CONTENTS

LIST OF ABBREVIATIONS

AF	Amplified-and-Forward.
AoF	Amount of Fading.
AWGN	Additive White Gaussian Noise.
BER	Bit Error Rate.
CDF	Cumulative Distribution Function.
CEP	Conditional Error Probability.
CSI	Channel-state Information.
DBPSK	Differential Binary Phase Shift Keying.
DF	Decode-and-Forward.
DGG	Double Generalized Gamma.
DH	Dual-hop.
EC	Ergodic Capacity.
EGBMGF	Extended Generalized Bivariate Meijer's G-function.
EGK	Extended Generalized-K.
EMI	Electromagnetic Interference.
FCC	Federal communications commission.
FSO	Free-Space Optical Communication.
GG	Generalized Gamma.
GNM	Generalized Nakagami-m.
i.i.d.	Independent and Identically Distributed.
i.n.i.d	Independent not Necessarily Identically Distributed.
IM/DD	Intensity Modulation/Direct Detection.
ISI	Inter-symbol Interference.
ISP	Internet service providers.
LAN	Local Area Network.
LED	Light-Emitting Diodes.
LN	Log-Normal.
LOS	Line-of-Sight.
MGF	Moment-Generating Function.
MIMO	Multiple-input Multiple-output.

NIR	Near Infrared.
OOK	On-off Keying.
OP	Outage Probability.
OWC	Optical wireless communication.
PDF	Probability Density Function.
RF	Radio frequency.
RV	Random Variable.
SC	Selection Combining.
SIMO	Single-input Multiple-output.
SISO	Single-input and Single-output.
SNR	Signal-to-noise Ratio.
SSC	Switched-and-stay Combining.
THz	Terahertz.
UVC	Ultraviolet Communications.
VLC	Visible Light Communications.
WBAN	Wireless Body Area Network.
WLAN	Wireless Local Area Network.

LIST OF SYMBOLS

$\Gamma(.)$	Gamma function.
$K_i(.)$	Modified Bessel function of the second kind of order i.
$\mathrm{G}_{p,q}^{m,n}[.]$	Meijer's G-function.
$\mathcal{M}_{.}(.)$	Moment-generating function of the random variable.
$I_0(.)$	Modified Bessel function of the first kind of order zero.
$\mathrm{E}[.]$	Expectation operation.
P_{out}	Outage probability.
$\Gamma(.\,,.)$	Complementary incomplete Gamma function.
$\psi(.)$	Digamma function.
$\boldsymbol{\Gamma}(.,.)$	Upper incomplete Gamma function.

LIST OF FIGURES

LIST OF TABLES

Chapter 1

Introduction

1.1 Background and Motivation

For the human being, communication is important for establishing a sense of social cohesion. Communication is defined as the activity of information exchange between two or more parties by speaking, writing, or using another medium through the same system of signs. Since man appeared on earth, communication took various forms starting from cave paintings. Other forms of long-distance communication have also existed such as drums, smoke signals, and pigeon post. Because these forms cannot be standardized, other forms were developed through writing, printed books and press, and sending mails.

As things evolve, there was a desire to transfer messages quickly and efficiently over longer distances. This desire was accommodated through the invention of the telegraph. The main principle behind the telegraph is to send electrostatically generated signals through a wire. The communication system consists of three main components, a battery for electricity generation, a key to break the circuit and an electromagnet at the receiving side. Using the telegraph was very popular, especially in the military services as it allowed sending instant messages across long distances. However, the cost associated with sending a telegraph was relatively high leading to its exclusion as a technology.

In 1876, Alexander Graham Bell noticed that sound vibrations travel through the air and can be received at a different end. By this observation, he patented the telephone in which these vibrations could be transferred across a wire by a continuous current. His discovery was widely accepted and is still used today.

During World War I, short-wave communications were utilized to transfer military messages. Once the war ended, this new form of communication unexpectedly took the world by storm. In 1920, commercial broadcasting started and by 1925 radio transmission was regulated by the Federal Communications Commission (FCC). Radio technology advanced so fast to become the hottest communication technology enabling transmission over long distances with better quality, less power and smaller devices. It was so popular that radios were to be found in every house.

The popularity of radio transmission demonstrated that the voice could be transmitted through air wirelessly, without the need for wires utilizing the electromagnetic spectrum. It also broadens the desire to transmit images and text instantly. Hence, in 1927 voice and images were available to be transferred via television. Since then and until 1960s, the technology advanced rapidly such that commercial telecommunication satellite was enabled and made a significantly major change in the market. The television became the source of accurate and timely news. Moreover, people relied on the television for constant entertainment.

After such a development in telecommunication, the market needed more full-duplex technologies allowing both parties to communicate simultaneously. In fact, the drive for most of these developments was for military purposes. As such, in 1967 the Internet, in which computers are allowed to exchange information, was originated. In the beginning, it was limited and then it went viral after several decades. The Internet usage includes information exchange via email and websites. Moreover, depending on the radio frequency carrier again, Martin Cooper invented the first mobile phone in 1973, allowing placing and receiving calls within a telephone service area. Mobile phones were widely accepted, as it is more convenient than landlines since they remove the need for wires.

During the early 2000s, wireless communications were attractive as network-enabled handled devices were evolving. Conventional wireless communication applications, involve both cellular and data, depend on the radio frequency (RF) to modulate the electrical signal whose range varies between 30 kHz and 300 GHz in the electromagnetic spectrum. RF communications are attractive since the waves are easily generated, spread in omni-directions, can travel long distances and finally can penetrate buildings, providing wider coverage. However, all these new applications require things to be taken into consideration. First concern is the bandwidth allocation which can be defined as the process of designating radio frequencies to different operators. Moreover, the RF spectrum is a national source that governments usually regulate, license and optimize to be used in radio broadcasting, industry, and commercial services for the public. In the United States as an example, the spectrum is regulated by the FCC.

Since the radio spectrum is a limited resource, it requires an effective and efficient allocation. Recent high demand of services and increases in the wireless data usage have led to two major issues in the communication industry, namely, the spectrum exhaustion and last mile access bottleneck. Spectrum exhaustion, crunch or congestion, is defined as the shortage of available wireless frequencies within the radio spectrum to accommodate a growing number of consumer devices, along with different government and private sector uses. This crunch is considered as a risk in wireless networking and telecommunication, leading to some undesirable future implications. On the other hand, last mile access bottleneck can be defined as the last mile link connecting the network to the Internet service providers (ISPs) network. For example, Internet connectivity is not available to some rural areas due to the lack of telecommunications infrastructure.

The research community, represented by scholars across universities, are driven to find realistic and effective solutions to these rising problems. One of the first trails was the cognitive radio (CR) that is based on the temporal use of the unoccupied spectrum. CR aims to increase the capacity per channel usage. Another interesting direction of solutions was proposed including the spatial usage of the spectrum via femtocells and multiple-input multiple-output (MIMO) systems, which enhance the capacity per square meter. The third solution proposed is to utilize different parts of the spectrum. It is achieved by optical wireless communication (OWC) systems. Our interest and main focus in this dissertation is the third direction as is described in the following sections.

1.1.1 Optical Wireless Communications

OWC offers an appealing, powerful, and attractive solution to replace and/or complement the conventional RF wireless communications for several reasons [2]. The first and most important reason is that the optical band in the electromagnetic spectrum is not licensed nor regulated, which reduces the operation cost since licensing fees are not needed anymore. In RF systems, it is required to design high-frequency circuits to perform back-and-forth conversion between baseband and transmission frequencies, whereas in OWC, this task is implemented by inexpensive light-emitting diodes (LED) and photodiodes. In comparison to RF, the range of the optical radiation can be easily controlled. Furthermore, the radiation cannot penetrate walls. All these properties cut down the interference between adjacent systems and enhance the security of the system. Lastly, utilizing the optical band implies the usage of unregulated frequencies at the terahertz (THz) range, leading to much higher data rates than conventional RF rates approaching gigabits per second, according to some experiments.

1.1.1.1 Historical Overview

Using OWC as a form of communication is not a new emerging technology. The earliest form was sunlight when the ancient Greeks and Romans utilized their shields to reflect sunlight. In 1880, Alexander Graham Bell, after patenting the telephone, invented the photophone that can be considered as the first wireless telephone system [3].

The photophone transfers sound on a beam of light. The voice is first projected via an instrument toward a mirror leading to noticeable vibrations. When sunlight is directed onto the mirror, the photophone receiver captures the oscillations and translates them back as voice. The photophone works similarly to the telephone but instead of relying on electricity, the information is transmitted using light. The photophone continued to be developed for military usage. However, after the invention of lasers in 1960s, there were many attempts for optical transmission. Goodwin in [4] listed various OWC demonstrations that have been performed using different types of lasers and modulation schemes during 1960-1970. Most of the experiments failed due to two reasons, namely, laser beam divergence and atmospheric turbulence. In the 1970s, fiber optics was developed to be a good choice for long-distance optical transmission. Hence, the interest in OWC shifted away and for years, remained limited to military and space applications only.

1.1.1.2 Current Status and Future Development

After the RF spectrum crunch, a number of companies have shown novel and efficient developments in OWC links that can be promising. These developments can be suitable for building future heterogeneous communication networks to support a wide range of service types and to meet the demands for higher data rates. Variations of OWC can be potentially employed in different communication applications, ranging from optical interconnects within integrated circuits through outdoor inter-building links to satellite communications. Based on the frequency range, the OWC can be divided into 3 types. The first is the near infrared (NIR) band (of wavelength 750-1550 nm) used in most terrestrial point-to-point OWC systems, that is called free-space optical (FSO) communications. These systems are applicable for inter-building connections. The second type is the visible band (of wavelength 390 – 750 nm) that is used to operate the visible light communications (VLC), taking advantage of LEDs to transmit and receive data ensuring human eye safety. The third type is the ultra violet band used by ultraviolet communication (UVC) systems for applications that require non-line-of-sight configurations. Also the OWC can be divided according to the applications as follows [5]:

- OWC is suitable for ultra-short range links such as inter-chip and intra-chip communications because of its higher bandwidth and low latency. This makes it a great replacement to copper-based interconnections which are considered a major bottleneck in system design.
- In the wireless body area network (WBAN), the RF technology is commonly used but it can cause some issues due to electromagnetic interference (EMI). Hence, VLC via LEDs is suitable for such short range links (order of 10 cm) [6].
- Due to recent development in solid state lighting, such as long life expectancy, high tolerance to humidity, lower power consumption, and reduced heat dissipation, OWC is applicable to medium range links (order of meters) as in wireless local area networks (WLANs). Some implementations are available in the literature as:
  - VLC can provide very high speeds up to 3.5 Gbps according to recent work [7, 8].
  - Some start-up companies based on the UK, France and Japan namely

PureVLC, Oledcomm, and Visilink have also been exploring the commercialization of this technology [5].

- OWC, in particular FSO, can also be utilized for longer distances up to several kilometers, providing high data rates and offering potential solutions for various problems, such as last mile access, cellular backhaul bottleneck, local area network (LAN) interconnections in enterprises or on campuses, broadband access to remote or/and rural areas [9], wireless video surveillance and backup links in disaster situations where existing infrastructure could be damaged or unreliable. Real-life events have proven the efficiency of deploying FSO technology as redundant links. Specifically, after the 9/11 terrorist attacks in New York City, FSO links were utilized to provide an emergency gateway to financial corporations in the Wall Street region, in which landlines were out of service [5].

- Moreover, the range of OWC links can extend to 10^4 kilometers from ground-to-satellite and satellite-to-satellite. In October 2013 as an example, NASA's Lunar Laser Communication Demonstration (LLCD) has shown the capability of establishing FSO links between the moon and earth while achieving a data rate of 622 Mbps over a distance of $384,600$ kilometers [10].

1.1.2 Free-space Optical Communications

In this dissertation, we focus mainly on FSO communication, since it is a potential solution for the bottleneck and spectrum exhaustion issues. FSO communications is a line-of-sight (LOS) and unidirectional technology that uses a modulated laser beam through the atmosphere to establish a communication link for several kilometers, providing data rates of giga-bits per seconds. For instance, state-of-the-art FSO systems support 10 Gb/s Ethernet that equals the bandwidth provided by the metro fiber optic systems [11]. Compared to fiber-optics, FSO systems deployment are both cost-and time-effective. On the other hand, FSO systems provide higher bandwidth compared to RF, license-free usage, inherited security and interference immunity. These features make FSO initially attractive for last mile access that connects the end user to exiting fiber optics networks.

Although FSO seems promising, there are still some challenges that need to be addressed. Indeed, as a laser beam propagates through the atmosphere, it is expected to experience some distortions in its power, which of course affects the stability of the receiving signal. In the following, further details on system loss factors are provided.

Absorption and Scattering The earth's atmosphere is an absorbing medium. In particular, any radiating photon is absorbed by a gaseous molecule and turned into kinetic energy and then the atmosphere becomes heated. Moreover, the wavelength is a major element in the absorption process. For example, O_2 and O_3 molecules can cancel the propagation of signals at a wavelength below 200 nm while it can be less effective at the visible wavelengths (i.e., $400 - 700$ nm).

Similarly, signal propagation through the atmosphere is prone to scattering which is also a function of wavelength. For instance, Rayleigh scattering is considered when air particles are smaller than the wavelength. In addition, when the size of the particles is much higher than the wavelength, such as in rain and snow, FSO transmission is relatively unaffected [12]. Generally, within the scale of metropolitan deployments (links are less than 1 km), typical rain can lead to attenuation on the order of 3 dB/km. However, severe rain can cause more attenuation, only in the case of deployments higher than 1 km [13]. On the other hand, Mie scattering is considered when the particles are of the same size as the wavelength, as in fog and haze. In this case, the signal can be highly attenuated even for short distances. As an example, experiments have shown that moderate fog over a distance of 50m leads to 90% loss in transmission power [14]. Another experiment in [15] conducted on the range of

785 to 1550 nm wavelength has shown that for foggy conditions, the attenuation is independent of the wavelength, while for haze it is not. In particular, fog particles (1000 nm - 20000 nm) are smaller than haze (10nm - 1000nm) and therefore haze conditions have low impact on the attenuation of the light beam.

Scattering and absorption lead to reduction and/or attenuation of the radiation in the atmosphere. This can be measured through the transmittance of the laser radiation, which is also related to the propagation path, described by Beer's law as:

$$\tau = \exp(-a(\lambda)L), \tag{1.1}$$

where L is the propagation path length and $a(\lambda)$ is called the attenuation coefficient defined as

$$a(\lambda) = A_a + S_a, \tag{1.2}$$

where A_s and S_a are the absorption and the scattering coefficient respectively.

It can be concluded from studying the impact of absorption and scattering effects on FSO systems that rain has a low effect on FSO while it is not the case for fog. It is totally the opposite in RF [13, 14]. This has motivated the integration of RF and FSO in communication networks.

Moreover, channel coherence bandwidth, which is inversely proportionally to the delay spread, is an important factor in modeling the communication channel. Under clear weather, there is negligible delay spread. However, fog and rain can increase the delay spread, which consequently induce inter-symbol interference (ISI). However, with the FSO high data rate, delay spread due to rain and fog scattering can be ignored. In some experiments, it has been reported that for a 1 km link, the delay spread due to rain is equal to less than 10 picoseconds, while it is limited to 50 picoseconds in the case of the presence of fog. Hence, the FSO channel is considered as frequency non-selective with no ISI.

Atmospheric Turbulence Induced Fading During transmission, the laser beam suffers from scintillation which can be defined as the temporal fluctuations of the laser beam intensity (irradiance), I_a, at the receiving end. More specifically, due to temperature and pressure inhomogeneity's caused by solar heat, the refractive index (defined as the ratio between the speed of light in a vacuum and the phase velocity of light in the medium) varies along the transmission path, leading to fluctuations in the signal amplitude and phase. The refractive index C_n^2 is considered as one of the most critical parameters to measure the strength of turbulence. It is an altitude dependent parameter defined as [16]:

$$\begin{aligned} C_n^2(h) = 0.00594 \left(\frac{v}{27}\right)^2 \left(10^{-5}h\right)^{10} \exp\left(-\frac{h}{1000}\right) \\ + 2.7 \times 10^{-16} \exp\left(-\frac{h}{1500}\right) + A \exp\left(-\frac{h}{100}\right), \end{aligned} \tag{1.3}$$

such that h is the height, v is the wind speed in meters per second and C_0 is the nominal value of the refractive index at the ground which is estimated to be $1.7 * 10^{-14}$. Typical C_n^2 values can vary between 10^{-14} $m^{2/3}$ indicating weak atmospheric turbulence and 10^{-12} $m^{\frac{2}{3}}$ for strong conditions. These fluctuations can definitely impact the system performance.

To quantify the effect of intensity fluctuations, the scintillation index is frequently considered in the studies. It can be defined as the normalized variance of irradiance fluctuations and can be expressed as

$$\sigma_{I_a}^2 = \frac{\mathbb{E}[I_a^2] - \mathbb{E}[I_a]^2}{\mathbb{E}[I_a]^2} = \frac{\mathbb{E}[I_a^2]}{\mathbb{E}[I_a^2]} - 1, \tag{1.4}$$

such that I_a denotes the beam irradiance and $\mathbb{E}[.]$ stands for the expectation operator. Another critical parameter to characterize the strength of turbulence is the Rytov variance

$$\sigma_R^2 = \delta C_n^2 \left(\frac{2\pi}{\lambda}\right)^{7/6} L^{11/6}, \tag{1.5}$$

such that L is the propagation path length, λ is the operational wavelength, C_n^2 is the refractive index, while $\delta = 1.23$ for plane waves and $\delta = 0.5$ for spherical waves. For weak turbulence conditions, the Rytov variance is proportional to the scintillation index, since it is the solution to Maxwell equations for electromagnetic wave propagation through a random medium. In stronger regimes, it indicates the turbulence strength by the increase of the refractive index or/and the path length. Hence, at weak turbulence conditions, the scintillation index is proportional to the Rytov variance. When turbulence gets worse, both the Rytov variance and scintillation index increase accordingly, reaching strong turbulence conditions. At this stage, the scintillation index reaches a maximum value and the Rytov variance is no longer a solution to the Maxwell equations. With the continuous increase in path length or inhomogeneity strength, the scintillation index reaches a saturation value close to unity. Saturation occurs because of the self-interference of the beam, so it loses its coherence. It can be concluded that the two major quantities are not independent as the optical wave propagates. Thus, the variations in both σ_R^2 and $\sigma_{I_a}^2$ could characterize the turbulence into 3 regimes as following [17–20]:

- When the Rytov variance is below 1, it describes the weak turbulence regime. In that case, the scintillation index becomes proportional to the Rytov variance.

- When the Rytov variance exceeds 1, the scintillation index increases to reach a maximum value of about 5 and 6 in spherical waves and 2 in plane waves [19]. This condition describes the moderate-to-strong turbulence, which can be called as well as focusing regime [17].

- Due to the continuous inhomogeneity's of temperature and increase of propagation path, σ_R^2 continues to increase [20], which leads to the saturation regime in which $\sigma_{I_a}^2 = 1$.

Assuming plane wave propagation, the turbulence conditions can be categorized into three regimes according to the Rytov variance, σ_R^2 [21]: a weak fluctuation regime ($\sigma_R^2 < 0.3$), a moderate-fluctuation regime ($0.3 \leq \sigma_R^2 < 5$), and a strong fluctuations regime ($\sigma_R^2 \geq 5$).

It is obvious that the performance of FSO communication systems can be severely affected by turbulence-induced scintillation. In other words, scintillation results in power loss at the photodetetor and random fluctuations of the received signal [22]. To capture the effect of such phenomena, mathematical models for the probability density function (PDF) of the instantaneous fading irradiance of the optical signal is introduced as to be illustrated in Chapter 2.

Geometric and Misalignment Loss The beam is prone to divergence when travels through the atmosphere leading to geometric loss. Beam divergence can be calculated using the link distance, divergence angle and aperture size. To effectively calculate the geometric loss, it is important to identify the optical wave model. For horizontal FSO transmissions, in the literature, it was shown that a Gaussian profile for the beam intensity is a good approximation. When the Gaussian bean has relatively high beam divergence in which it statistical characteristics is similar to point source. Thus, the approximations of plane or spherical wave can be used.

Moreover, beam divergence can affect the alignment between the transmitter and the receiver. Beam misalignment can also occur due to beam wander in which the large-scale eddies that deviates the beam from original path. Also, misalignment can be resulted from building sway, thermal expansion, and small earth quakes.

Eye safety Optical devices can pose critical health concerns if used incorrectly. Hence, eye safety is an important aspect when employing optical wireless commu-

	$650nm$	$880nm$	$1310nm$	$1550nm$
Class 1	up to 0.2 mW	up to 0.5 mW	up to 8.8 mW	up to 10 mW
Class 2	0.2-1 mW	N/A	N/A	N/A
Class 3A	1-5 mW	0.5-2.5 mW	8.8-45 mW	10-50 mW
Class 3B	5-500 mW	2.5-500 mW	45-500 mW	50-500 mW

Table 1.1: Laser safety classifications for a point-source emitter.

nication systems. Moreover, safety standards have been imposed in which the optical sources are classified with respect to the total emitting power as seen in Table. 1.1.

In general, the optical power emitted from the transmitter can be increased in order to overcome all obstacles facing the beam as propagates. However, the power must be limited to be complied with safety standards. All segments of OWC lead to eye damage of the energy at specific wavelength exceeds safety levels. For outdoor applications, high-power lasers are required for operation which are classified in the Class 3B band. Therefore, these systems are advised to be placed away from human contact preferably in rooftops. On the other hand, safety standards impose that indoor applications must be class 1 safe under all circumstances making it another challenges [23]. According to the table, launching power of indoor laser sources should not exceed 0.5 mW which is considered very low. However, using LEDs instead of laser sources offer much higher power while remaining Class 1 eye safe. It is because LEDs are large-area devices unlike lasers that are point source devices. Hence, using low cost LEDs as emitters either singly or in arrays become preferable in most indoor systems.

1.2 Thesis Objective

The aim of this thesis is to provide generalized models for the turbulence and misalignment. Also, scintillation mitigation methods are investigated using space diversity and relaying. In particular, this thesis contributes to the literature as follows:

- A performance analysis of generalized turbulence model based on double generalized Gamma distribution is provided taking into account the effect of symmetric pointing error effects.

- Generalized misalignment model statistics based on the Beckmann distribution is provided along with the asymptotic ergodic capacity based on the moment approach.

- A performance analysis of selection combining diversity technique over dual-branch FSO system is offered.

- A performance analysis of asymmetric amplify-and-forward relay-assisted FSO links is given.

1.3 Thesis Structure

This thesis is organized as follows. It first starts with the introduction in Chapter 1. In Chapter 2, the system and channel model considered in this work are proposed. Next, the performance analysis of a single FSO link over the double generalized Gamma channel is investigated in Chapter 3. Chapter 4 focuses on the asymptotic capacity, assuming a generalized model of pointing error. Following this, Chapters 5 and 6 study some diversity combining techniques over dual-branch FSO for weak and strong turbulence conditions, respectively. The performance analysis of dual-hop relay-assisted FSO link is then provided in Chapter 7. This work is finally concluded with a summary of contributions in Chapter 8. [24]

Chapter 2

Free-Space Optical Communication Channel Characterization and Modeling

2.1 Introduction

Mathematical modeling is crucial in the performance analysis of communication systems. It enables the prediction of the capabilities of the system before real employment. For FSO systems, the scintillation index in 1.4 is first utilized to categorize the turbulence strength. It can be used for further investigation to identify the distribution of turbulence-induced fading. This problem was widely tackled in the literature. For instant, log-normal (LN) model is accepted to describe the turbulence in weak regime [18]. On the other hand, different statistical models were investigated to fully characterize moderate-to-strong turbulence conditions. First, the negative exponential model was identified to describe the limit distribution for the intensity in the saturation regime [17]. Furthermore, The K-distribution was studied to characterize the channel in the strong regime [25]. Later, there has been notable research work that aim to come up with a universal model to span all turbulence conditions. These efforts depend on doubly stochastic theory of scintillation in which the large-scale and small-scale fluctuations of the beam are assumed to be generated from refractive and diffractive effects [18]. Hence, the K-distribution was extended to double-stochastic I-K distribution in [26, 27]. However, it was shown in [28] that I-K model might not match experimental work. Several distributions such as Log-normally-modulated exponential, exponential Weibull and Log-normal Rice have been studied in [17, 29–31].

In the current literature, the Gamma-Gamma ($\Gamma\Gamma$) scintillation model has gained a wide acceptance to describe moderate-to-strong turbulence conditions [17, 18]. In a recent study by [32], the double generalized Gamma (DGG) was proposed as a general model to span different turbulence conditions. According to some simulation results, the double generalized Gamma showed some superiority over the Gamma-Gamma model.

In addition to the turbulence effect, a misalignment between the transmitter and the receiver can lead to pointing errors and additional performance degradation. The misalignment originates from either mechanical error in the tracking system or mechanical vibrations in the system due to winds or/and building sway [33]. More specifically, pointing error results from the displacement of the laser beam along vertical (elevation) and horizontal (azimuth) directions that are typically assumed to be independent Gaussian random variables. A pointing error has two main components: the boresight and the jitter. The boresight is caused by thermal expansion of the laser beam and defined as the fixed displacement between the beam footprint center and the center of detection plane. On the other hand, the jitter is the random offset of the beam center at the detector plane, typically caused by building sway, weak earthquakes, and dynamic wind loads [34]. In the literature, several studies have been reported to model the pointing error effectively. For example, Farid and Hranilovic in [35] assumed zero boresight and same jitter variance for vertical and horizontal displacements. In the same fashion, Wang *et al* [34] generalized the model in [35] by considering a nonzero boresight. On the other hand, Gappmair *et al* in [36] considered zero boresight but different jitter variances for the two directions. In our work, we consider a generalized pointing error model taking into account a nonzero boresight component and different jitter variances.

To capture the effect of these drawbacks on the performance of FSO systems, combined statistics of turbulence and pointing errors is essential. Significant attempts were reported in the literature for Gamma-Gamma\Rayleigh channel model in [37], for double generalized Gamma\Rayleigh channel in [38], for Log-Normal\Rician in [34], and for Málaga ($\mathcal{M}$)\Rayleigh channel model in [39]. Finding the combined effect of pointing errors and turbulence becomes a harder task when considering general models of each (i.e. considering Beckmann model for the pointing error effect).

In this chapter, we present the models for turbulence and pointing errors considered throughout the work. In particular, we first investigate the most well-known models of different atmospheric turbulence conditions. Then, we focus on the pointing errors effect to explore the various models visited in the literature. In particular, we introduce our general model to cover different scenarios of misalignment. Finally, closed-form for a composite channel model is proposed.

2.2 Modeling of FSO Atmospheric Turbulence

The irradiance of the received optical wave I is defined as $I = I_0 I_a I_p$ where I_0 is the path loss effect and it is assumed to be normalized to 1, while I_a and I_p reflect the turbulence-induced fading and the pointing error effect, respectively [40]. The fading due to the atmospheric turbulence conditions I_a can be viewed as the modulation of large-scale (refractive) and small-scale (diffractive) fluctuations (i.e. if the turbulence cells are larger than the beam diameter and vise versa). Mathematically, it can be written as [17]

$$I_a = I_x I_y \,, \tag{2.1}$$

where I_x and I_y are statistically independent unit mean processes representing large-scale and small-scale effects, respectively.

In this section, various turbulence models are visited. In specific, the irradiance I_a which is considered as a random variable (RV) can follow different distributions according to the turbulence conditions.

2.2.1 Weak Turbulence Channel Model

For weak turbulence conditions, in which large-scale fluctuations dominate, I_a is modeled as [16]

$$I_a = \exp(2X)\,, \tag{2.2}$$

where $X \sim \mathcal{N}(\mu_X, \sigma_X^2)$ is the log-amplitude of the optical intensity such that $\sigma_X^2 \approx \sigma_R^2/4 = 0.30545\, k^{7/6}\; C_n^2 z^{11/6}$ [35] where σ_R^2 is the Rytov variance[1], C_n^2 is the index of refraction structure parameter of atmosphere defined in (1.3), and $k = 2\pi/\lambda$ is the optical wavenumber with λ being the wavelength [41]. Then the PDF of I_a can be given as

$$f_{I_a}(I) = \frac{1}{I\sigma_I\sqrt{2\pi}} \exp\left\{-\frac{(\ln(I)-\mu_I)^2}{2\sigma_I^2}\right\}\,, \tag{2.3}$$

where $\mu_I = 2\mu_X$ and $\sigma_I^2 = 4\sigma_X^2$ are the mean and standard deviation of I_a. To ensure that the average power is not amplified by fading, the irradiance is normalized (i.e $\mathbb{E}[I_a] = 1$ and $\mu_I = -2\sigma_X^2$) [42]. The nth moment for a LN RV I_a can then be calculated as

$$\mathbb{E}[I_a^n] = \exp\left(n\mu_I + \frac{n^2\sigma_I^2}{2}\right) = \exp\left(2n\sigma_X^2(n-1)\right)\,, \tag{2.4}$$

where E[.] is the expectation operation.

2.2.2 Moderate-to-Strong Turbulence Channel Model

Moderate-to-strong turbulence conditions result from combined effect of the large-scale and small-scale fluctuations as in (2.1). Hence, the second moment of the

---

[1] For plane wave propagation, the Rytov variance is given as $\sigma_R^2 = 1.23\, k^{7/6}\; C_n^2 z^{11/6}$ and $\sigma_X^2 = 0.30545\, k^{7/6}\; C_n^2 z^{11/6}$. However, for spherical wave propagation, the Rytov variance is equal to $\sigma_R^2 = 0.5\, k^{7/6}\; C_n^2 z^{11/6}$ and therefore, $\sigma_X^2 = 0.1250\, k^{7/6}\; C_n^2 z^{11/6}$ [16, Eq. (97)].

irradiance can be defined as

$$\mathbb{E}[I_a^2] = \mathbb{E}[I_x^2]\mathbb{E}[I_y^2]. \tag{2.5}$$

Since I_x and I_y are assumed to be unit mean independent random variables, then (2.5) can be written as

$$\mathbb{E}[I_a^2] = (1 + \sigma_{I_x}^2)(1 + \sigma_{I_y}^2), \tag{2.6}$$

where $\sigma_{I_x}^2$ and $\sigma_{I_y}^2$ are normalized variances of I_x and I_y, respectively. Then, the scintillation index in (1.4) is expressed as

$$\sigma_{I_a}^2 = (1 + \sigma_{I_x}^2)(1 + \sigma_{I_y}^2) - 1 = \sigma_{I_x}^2 + \sigma_{I_y}^2 + \sigma_{I_x}^2\sigma_{I_y}^2. \tag{2.7}$$

According to the novel work by [17], I_x and I_y are generally modeled as Gamma random variables leading to I_a modeled as a $\Gamma\Gamma$ RV with a PDF given by [17, Eq. 13]

$$f_{I_a}(I) = \frac{2(\alpha\beta I)^{\frac{\alpha+\beta}{2}}}{\Gamma(\alpha)\Gamma(\beta)I} K_{\alpha-\beta}\left(2\sqrt{\alpha\beta I}\right). \tag{2.8}$$

The PDF in (2.8) can be rewritten as

$$f_{I_i}(I) = \frac{(\alpha_i\beta_i I)^{\frac{\alpha_i+\beta_i}{2}}}{\Gamma(\alpha_i)\Gamma(\beta_i)I} \mathrm{G}_{0,2}^{2,0}\left(\alpha_i\beta_i I \,\middle|\, \begin{matrix} - \\ \frac{\alpha_i-\beta_i}{2}, \frac{\beta_i-\alpha_i}{2} \end{matrix}\right), \tag{2.9}$$

where $\mathrm{G}_{p,q}^{m,n}[.]$ is the Meijer's G-function as defined in [43, Eq.(9.301)], $\Gamma(.)$ is the Gamma function defined in [43, Eq.(8.310)], $K_i(.)$ is the modified Bessel function of order i, α and β are the fading parameters of large-scale and small-scale fluctuations[2].

---

[2] α represents the effective number of large-scale eddies while β is the effective number of small-scale eddies. The condition $\alpha > \beta$ always applies.

The nth moment of I_a can be derived by utilizing [44, Eq. 07.34.21.0009.01] as

$$\mathbb{E}[I_a^n] = \frac{\Gamma(\alpha+n)\Gamma(\beta+n)}{(\alpha\beta)^n\Gamma(\alpha)\Gamma(\beta)}, \tag{2.10}$$

and the second moment can be written as

$$\mathbb{E}[I_a^2] = \left(1+\frac{1}{\alpha}\right)\left(1+\frac{1}{\beta}\right). \tag{2.11}$$

Comparing (2.6) and (2.11), the following relations are trivial

$$\alpha = \frac{1}{\sigma_{I_x}^2}, \quad \beta = \frac{1}{\sigma_{I_y}^2}, \tag{2.12}$$

$$\sigma_{I_a}^2 = \frac{1}{\alpha} + \frac{1}{\beta} + \frac{1}{\alpha\beta}. \tag{2.13}$$

The variances of small-scale and large-scale fluctuations are expressed in terms of the Rytov variance in [17, Eqs. (18) and Eq. (19)]. In the case of plane wave as an example, the turbulence parameters α and β can be defined as

$$\begin{aligned}\alpha &= \left[\exp\left(\frac{0.94\sigma_R^2}{(1+1.11\sigma_R^{12/5})^{7/6}}\right)-1\right]^{-1},\\ \beta &= \left[\exp\left(\frac{0.51\sigma_R^2}{(1+0.69\sigma_R^{12/5})^{7/6}}\right)-1\right]^{-1}.\end{aligned} \tag{2.14}$$

2.2.3 Generalized Turbulence Channel Model

In this section, we discuss a newly proposed model, namely the double generalized Gamma developed by [32]. The model spans a wide range of turbulence conditions and perfectly matches the simulation data as seen in [32, Figs. (1), (2) and (3)]. Under this model, the large-scale and small-scale fluctuations, I_x and I_y respectively, are assumed to follow generalized Gamma (GG) distribution [45, 46] i.e. $I_x \sim GG(\alpha_1, \beta_1, \Omega_1)$ and $I_y \sim GG(\alpha_2, \beta_2, \Omega_2)$, where β_1 and β_2 are shaping parameters defining the turbulence-induced fading while $\alpha_1, \alpha_2, \Omega_1, \Omega_2$ are identified using the variance of the small and large scale fluctuations from [17, Eq. (18)-(20)] inserted in [46, Eq. (8a), (8b), (9)]. Hence, the PDF of I_a can be written as [46, Eq. (4)]

$$f_{I_a}(I_a) = \frac{\alpha_2 \lambda \sigma^{\beta_1 - \frac{1}{2}} \lambda^{\beta_2 - \frac{1}{2}} (2\pi)^{1-\frac{\sigma+\lambda}{2}}}{\Gamma(\beta_1)\Gamma(\beta_2) I_a} \mathrm{G}_{\lambda+\sigma,0}^{0,\lambda+\sigma}\left(\left(\frac{\Omega_2}{I_a^{\alpha_2}}\right)^{\lambda} \frac{\lambda^\lambda \sigma^\sigma \Omega_1^\sigma}{\beta_1^\sigma \beta_2^\lambda} \middle| \begin{matrix} 1-\kappa_0 \\ - \end{matrix} \right), \tag{2.15}$$

where $\kappa_0 = \Delta(\sigma : \beta_1), \Delta(\lambda : \beta_2)$, λ and σ are positive integers such as $\frac{\lambda}{\sigma} = \frac{\alpha_1}{\alpha_2}$ and $\Delta(x : y) \triangleq \frac{y}{x}, \frac{y+1}{x} \dots, \frac{y+x-1}{x}$.

The parameters λ and σ can be easily identified by first taking some possible values of λ (or σ) then calculate the other parameter using the relation $\sigma = \lceil \frac{\lambda \times \alpha_2}{\alpha_1} \rceil$ $\left(\lambda = \lceil \frac{\sigma \times \alpha_1}{\alpha_2} \rceil\right)$. This results in different combinations of λ and σ as shown in Table. 2.1. The perfect pair is chosen when the ratio error (i.e. error $= |\frac{\alpha_1}{\alpha_2} - \frac{\lambda}{\sigma}| \times \frac{\alpha_2}{\alpha_1}$) is the minimum as marked in blue in Table. 2.1. Moreover, Fig. 2.1 shows that different values of λ and σ lead to the same result.

It is very important to note that ((2.15) coincides numerically with Extended Generalized-K (EGK) PDF given in [47, Eq. (3)] and [48, Eq. (26)]. Also, the Malaga distribution [49] that has been proposed as a unifying model for all turbulence conditions reduces to the double GG by setting the appropriate parameters based on the amount of fading (AoF) matching.

2.3 Pointing Error Impairments Mathematical Modeling

Pointing error impairments can lead to considerable loss. In this section, the statistical model of the pointing error random variable, I_p, is discussed in details.

Table 2.1: Possible values of λ and σ.

λ	σ	Error	σ	λ	Error
1	1	58.98	1	3	23.05
2	1	17.96	2	5	2.55
3	2	38.47	3	8	9.38
4	2	17.96	4	10	2.55
5	3	31.63	5	13	6.65
6	3	17.96	6	15	2.55
7	3	4.29	7	18	5.48
8	4	17.96	8	20	2.55
9	4	7.70	9	22	0.27
10	5	17.96	10	25	2.55
11	5	9.76	11	27	0.69
12	5	1.56	12	30	2.55
13	6	11.13	13	32	0.97
14	6	4.21	14	35	2.55
15	7	12.10	15	37	1.18
16	7	6.24	16	40	2.55
17	7	0.38	17	42	1.34
18	8	7.71	18	44	0.27
19	8	2.59	19	47	1.47
20	9	8.85	20	49	0.50

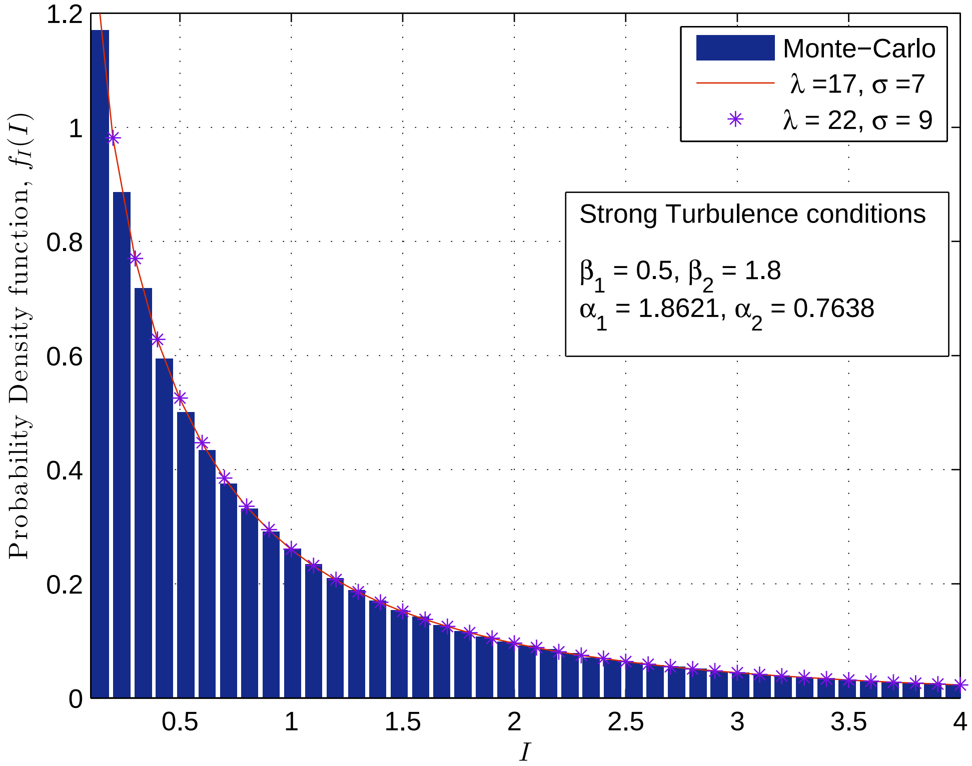

Figure 2.1: Comparison between PDFs obtained analytically and via Monte-Carlo simulations for different values of λ and σ.

2.3.1 Generalized Misalignment Channel Model

Assuming Gaussian beam with initial beamwaist, w_0, and radius of curvature, F_0, propagating through atmospheric turbulence of distance z, the beam waist at the receiver of radius a in long term, w_z, can be defined [18, Eq. 45, p.238]. Given a radial displacement r, the fraction of collected power at distance z can be approximated by

$$I_p(r:z) \approx A_0 \exp\left(-\frac{2r^2}{w_{z_{eq}}^2}\right) , \tag{2.16}$$

where $w_{z_{eq}}$ is the equivalent beamwidth defined as $w_{z_{eq}} = w_z^2 \frac{\sqrt{A_0 \pi}}{2v \exp\{-v^2\}}$ such that $A_0 = [\text{erf}(v)]^2$ is the maximum fraction of the collected power (i.e. the fraction of power at $r = 0$) , $v = \sqrt{\frac{a^2\pi}{2w_z^2}}$ is the ratio between the aperture radius a and the

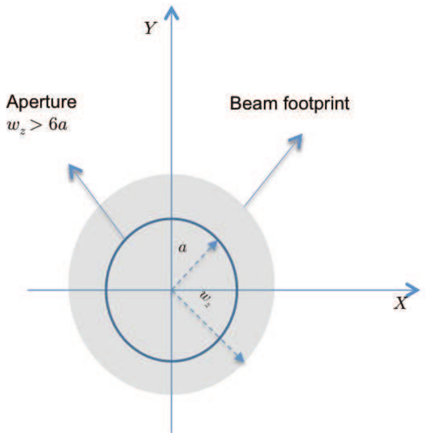

(a) Zero boresight: No misalignment

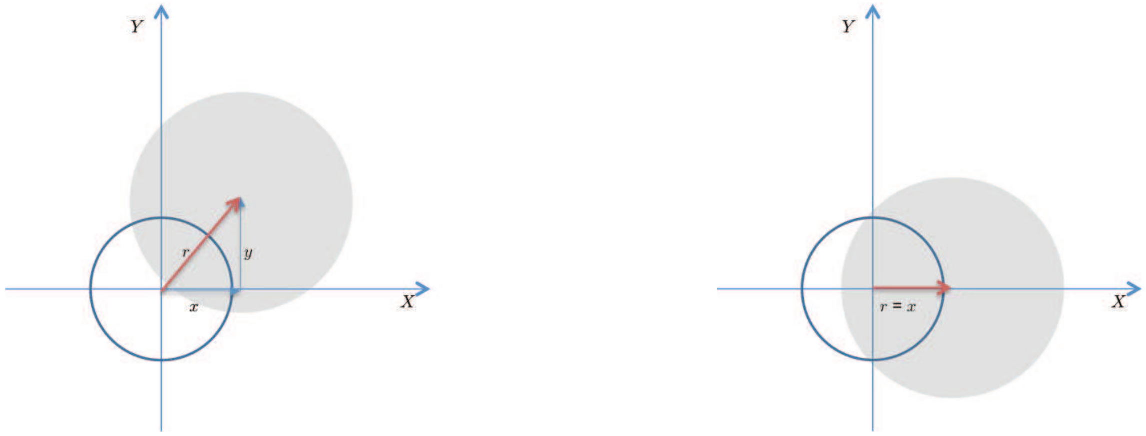

(b) Bi-Directional misalignment: zero boresight and identical jitters [35]

(c) Uni-Directional misalignment: zero boresight [50]

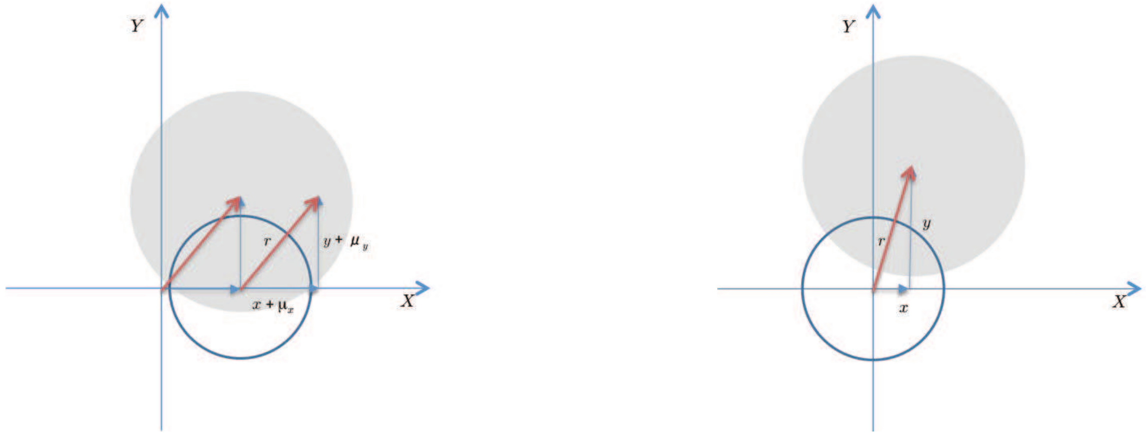

(d) Bi-Directional misalignment: non-zero boresight and identical jitters

(e) Bi-Directional misalignment: zero boresight and non-identical jitters

Figure 2.2: Beam footprint on the detector plane.

beamwidth w_z [35]. It is important to note that the approximation in (2.16) is valid when $w_z > 6a$ [34]. At the receiver, the radial displacement vector can be expressed as $\mathbf{r} = \left[\begin{smallmatrix} x & y \end{smallmatrix}\right]^T$, where x and y represent the vertical and horizontal displacements of the beam in the detector plane. Thus, the distribution of $r = |\mathbf{r}| = \sqrt{x^2 + y^2}$ depends on the distribution of x and y. Assuming independent Gaussian displacements along the horizontal and elevation axes, then r can be distributed according to the following distributions.

2.3.1.1 Beckmann Distribution

The Beckmann distribution[3] is a versatile model that includes many distributions as special cases. It is a four-parameter distribution modeling the envelope of two independent Gaussian RVs. In our case, if both displacements are nonzero mean Gaussian RVs with different jitters, i.e. $x \sim \mathcal{N}(\mu_x, \sigma_x)$ and $y \sim \mathcal{N}(\mu_y, \sigma_y)$, then $r = |\mathbf{r}| = \sqrt{x^2 + y^2}$ follows the Beckmann distribution [1, Eq. 2.37] [51, Eq. (31)] with PDF given by

$$f_r(r) = \frac{r}{2\pi\sigma_x\sigma_y} \int_0^{2\pi} \exp\left(-\frac{(r\cos\theta - \mu_x)^2}{2\sigma_x^2} - \frac{(r\sin\theta - \mu_y)^2}{2\sigma_y^2} \right) d\theta. \tag{2.17}$$

With the PDF of r, we can calculate the nth moment of I_p defined in (2.16) as

$$\mathbb{E}[I_p^n] = \mathbb{E}\left[A_0^n \exp\left(-\frac{2nr^2}{w_{z_{eq}}^2} \right) \right] = A_0^n \mathcal{M}_{r^2}\left(-\frac{2n}{w_{z_{eq}}^2} \right), \tag{2.18}$$

---

[3] The Beckmann distribution [51] is a four-parameter distribution corresponding to the envelope of two independent Gaussian RVs, each with their own mean and variance. It is different than the Log-Normal Rican distribution which can be also called as Beckamann distribution [17].

where $\mathcal{M}_{r^2}(.)$ is the moment-generating function of the random variable r^2 and given by [1, Eq. (2.38)]

$$\mathcal{M}_{r^2}(s) = \frac{1}{\sqrt{(1-\sigma_x^2 s)(1-\sigma_y^2 s)}} \exp\left(\frac{\mu_x^2 s}{1-2\sigma_x^2 s} + \frac{\mu_y^2 s}{1-2\sigma_y^2 s}\right). \tag{2.19}$$

Therefore, the nth moment of I_p becomes in this case

$$\mathbb{E}[I_p^n] = \frac{A_0^n \xi_x \xi_y}{\sqrt{(n+\xi_x^2)(n+\xi_y^2)}} \exp\left(-\frac{2n}{w_{z_{eq}}^2}\left[\frac{\mu_x^2}{1+\frac{n}{\xi_x^2}} + \frac{\mu_y^2}{1+\frac{n}{\xi_y^2}}\right]\right), \tag{2.20}$$

where $\xi_x = \frac{w_{z_{eq}}}{2\sigma_x}$ and $\xi_y = \frac{w_{z_{eq}}}{2\sigma_y}$, are the ratio between the equivalent beam width and the jitter variance for each direction.

2.3.1.2 Rayleigh Distribution

When both displacements have zero mean and common variance, i.e. $\mu_x = \mu_y = 0$ and $\sigma_x = \sigma_y = \sigma$ as illustrated in Fig. 2.2b, r is a Rayleigh distributed RV whose PDF is given by

$$f_r(r) = \frac{r}{\sigma^2} \exp\left(-\frac{r^2}{2\sigma^2}\right). \tag{2.21}$$

The PDF of I_p reduces in this case to [35]

$$f_{I_p}(I_p) = \frac{\xi^2}{A_0^{\xi^2}} I_p^{\xi^2-1}, \tag{2.22}$$

where $\xi = \frac{w_{z_{eq}}}{2\sigma}$. The nth moment can be deduced from (2.20) as

$$\mathbb{E}[I_p^n] = \frac{A_0^n \xi^2}{n+\xi^2}. \tag{2.23}$$

2.3.1.3 Rician Distribution

If both displacements have distinct nonzero mean and common variance, i.e. $\mu_x \neq \mu_y$, $\sigma_x = \sigma_y = \sigma$, as shown in Fig. 2.2d, then r is a Rician distributed RV with PDF given by

$$f_r(r) = \frac{r}{\sigma^2} \exp\left(\frac{-(r^2+s^2)}{2\sigma^2}\right) I_0\left(\frac{rs}{\sigma^2}\right), \tag{2.24}$$

where $s = \sqrt{\mu_x^2 + \mu_y^2}$ and $I_0(.)$ is the modified Bessel function of the first kind of order zero. This case has been visited in [34] and the PDF of the pointing error has been derived as

$$f_{I_p}(I_p) = \frac{\xi^2 \exp\left(\frac{-s^2}{2\sigma^2}\right)}{A_0^{\xi^2}} I_p^{\xi^2-1} I_0\left(\frac{s}{\sqrt{2}\sigma^2}\sqrt{-w_{z_{eq}} \ln\left(\frac{I_p}{A_0}\right)}\right). \tag{2.25}$$

The nth moment can be deduced also from (2.20) as

$$\mathbb{E}[I_p^n] = \frac{A_0^n \xi^2}{n+\xi^2} \exp\left(-\frac{2\, n\, \xi^2\, s}{w_{z_{eq}}^2 (n+\xi^2)}\right), \tag{2.26}$$

which matches [34, Eq. 6].

2.3.1.4 Hoyt Distribution

Here, zero mean but different variances are assumed for the two displacements directions (i.e. $\mu_x = \mu_y = 0$ and $\sigma_x \neq \sigma_y$) as shown in Fig. 2.2e. In this case, r becomes a Hoyt distributed RV with PDF given by

$$f_r(r) = \frac{r}{q\sigma_y^2} \exp\left(-\frac{r^2(1+q^2)}{4q^2\sigma_y^2}\right) I_0\left(\frac{r^2(1-q^2)}{4q^2\sigma_y^2}\right), \tag{2.27}$$

where $q = \frac{\sigma_x}{\sigma_y} = \frac{\xi_y}{\xi_x}$. This special case was studied in [36] and the PDF of I_p was found to be given by

$$f_{I_p}(I_p) = \frac{\xi_x \xi_y}{A_0} \left(\frac{I_p}{A_0} \right)^{\frac{\xi_x^2(1+q^2)}{2} - 1} I_0 \left(\frac{\xi_x^2 (1-q^2)}{2} \ln \frac{I_p}{A} \right), \quad 0 \le I_p \le A. \tag{2.28}$$

The nth moment can be deduced from (2.20) as

$$\mathbb{E}[I_p^n] = \frac{A_0^n \xi_x \xi_y}{\sqrt{(\xi_x^2 + n)(\xi_y^2 + n)}}. \tag{2.29}$$

2.3.1.5 Zero-mean Single-sided Gaussian Distribution

In this scenario, the displacement occurs in only one direction either parallel or orthogonal to the detection plane (i.e. $\mu_x = \mu_y = 0$, $\sigma_x = \sigma$, and $\sigma_y = 0$). This model was first introduced in [50] and the PDF of I_p can be derived in this case by simple RV transformation of (2.16), yielding

$$f_{I_p}(I_p) = \frac{\xi I_p^{\xi^2 - 1}}{A_0^{\xi^2} \sqrt{\pi \ln \left(\frac{A_0}{I_p} \right)}}, \tag{2.30}$$

and the resulting nth moment can be expressed as

$$\mathbb{E}[I_p^n] = \frac{\xi A_0^n}{\sqrt{n + \xi^2}}. \tag{2.31}$$

2.3.1.6 Non-zero Mean Single-sided Gaussian Distribution

In this case, we assume $\mu_x = \mu_y = \mu$, $\sigma_x = \sigma$, and $\sigma_y = 0$ and we can obtain the PDF of I_p as

$$f_{I_p}(I_p) = I_p^{\xi^2 - 1} \xi^2 \sqrt{\frac{\mu\sqrt{2}}{w \sqrt{\ln \frac{A_0}{I_p}}}} \exp\left(-\frac{2\mu^2 \xi^2}{w^2} \right) I_{-\frac{1}{2}} \left(\frac{2\mu\xi^2}{w} \sqrt{2 \ln \frac{A_0}{I_p}} \right), \tag{2.32}$$

and then the nth moment can as a result be expressed as

$$\mathbb{E}[I_p^n] = \frac{A_0^n \xi}{\sqrt{n+\xi^2}} \exp\left(-\frac{2n\mu^2(n+2\xi^2)}{w^2(n+\xi^2)}\right). \tag{2.33}$$

2.4 Modeling of Composite Channels

In this section, the combined effect of turbulence and pointing errors is presented. Due to some mathematical restrictions, the turbulence is modeled by double GG and the pointing error is modeled by the Rayleigh distribution. In specific, the joint distribution of $I = I_a I_p$ is given by [40, 52, 53]

$$f_I(I) = \int_{I_p} f_{I|I_p}(I|I_p) f_{I_p}(I_p)\, dI_p\,, \quad 0 \le I_p \le A_0\,, \tag{2.34}$$

with

$$f(I|I_p) = \frac{1}{I_p} f_{I_a}\left(\frac{I}{I_p}\right), 0 \le I \le A_0 I_a\,. \tag{2.35}$$

Inserting (2.22) and (2.15) in (2.34), and using [44, Eq. (07.34.21.0084.01)] yields

$$f_I(I) = \frac{\xi^2 \sigma^{\beta_1-\frac{1}{2}} \lambda^{\beta_2-\frac{1}{2}} (2\pi)^{1-\frac{\lambda+\sigma}{2}}}{\Gamma(\beta_1)\Gamma(\beta_2) I} \mathrm{G}^{0,\lambda+\sigma+1}_{\lambda+\sigma+1,1}\left(\frac{\lambda^\lambda \sigma^\sigma \Omega_1^\sigma \Omega_2^\lambda}{\beta_1^\sigma \beta_2^\lambda}\left(\frac{A_0}{I}\right)^{\alpha_2\lambda} \middle| \begin{matrix}\kappa_1\\ \kappa_2\end{matrix}\right), \tag{2.36}$$

where $\kappa_1 = 1 - \frac{\xi^2}{\alpha_2\lambda}, \Delta(\sigma : 1-\beta_1), \Delta(\lambda : 1-\beta_2)$, and $\kappa_2 = \frac{-\xi^2}{\alpha_2\lambda}$. It is important to note that when the pointing error effect approaches zero[4], (2.36) coincides mathematically and numerically with [46, Eq. (4)].

---

[4] Non-pointing error case occurs when $\xi \to \infty$ and $A_0 \to 1$.

2.5 Conclusion

In this chapter, we focused on two impairments which affect FSO systems and which typically lead to considerable loss namely, atmospheric turbulence and beam misalignment. First, different statistical distributions of atmospheric conditions were visited. Then, a new and general model for the pointing error impairments based on the generalized Beckmann distribution was discussed. The pointing error model is generic and includes previously published models as special cases. Then, we derived the joint PDF of the irradiance under the impact of Rayleigh pointing errors over double GG turbulence channel. Our PDF expression matches Kashani *et al.* [32] results mathematically and numerically when the pointing errors effect approaches zero.

Chapter 3

Performance of FSO Links over Double Generalized Gamma Channels with Pointing Errors

3.1 Introduction

In this chapter, we propose a new unified model for the performance analysis of a single FSO communication link that accounts for the impact of pointing errors and type of receiver detector. More specifically, we present unified closed-form expressions for the cumulative distribution function, the probability density function, the moment-generating function, and the moments of the end-to-end signal-to-noise ratio (SNR) of a single link FSO transmission system. We then use these unified expressions to evaluate performance measures such as the average bit error rate (BER), the outage probability (OP), and the ergodic capacity (EC) of a single FSO link operating over double GG fading channel model and under the impact of pointing errors.

3.2 System Model

Let us consider a single FSO link with two types of detection techniques, namely heterodyne and Intensity Modulation/Direct Detection (IM/DD)[1]. Data transmission is affected by path loss, atmospheric turbulence conditions, pointing errors, and additive white Gaussian

---

[1] Heterodyne detection mixes the optical field once it is received with locally generated signal and then detection is carried on. Heterodyne provides better performance, however, it is complex to implement. On the other hand, IM/DD is widely used in current FSO systems due to its simplicity. IM/DD depends on the intensity of the optical field to detect the transmitted data.

noise (AWGN)[2] that can be modeled as

$$y = \eta I x + w \quad , \tag{3.1}$$

where y is the received signal, η is the effective photoelectric conversion ratio, $x \in \{0, 2P_t\}$ is the on-off keying (OOK) modulated transmitted signal (i.e. $P_t = 1/2$), w refers to the AWGN sample with power spectral density equals to N_0, and I is the receiver irradiance that is defined as $I = I_a I_p$ where I_a reflects the turbulence-induced fading and follows double GG distribution with PDF given by (2.15) and I_p reflects the pointing error effect with PDF equals to (2.22). The joint PDF of I is expressed in (2.36) [40].

3.3 Statistical Properties of the Signal-to-Noise Ratio

In order to carry out a performance analysis of any FSO communication system, it is crucial to identify the statistics of the end-to-end SNR, γ. Examining several research work reported in the literature, it is noticed that the SNR is defined differently with respect to the receiver detector. In this section, we first examine each definition of the SNR to conclude with a unified expression accounting for any receiver detector. Then, based on the general definition of the electrical SNR, we find the statistical properties.

3.3.1 Probability Density Function

Heterodyne Detection In the case of this receiver, the average SNR μ_1 is defined as [53]

$$\mu_1 = \frac{\eta \mathrm{E}[I]}{N_0}, \tag{3.2}$$

---

[2] Most optical wireless systems operate in shot-noise limited regime and in that case the ambient light shot noise component dominants the shot noise generated from signal and the circuit. Thus, the resulting noise of the channel becomes white shot noise and can be distributed as Poisson random variables. By the central limit theorem, as the number of random variables approaches infinity, the cumulative distribution function is approximated by Gaussian distribution [2].

where $\mathrm{E}[I]$ is the first moment of I which can be found by

$$\mathbb{E}[I] \triangleq \int_0^\infty I f_I(I) dI, \tag{3.3}$$

where $f_I(I)$ is defined in (2.36). After solving the integration followed by some mathematical manipulations, $\mathbb{E}[I]$ is expressed as

$$\mathrm{E}[I] = \frac{A_1 B_1 A_0}{(1+\xi^2) A_2^{\frac{1}{\alpha_2 \lambda}}} = h A_0 \,, \tag{3.4}$$

where $A_1 = \frac{\xi^2 \sigma^{\beta_1 - \frac{1}{2}} \lambda^{\beta_2 - \frac{1}{2}} (2\pi)^{1-\frac{\lambda+\sigma}{2}}}{\Gamma(\beta_1)\Gamma(\beta_2)}$, $A_2 = \frac{\beta_1^\sigma \beta_2^\lambda}{\lambda^\lambda \sigma^\sigma \Omega_1^\sigma \Omega_2^\lambda}$, $B_1 = \prod_{i=1}^{\sigma+\lambda} \Gamma\left(\frac{1}{\alpha_2 \lambda} + \kappa_{0,i}\right)$, where $\kappa_{u,v}$ is the vth-term of κ_u, and $h = A_1 B_1 / (1+\xi^2) A_2^{\frac{1}{\alpha_2 \lambda}}$. It can be deduced from (3.2) that the SNR at the output of heterodyne receiver is defined as

$$\gamma = \frac{\eta I}{N_0} \,, \tag{3.5}$$

where $\frac{\eta}{N_0} = \frac{\mu_1}{h A_0}$. Following simple RV transformation of (2.36), the PDF of γ can be then expressed as

$$f_\gamma(\gamma) = \frac{A_1}{\gamma} \mathrm{G}_{\lambda+\sigma+1,1}^{0,\lambda+\sigma+1} \left(A_2^{-1} h^{-\alpha_2 \lambda} \left(\frac{\mu_1}{\gamma}\right)^{\alpha_2 \lambda} \middle| \begin{matrix} \kappa_1 \\ \kappa_2 \end{matrix} \right). \tag{3.6}$$

Intensity Modulation/Direct Detection Under this type of detection, the average electrical SNR is given by [40]

$$\mu_2 = \frac{(\eta \mathrm{E}[I])^2}{N_0}, \tag{3.7}$$

where $\mathbb{E}[I]$ is defined in (3.4). This leads to define the electrical SNR as

$$\gamma = \frac{(\eta I)^2}{N_0}, \tag{3.8}$$

where $\frac{\eta^2}{N_0} = \frac{\mu_2}{h^2 A_0^2}$. Again, the PDF of γ can be derived by RV transformation of (2.36)

$$f_\gamma(\gamma) = \frac{A_1}{2\gamma}\, \mathrm{G}_{\lambda+\sigma+1,1}^{0,\lambda+\sigma+1}\left(A_2^{-1} h^{-\alpha_2\lambda} \left(\frac{\mu_2}{\gamma}\right)^{\frac{\alpha_2\lambda}{2}} \middle| \begin{matrix} \kappa_1 \\ \kappa_2 \end{matrix} \right). \tag{3.9}$$

<u>Unified Expression</u> Observing (3.6) and (3.9) and utilizing [44, Eq. (07.34.17.0012.01)], a unified PDF can be obtained as

$$f_\gamma(\gamma) = \frac{A_1}{r\gamma}\, \mathrm{G}_{1,\lambda+\sigma+1}^{\lambda+\sigma+1,0}\left(A_2 h^{\alpha_2\lambda} \left(\frac{\gamma}{\mu_r}\right)^{\frac{\alpha_2\lambda}{r}} \middle| \begin{matrix} \tilde{\kappa}_2 \\ \tilde{\kappa}_1 \end{matrix} \right), \tag{3.10}$$

with[3]

$$\mathbb{E}[\gamma] = \overline{\gamma}_r = \frac{\mathrm{E}[I^r]}{\mathrm{E}[I]^r}\mu_r, \tag{3.11}$$

where $\tilde{\kappa}_1 = 1 - \kappa_1 = \frac{\xi^2}{\alpha_2\lambda}, \Delta(\sigma : \beta_1), \Delta(\lambda : \beta_2)$, $\tilde{\kappa}_2 = 1 - \kappa_2 = \frac{\alpha_2\lambda+\xi^2}{\alpha_2\lambda}$, $\mu_r = (\eta\mathbb{E}[I])^r/N_0$, and r refers to the detection method (i.e. $r = 1$ represents heterodyne detection and $r = 2$ represents IM/DD). This resulting PDF is generic and it reduces to the Gamma-Gamma fading model with pointing errors case when $\alpha_1 = \alpha_2 = 1$, $\Omega_1 = \Omega_2 = 1$, $\lambda = \sigma = 1$, $\beta_1 = \alpha$, and $\beta_2 = \beta$ as in [37, Eq. (3)] [37, Eq. (1)].

3.3.2 Cumulative Distribution Function

The cumulative distribution function (CDF) is defined as

$$F_\gamma(\gamma) = \int_0^\gamma f_\gamma(\gamma)\, d\gamma, \tag{3.12}$$

---

[3] The average SNR $\overline{\gamma}$ is defined as $\overline{\gamma}_r = \eta^r \mathrm{E}[I^r]/N_0$ while the average electrical SNR μ_r is given by $\mu_r = \eta^r \mathbb{E}[I]^r/N_0$ [54]. Thus, the relation between the average SNR and the average electrical SNR is trivial given that $\frac{\mathrm{E}[I^2]}{\mathrm{E}[I]^2} \triangleq \sigma_{si}^2 + 1$, where σ_{si}^2 is the scintillation index [55].

can be obtained by utilizing [44, Eq. (07.34.21.0084.01)] yielding

$$F_\gamma(\gamma) = \frac{\xi^2 \sigma^{\beta_1-\frac{1}{2}} \lambda^{\beta_2-\frac{1}{2}} (2\pi)^{1-\frac{r(\lambda+\sigma)}{2}} r^{\beta_1+\beta_2-2}}{\alpha_2 \lambda \Gamma(\beta_1)\Gamma(\beta_2)} \mathrm{G}^{u,1}_{r+1,u+1}\left(C\left(\frac{\gamma}{\mu_r}\right)^v \middle| \begin{matrix} 1, \kappa_3 \\ \kappa_4, 0 \end{matrix} \right), \tag{3.13}$$

where $v = \alpha_2\lambda$, $u = r(\lambda+\sigma+1)$, $C = \left(A_2 h^{\alpha_2\lambda}/r^{\lambda+\sigma}\right)^r$, $\kappa_3 = [\Delta(r : \tilde{\kappa}_2)]$ comprised of r terms, and $\kappa_4 = [\Delta(r : \tilde{\kappa}_1)]$ comprised of $r(\lambda+\sigma+1)$ terms such that $[\Delta(z : a_m)] \triangleq \Delta(z : a_1), \Delta(z : a_2) \ldots, \Delta(z : a_m)$. The CDF can be given in a simpler form in terms of basic elementary functions by first inverting the argument of the Meijer's G function using [43, Eq. (9.31.2)] and then applying [37, Eq. (24)] as

$$\lim_{x\to\infty} \mathrm{G}^{m,n}_{p,q}\left(x \middle| \begin{matrix} a_1, \ldots, a_n, \ldots, a_p \\ b_1, \ldots, b_m, \ldots, b_q \end{matrix} \right) = \sum_{k=1}^{n} x^{a_k-1} \frac{\prod_{l=1;l\neq k}^{n} \Gamma(a_k - a_l) \prod_{l=1}^{m} \Gamma(1 + b_l - a_k)}{\prod_{l=n+1}^{p} \Gamma(1 + a_l - a_k) \prod_{l=m+1}^{q} \Gamma(a_k - b_l)}, \tag{3.14}$$

with $a_k - a_l \neq 0, \pm 1, \pm 2, \cdots : (k, l = 1, \ldots n; k \neq l)$ and $a_k - b_l \neq 1, 2, 3, \ldots; (k = 1, \ldots, n; l = 1, \ldots, m)$. Thus, the CDF in (3.13) can be expressed asymptotically at high SNR as

$$\begin{aligned} F_\gamma(\gamma) \underset{\mu_r \gg 1}{\approxeq} & \frac{\xi^2 \sigma^{\beta_1-\frac{1}{2}} \lambda^{\beta_2-\frac{1}{2}} (2\pi)^{1-\frac{r(\lambda+\sigma)}{2}} r^{\beta_1+\beta_2-2}}{\alpha_2 \lambda \Gamma(\beta_1)\Gamma(\beta_2)} \\ & \times \sum_{k=1}^{u} \left[C^{-1} \left(\frac{\mu_r}{\gamma}\right)^v \right]^{-\kappa_{4,k}} \frac{\prod_{l=1, l\neq k}^{u} \Gamma\left(\kappa_{4,l} - \kappa_{4,k}\right)}{\kappa_{4,k} \prod_{l=1}^{r} \Gamma\left(\kappa_{3,l} - \kappa_{4,k}\right)}. \end{aligned} \tag{3.15}$$

Hence, the asymptotic expression of the CDF is dominated by $\min(\frac{\xi^2}{rv}, \frac{\beta_1}{r\sigma}, \frac{\beta_2}{r\lambda})$, where $\frac{\xi^2}{rv}$ represents the first term, $\frac{\beta_1}{r\sigma}$ represents the $(r+1)^{th}$ term and $\frac{\beta_2}{r\lambda}$ represents the $(r + r\sigma + 1)^{th}$ term in κ_4 i.e. when the difference between the parameters is large enough then the asymptotic expression of the CDF in (**??**) is dominated by a single term corresponding to the minimum of the three parameters. On the other hand, if the difference between any two parameters is not significant, then the asymptotic expression of the CDF in (**??**) is dominated by the summation of two terms corresponding to the first and second ranked minimum of the three parameters mentioned above.

3.3.3 Moment Generating Function

The moment generating function (MGF) that is defined as

$$\mathcal{M}_\gamma(s) \triangleq \mathbb{E}[e^{-\gamma s}], \tag{3.16}$$

can be expressed in terms of the CDF using integration by parts as [37, Eq. (6)]

$$\mathcal{M}_\gamma(s) = s\int_0^\infty \exp(-\gamma s) F_\gamma(\gamma). \tag{3.17}$$

Substituting (3.13) in (3.17) and utilizing [44, Eq. (07.34.21.0088.01)], the MGF can be expressed as

$$\mathcal{M}_\gamma(s) = \frac{\xi^2 \sigma^{\beta_1-\frac{1}{2}} \lambda^{\beta_2-\frac{1}{2}} (2\pi)^{\frac{3-r(\lambda+\sigma)-\alpha_2\lambda}{2}} r^{\beta_1+\beta_2-2}}{\sqrt{\alpha_2\lambda}\,\Gamma(\beta_1)\Gamma(\beta_2)} \mathrm{G}^{u,v}_{r+v,u}\left(C\left(\frac{v}{s\mu_r}\right)^{v} \left| \begin{matrix} \Delta(v:1), \kappa_3 \\ \kappa_4 \end{matrix} \right. \right). \tag{3.18}$$

In a similar fashion, the MGF can be expressed asymptotically at high SNRs as

$$\begin{aligned} \mathcal{M}_\gamma(s) \underset{\mu_r \gg 1}{\approxeq} & \frac{\xi^2 \sigma^{\beta_1-\frac{1}{2}} \lambda^{\beta_2-\frac{1}{2}} (2\pi)^{\frac{3-r(\lambda+\sigma)-\alpha_2\lambda}{2}} r^{\beta_1+\beta_2-2}}{\sqrt{\alpha_2\lambda}\,\Gamma(\beta_1)\Gamma(\beta_2)} \\ & \times \sum_{k=1}^{u} \left[C^{-1}\left(\frac{s\mu_r}{v}\right)^{v}\right]^{-\kappa_{4,k}} \frac{\prod_{l=1,l\neq k}^{u} \Gamma\left(\kappa_{4,l}-\kappa_{4,k}\right) \prod_{l=1}^{v} \Gamma\left(\{\Delta(v:0)\}_l + \kappa_{4,k}\right)}{\prod_{l=1}^{r} \Gamma\left(\kappa_{3,l}-\kappa_{4,k}\right)}. \end{aligned} \tag{3.19}$$

Again, the dominant terms can be derived in a similar fashion as the CDF in Section 3.3.2.

3.3.4 Moments

The moments of γ is defined as

$$\mathbb{E}[\gamma^n] \triangleq \int_0^\infty \gamma^n f_\gamma(\gamma) d\gamma. \tag{3.20}$$

Placing (3.10) in (3.20) and utilizing [43, Eq. (7.813.1)], the moments can be obtained in a simple closed-form expression as

$$\mathbb{E}[\gamma^n] = \frac{A_1 B_2 \mu_r^n}{(nr+\xi^2) h^{nr} A_2^{\frac{nr}{\alpha_2 \lambda}}} \quad , \tag{3.21}$$

where $B_2 = \prod_{i=1}^{\sigma+\lambda} \Gamma\left(\frac{nr}{v} + \kappa_{0,i}\right)$.

3.4 Performance Analysis Measures

In this section, the performance of a single FSO link operating over double GG fading channel is studied based on the results provided in Section 3.3. In specific, closed-form expressions of the OP, AoF, BER and EC are derived.

3.4.1 Outage Probability

The outage probability P_{out} is defined as follows:

$$P_{out} = \Pr[\gamma < \gamma_{th}] = F_\gamma(\gamma_{th}). \tag{3.22}$$

Accordingly, the OP of the link is obtained by substituting (3.13) into (3.22).

3.4.2 Higher-Order Amount of Fading

In this section, the amount of fading that can be considered as an important measure to assess the performance of any wireless communication system is presented. The

Parameters p and q	**Modulation scheme**
$p = 0.5$ and $q = 0.5$	Orthogonal coherent binary frequency shift keying (CBFSK)
$p = 0.5$ and $q = 1$	Antipodal coherent binary phase shift keying (CBPSK)
$p = 1$ and $q = 0.5$	Orthogonal noncoherent binary frequency shift keying (NCBFSK)
$p = 1$ and $q = 1$	Antipodal differentially coherent binary phase shift keying (DBPSK)

Table 3.1: Different Modulation schemes with respect to the parameters p and q [1].

AoF aims to define the distribution of the SNR of the received signal [56]. The n^{th}-order AoF for γ is defined as [57]

$$AF_{\gamma} = \frac{\mathrm{E}[\gamma^n]}{\mathrm{E}[\gamma]^n} - 1. \tag{3.23}$$

Using this definition and substituting (3.21) into it, the n^{th}-order AF can be rewritten as

$$AF_{\gamma}^{(n)} = \frac{(r+\xi^2)^n}{A_1^{n-1} B_2^{n-1} (nr+\xi^2)} - 1\,. \tag{3.24}$$

3.4.3 Average Bit Error Rate

The average bit error rate, $\overline{P}_b$, is the average number of bit errors per unit time. To obtain an analytical expression of the average BER of the system, the conditional error probability (CEP) formula for an AWGN channel is averaged over the fading distribution. In other words, Wojnar in [58] unified the CEP to span coherent, differentially coherent and noncoherent modulations of binary signaling transmitted over the AWGN channel as

$$P_e(\epsilon|\gamma) = \frac{\Gamma(p, q\gamma)}{2\Gamma(p)}, \tag{3.25}$$

where p and q refer to different modulation/detection schemes as shown in Table. 3.1 and $\Gamma(.,.)$ is the complementary incomplete gamma function. Hence, the average

BER is then obtained by averaging (3.25) over the fading PDF as

$$\overline{P}_b = \int_0^\infty \frac{\Gamma(p, q\gamma)}{2\Gamma(p)} f_\gamma(\gamma) d\gamma, \tag{3.26}$$

$$= \int_0^\infty \frac{\Gamma(p, q\gamma)}{2\Gamma(p)} dF_\gamma(\gamma), \tag{3.27}$$

and after applying integration part in (3.27), the average BER can be expressed in terms of the CDF of the fading RV as [59, Eq. (12)]

$$\overline{P}_b = \frac{q^p}{2\Gamma(p)} \int_0^\infty \exp(-q\gamma)\gamma^{p-1} F_\gamma(\gamma) d\gamma\,. \tag{3.28}$$

Assuming double GG fading channel with pointing error impairments, $\overline{P}_b$ can be derived by placing (3.13) into (3.28) and utilizing [44, Eq. (07.34.21.0088.01)] as

$$\overline{P}_b = \frac{\xi^2 \sigma^{\beta_1-\frac{1}{2}} \lambda^{\beta_2-\frac{1}{2}} (2\pi)^{\frac{3-r(\lambda+\sigma)-\alpha_2\lambda}{2}} r^{\beta_1+\beta_2-2}}{2\Gamma(p)\Gamma(\beta_1)\Gamma(\beta_2)(\alpha_2\lambda)^{\frac{3}{2}-p}} \mathrm{G}^{u,v+1}_{r+v+1,u+1}\left(C\left(\frac{v}{q\mu_r}\right)^{v} \middle| \begin{matrix} \Delta(v:1-p), 1, \kappa_3 \\ \kappa_4, 0 \end{matrix} \right). \tag{3.29}$$

Interestingly, the expression in (3.29) can be also approximated at high SNR using elementary functions as follows

$$\overline{P}_b \underset{\mu_r \gg 1}{\approx} \frac{\xi^2 \sigma^{\beta_1-\frac{1}{2}} \lambda^{\beta_2-\frac{1}{2}} (2\pi)^{\frac{3-r(\lambda+\sigma)-\alpha_2\lambda}{2}} r^{\beta_1+\beta_2-2}}{2\Gamma(p)\Gamma(\beta_1)\Gamma(\beta_2)(\alpha_2\lambda)^{\frac{3}{2}-p}} \times \sum_{k=1}^{u} \left[C^{-1} \left(\frac{q\mu_r}{v}\right)^{v} \right]^{-\kappa_{4,k}} \frac{\prod_{l=1, l\neq k}^{u} \Gamma\left(\kappa_{4,l} - \kappa_{4,k}\right) \prod_{l=1}^{v} \Gamma\left(\{\Delta(v:p)\}_l + \kappa_{4,k}\right)}{\kappa_{4,k} \prod_{l=1}^{r} \Gamma\left(\kappa_{3,l} - \kappa_{4,k}\right)}. \tag{3.30}$$

The dominant terms for $\overline{P}_b$ are obtained the same way as the CDF was treated in Section 3.3.2. If the conditions of a single dominant term are satisfied then (3.30) can be reduced to the very simple form as [60]

$$\overline{P}_b \approxeq (G_c \cdot \mu_r)^{-G_d}, \tag{3.31}$$

where G_c refers to the coding gain while G_d is referred to as the diversity gain. Therefore, the diversity and coding gains of the system under consideration can be simply expressed in terms of elementary functions as follows

$$G_d = v \min\left(\frac{\xi^2}{rv}, \frac{\beta_1}{r\sigma}, \frac{\beta_2}{r\lambda}\right), \tag{3.32}$$

and

$$\begin{aligned} G_c = \frac{C^{-1/v} q}{v} \times \Bigg[& \frac{\xi^2 \sigma^{\beta_1-\frac{1}{2}} \lambda^{\beta_2-\frac{1}{2}} (2\pi)^{\frac{3-r(\lambda+\sigma)-\alpha_2\lambda}{2}} r^{\beta_1+\beta_2-2}}{2\Gamma(p)\Gamma(\beta_1)\Gamma(\beta_2)(\alpha_2\lambda)^{\frac{3}{2}-p}} \\ & \times \frac{\prod_{l=1, l\neq k}^{u} \Gamma\left(\kappa_{4,l}-\kappa_{4,k}\right) \prod_{l=1}^{v} \Gamma\left(\{\Delta(v:p)\}_l + \kappa_{4,k}\right)}{\kappa_{4,k} \prod_{l=1}^{r} \Gamma\left(\kappa_{3,l}-\kappa_{4,k}\right)} \Bigg]^{-1/G_d}, \end{aligned} \tag{3.33}$$

where k is the index of the $\min\left(\frac{\xi^2}{rv}, \frac{\beta_1}{r\sigma}, \frac{\beta_2}{r\lambda}\right)$ which can be one of the following possibilities $k = 1$ or $k = r + 1$ or $k = r + r\sigma + 1$.

3.4.4 Ergodic Capacity

The Shannon capacity of a communication channel is defined as the upper bound for the maximum rate of transmission at small BER. Applying the theorem to AWGN channel, the capacity can be written as

$$C = B \ \log_2(1 + \gamma_{end}), \tag{3.34}$$

where B is the channel bandwidth and γ_{end} is the end-to-end SNR of the communication channel. Since the end-to-end SNR for fast fading channel is a random variable, then the channel capacity must be considered as random too and its average, known as ergodic capacity, is defined as the average practical best rate for error-free transmission[4].

Considering that perfect channel-state information (CSI) at both the receiver and the transmitter of an FSO communication system, the ergodic capacity can be defined as

$$\begin{aligned}\overline{C} &\triangleq \mathbb{E}[\log_2(1+\delta\gamma)] && (3.35)\\ &= \int_0^\infty \log_2(1+\delta\gamma) f_\gamma(\gamma) d\gamma, && (3.36)\end{aligned}$$

where $\delta = 1$ for heterodyne detection ($r = 1$) and $\delta = e/2\pi$ for IM/DD ($r = 2$). It is very important to note that the expression in (3.35) is exact for $r = 1$ while it is a lower bound for the case of $r = 2$ [62, Eq. (26)] [63, Eq. (7.43)].

Expressing $\log_2(1+\delta\gamma)$ as $\frac{\ln(1+\delta\gamma)}{\ln(2)}$, $\overline{C}$ is obtained by using (3.36) along with the identities [44, Eq. (07.34.21.0013.01)] and

$$\ln(1+x) = \mathrm{G}_{2,2}^{1,2}\left(x \,\middle|\, \begin{matrix}1,1\\ 1,0\end{matrix}\right), \tag{3.37}$$

yielding

$$\overline{C} = \frac{\xi^2 \sigma^{\beta_1-\frac{1}{2}} \lambda^{\beta_2-\frac{1}{2}} (2\pi)^{2-\alpha_2\lambda-\frac{r(\lambda+\sigma)}{2}} r^{\beta_1+\beta_2-2}}{\ln(2)\Gamma(\beta_1)\Gamma(\beta_2)\alpha_2\lambda} \mathrm{G}_{r+v+1,u+v+1}^{u+v+1,v}\left(C\left(\frac{1}{\delta\mu_r}\right)^v \,\middle|\, \begin{matrix}\Delta(v:0),1,\kappa_3\\ \kappa_4,\Delta(v:0),0\end{matrix}\right). \tag{3.38}$$

---

[4] Although optical channel is well described as slow varying channel where coherence time is much greater than transmission time, ergodic capacity is still a widely adopted metric. The suitability of ergodic capacity as performance metric improves in this work as we consider pointing errors which typically increase the rate of channel fluctuations. In the case of heterodyne detection (r = 1) the expression $\overline{C} = \mathbb{E}[\log_2(1+\delta\gamma_{end})]$ represents the exact ergodic capacity where $\delta = 1$. However, in the case of IM/DD ($r = 2$) the expression $\overline{C} = \mathbb{E}[\log_2(1+\delta\gamma)]$ where $\delta = e/2\pi$ represents a tight lower bound for capacity is given as [61] [62, Eq. (26)] [63, Eq. (7.43)].

Moreover, $\overline{C}$ can be written asymptotically at high SNR as

$$\overline{C} \underset{\mu_r \gg 1}{\approxeq} \frac{\xi^2 \sigma^{\beta_1-\frac{1}{2}} \lambda^{\beta_2-\frac{1}{2}} (2\pi)^{2-\alpha_2\lambda-\frac{r(\lambda+\sigma)}{2}} r^{\beta_1+\beta_2-2}}{\ln(2)\Gamma(\beta_1)\Gamma(\beta_2)\alpha_2\lambda} \times \sum_{k=1}^{u+v+1} \left[C^{-1}\left(\delta\mu_r\right)^v\right]^{-\kappa_{7,k}} \frac{\prod_{l=1,l\neq k}^{u+v+1}\Gamma\left(\kappa_{7,l}-\kappa_{7,k}\right)\prod_{l=1}^{v}\Gamma\left(\{\Delta(v:1)\}_l+\kappa_{7,k}\right)}{\Gamma(1-\kappa_{7,k})\prod_{l=1}^{r}\Gamma\left(\kappa_{3,l}-\kappa_{7,k}\right)}, \tag{3.39}$$

where $\kappa_7 = \kappa_4, \Delta(v:0), 0$ and can be reduced to the dominant terms slightly different then in the case of Sec. 3.3.2. The asymptotic expression of the capacity in (3.39) is dominated by the summation of two terms, one corresponds to $\min\left(\frac{\xi^2}{rv}, \frac{\beta_1}{r\sigma}, \frac{\beta_2}{r\lambda}, \frac{\epsilon}{v}\right)$ such that $\frac{\epsilon}{v}$ is the $(u+1)^{th}$ term in κ_7 where ϵ is a small error introduced to validate the conditions of [37, Eq. (24)]. The second term corresponds to the $(u+2)^{th}$ of κ_7.

In another way, the channel capacity can be written in terms of the AoF at high SNR as [48, Eqs. (8) and (9)]

$$\overline{C} \underset{\mu_r \gg 1}{\approxeq} \log(\overline{\gamma}) + \frac{\partial}{\partial n} AF_{\gamma}^{(n)}\bigg|_{n=0}, \tag{3.40}$$

and with simple algebraic manipulation, it can be simplified further to [37]

$$\overline{C} \underset{\mu_r \gg 1}{\approxeq} \log(\overline{\gamma}) + \frac{\partial}{\partial n}\left(\frac{\mathbb{E}[\gamma^n]}{\mathbb{E}[\gamma]^n} - 1\right)\bigg|_{n=0}, \tag{3.41}$$

$$\begin{aligned} &= \log(\overline{\gamma}) + \left(\frac{1}{\mathbb{E}[\gamma]^n}\frac{\partial}{\partial n}\mathbb{E}[\gamma^n] + \mathbb{E}[\gamma^n]\frac{\partial}{\partial n}\frac{1}{\mathbb{E}[\gamma]^n}\right)\bigg|_{n=0}, \\ &= \log(\overline{\gamma}) + \left(\frac{1}{\mathbb{E}[\gamma]^n}\frac{\partial}{\partial n}\mathbb{E}[\gamma^n] - \frac{\mathbb{E}[\gamma^n]}{\mathbb{E}[\gamma]^n}\log(\mathbb{E}[\gamma])\right)\bigg|_{n=0}, \\ &= \log(\overline{\gamma}) + \left(\frac{1}{\mathbb{E}[\gamma]^n}\frac{\partial}{\partial n}\mathbb{E}[\gamma^n] - \frac{\mathbb{E}[\gamma^n]}{\mathbb{E}[\gamma]^n}\log(\overline{\gamma})\right)\bigg|_{n=0}, \\ &= \frac{\partial}{\partial n}\mathbb{E}[\gamma^n]\bigg|_{n=0}. \end{aligned} \tag{3.42}$$

Thus, high SNR approximation for the ergodic capacity can be obtained by evaluating the first derivative of the moments (3.21) at $n = 0$ which is given by

$$\frac{\partial}{\partial n}\mathbb{E}[\gamma^n] = \frac{A_1 B_2 \mu_r^n}{(nr+\xi^2)h^{nr}A_2^{\frac{nr}{v}}}\left[\log(\mu_r) - r\log(h) - \frac{r\log(A_2)}{v} + \frac{r}{v}B_3 - \frac{r}{nr+\xi^2}\right], \tag{3.43}$$

where $B_3 = \sum_{i=1}^{\sigma+\lambda}\psi\left(\frac{nr}{v}+\kappa_{0,i}\right)$, such that $\psi(.)$ is the digamma function [43, Eq. (8.360.1)]. Evaluating (3.43) at $n = 0$, the ergodic capacity at high SNR can be simply expressed as

$$\overline{C} \underset{\mu_r \gg 1}{\approxeq} \frac{A_1 B_2|_{n=0}}{\xi^2}\left[\log(\delta\mu_r) - r\log(h) - \frac{r\log(A_2)}{v} + \frac{r}{v}B_3|_{n=0} - \frac{r}{\xi^2}\right]. \tag{3.44}$$

In addition, the ergodic capacity at low SNR regime can be approximated by the first moment of the SNR. Placing $n = 1$ in the moments (3.21), the asymptotic ergodic capacity at low SNR can be expressed in terms of elementary functions as

$$\overline{C} \underset{\mu_r \ll 1}{\approxeq} \frac{A_1 B_2 \delta\mu_r}{(r+\xi^2)h^r A_2^{\frac{r}{\alpha_2\lambda}}}. \tag{3.45}$$

3.5 Numerical Examples

In this section, we present some selected numerical examples to prove the validity of the analytical results. Also, the impact of turbulence conditions and pointing errors on the performance of the system under both detection techniques (i.e heterodyne and IM/DD) is shown. In the simulations, two scenarios of atmospheric turbulence conditions are considered, namely strong (i.e lower values of β_1 and β_2) and moderate based on the results reported in [32]. For strong turbulence, we consider the following set of parameters: $\beta_1 = 0.5$, $\beta_2 = 1.8$, $\alpha_1 = 1.8621$, $\alpha_2 = 1$, $\Omega_1 = 1.5074$, and $\Omega_2 = 1$ such that λ and σ are chosen to satisfy the conditions to be 17 and 9, respectively. On the other hand, for moderate turbulence conditions, we assume $\alpha_1 = 2.1690$, $\alpha_2 = 1$,

$\beta_1 = 0.55$, $\beta_2 = 2.35$, $\Omega_1 = 1.5793$, and $\Omega_2 = 1$ where λ and σ are chosen to be 28 and 13, respectively [46]. In both cases, it is assumed that α_2 is an integer to satisfy the condition $\alpha_2\lambda$ being an integer.

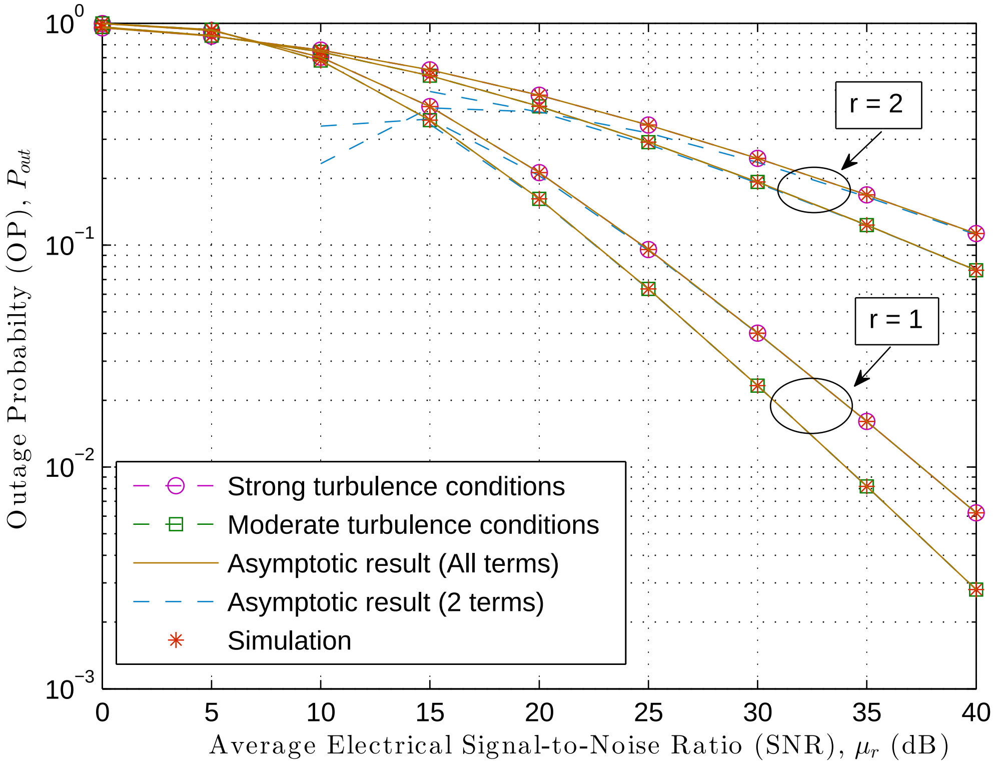

Figure 3.1: Outage probability of a single FSO link under strong and moderate turbulence conditions for both detection techniques, heterodyne ($r = 1$) and IM/DD ($r = 2$) with $\xi = 1$.

Starting with the outage probability of a single FSO link under two types of detection techniques experiencing different turbulence condition is presented in Fig. 3.1. Moreover, the impact of pointing error is presented in Fig. 3.2. It is worthy of note that simulation results match the analytical work. In particular, the asymptotic results based on all terms match the analytical ones perfectly while the rest of the results (based on two or single terms) converge very fast even for low SNR values. It is observed as well that when the system operates on IM/DD, it is prone to outage more than if heterodyne is considered. Moreover, high pointing errors effect (i.e $\xi \to 0$)

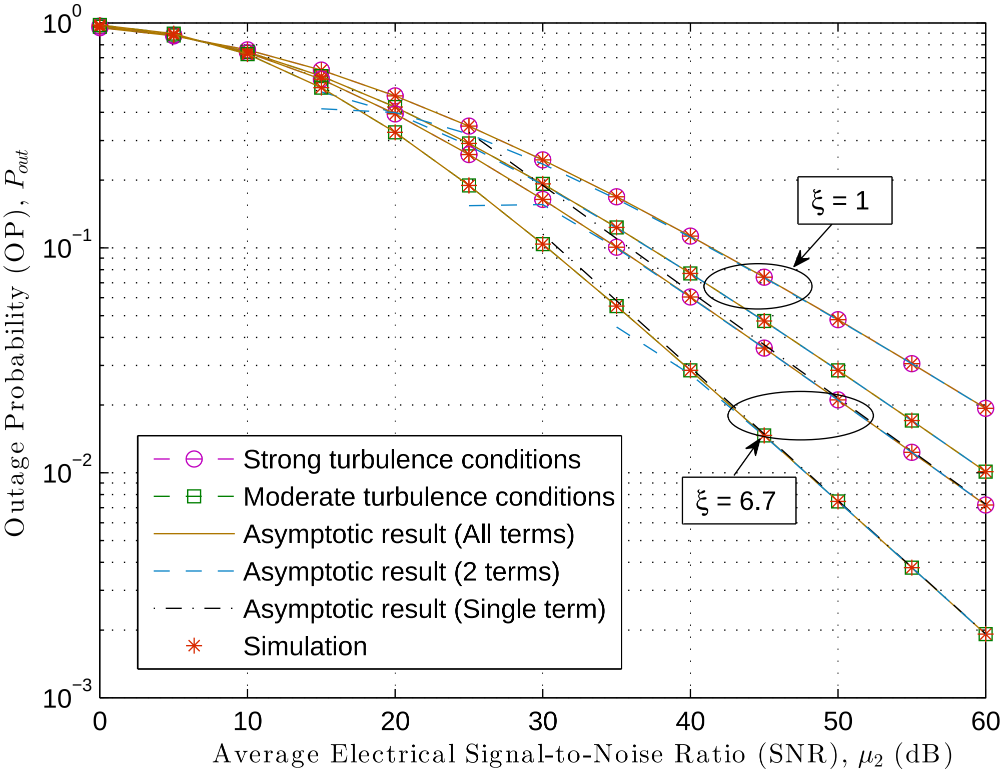

Figure 3.2: The impact of pointing errors on the outage probability of a single FSO link under strong and moderate turbulence conditions using IM/DD technique ($r = 2$) with varying pointing errors.

leads to higher probability of system outage.

In addition, the average BER performance under differential binary phase shift keying (DBPSK) modulation, where $p = 1$ and $q = 1$, for single link FSO system was evaluated in Figs. 3.3 and 3.4. We can observe that the simulation results along with the asymptotic (utilizing all terms in the summation as in (3.30)) are matching with the exact analytical results. However, lower values of ξ (i.e. high pointing errors effect) affect the convergence of asymptotic results (utilizing only the dominant terms). Specifically, in Fig. 3.4, we get asymptotic results by utilizing a single dominant term of Eq. (3.15) only for the case of $\xi = 6.7$. This is mainly due to a significance difference between $\frac{\xi^2}{rv}, \frac{\beta_1}{r\sigma}, \frac{\beta_2}{r\lambda}$ which leads to a dominate term corresponding to $\min(\frac{\xi^2}{rv}, \frac{\beta_1}{r\sigma}, \frac{\beta_2}{r\lambda})$. In general, turbulence conditions and pointing errors result

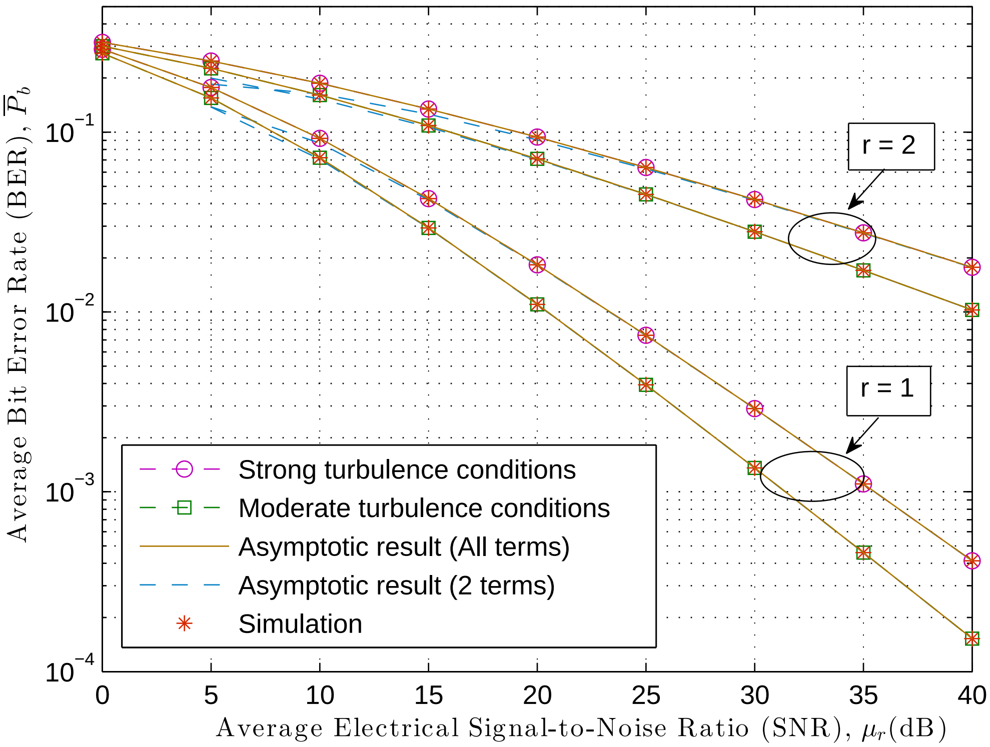

Figure 3.3: Average bit error rate of a single FSO link under strong and moderate turbulence conditions for both detection techniques, heterodyne ($r = 1$) and IM/DD ($r = 2$) with $\xi = 1$.

in a considerable degradation in the error performance. Yet, heterodyne detection provides better performance than IM/DD.

Finally, we show the impact of pointing errors on the ergodic capacity of a single FSO link under double GG strong turbulence for IM/DD with varying ξ in Fig. 3.5. We can notice that high pointing errors effect reduces the capacity of the system. In addition, we have evaluated the asymptotic results via two methods (i.e Meijer's G-function expansion and moments approximation). The asymptotic results derived in (3.39) (utilizing all terms in the summation) match the exact results perfectly while the other asymptotic (utilizing the dominant terms) converge faster for the case of low pointing errors effect. In the same way, the exact ergodic capacity and asymptotic results for low SNR regime is presented in Fig. 3.6 as derived earlier in (3.45).

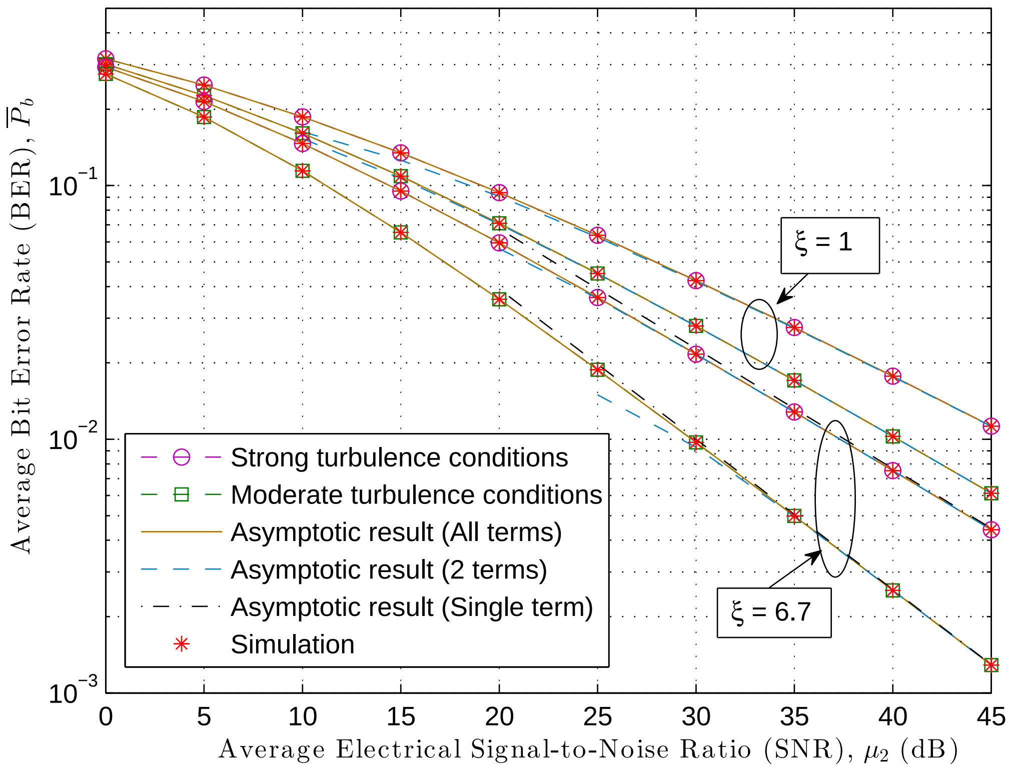

Figure 3.4: The impact of pointing errors on the average bit error rate of a single FSO link under strong and moderate turbulence conditions using IM/DD technique ($r = 2$) with varying pointing errors.

3.6 Conclusion

In this chapter, we derived unified, novel, and closed-form expressions for statistical properties of the end-to-end SNR of a single FSO link transmission system taking pointing errors into account. Moreover, we presented link performance analysis by offering closed-form expressions for the outage probability, the average BER, the higher amount of fading in addition to the ergodic capacity in terms of the Meijer's G-function. Finally, for high SNR regime we expressed all of our derivations in terms of elementary functions utilizing an asymptotic expansion for the Meijer's G-function.

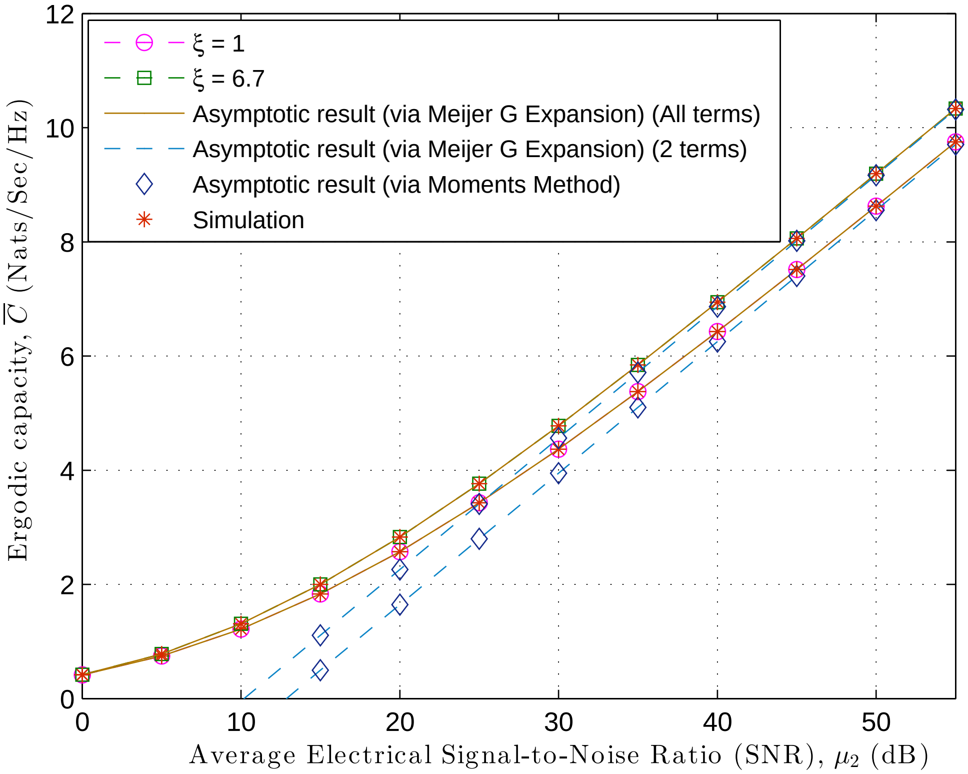

Figure 3.5: Ergodic capacity of a single FSO link under strong turbulence conditions for IM/DD ($r = 2$) with varying ξ along with asymptotic results at high SNR.

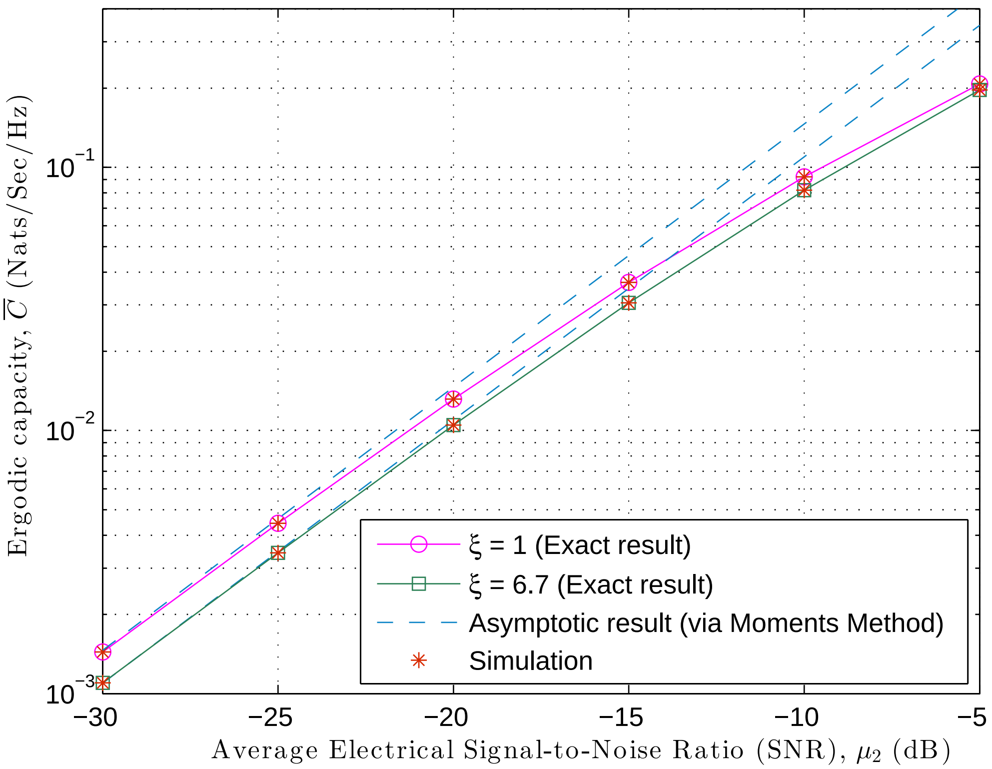

Figure 3.6: Ergodic capacity of a single FSO link under strong turbulence conditions for IM/DD ($r = 2$) with varying ξ along with asymptotic results at low SNR.

Chapter 4

Performance of FSO Links Under a Generalized Pointing Error Model

4.1 Introduction

Identifying the statistical model of the received irradiance that counts for both scintillation and pointing error facilities the performance analysis of FSO systems. To illustrate, the scintillation effect is widely modeled as Log-Normal for weak turbulence, Gamma-Gamma for strong turbulence [16, 17, 64–68], and double GG for wide range of turbulence conditions [46]. In terms of the pointing error, it was first modeled in [35] by a Rayleigh distribution, in [36] by a Hoyt distribution, in [34] by a Rician distribution and more generally by a Beckmann distribution [51, 69]. Considering aggregated channels in which the combined effect of the pointing errors and turbulence is taken into account becomes a harder task, especially when considering general models of each. However, there are some attempts reported in the literature. Namely, the Gamma-Gamma\Rayleigh channel model was investigated in [37], the double generalized Gamma\Rayleigh channel was investigated in [38], the Log-Normal\Rician was investigated in [34], and the Málaga ($\mathcal{M}$) \Rayleigh channel model was investigated in [39]. So far, there is lack of studies on the performance analysis FSO systems assuming Beckmann distribution for the pointing error. Moreover, obtaining closed-form expressions of any of the performance measures might not be feasible especially in the case of the irradiance being a mixture of two independent processes. This has raised the interest to investigate the asymptotic limit at high signal-to-noise ratio.

-		Turbulence Only	Turbulence and Pointing Error
IM/DD	ΓΓ	[66, 70, 71]	[40], [37]
	LN	[66, 70]	*
	Other	[72] [73]	[38]
Heterodyne Detection	ΓΓ	*	[74], [37]
	LN	*	*
	Other	*	[38]

Table 4.1: Summary of research work on ergodic capacity.

In this chapter, the focus is on of the fundamental information-theoretic measures, namely on the channel capacity as explained in Sec. 3.4.4. Several research works have been reported in the literature aiming to find closed-form expressions of the ergodic capacity of FSO systems as summarized in Table. 4.1. It is noticed that the studies focusing on the joint effect of turbulence and pointing errors assume zero boresight and the same jitter variance for horizontal and vertical misalignment.

4.2 Outline and Objective

In this chapter, based on the generalized pointing error model introduced in Sec. 2.3.1.1. We derive the asymptotic ergodic capacity of FSO systems under the joint impact of turbulence and generalized pointing error impairments.

4.3 System Model

In this section, we assume that the beam is not perfectly aligned to the center of the detection plane as seen in Fig. 4.1. In specific, the beam is initially pointing at $\mathcal{A} = [q\,p]^t$ in the detection plane and it is detected by the aperture of radius a placed at $\mathcal{B} = [u\,v]^t$. Moreover, due to important initialization or other effect, $\mathcal{A}$ may not collocated with $\mathcal{B}$. Also, the beam may experience random displacements in two directions namely, horizontal, x and vertical, y as the result of building sway. It is commonly assumed that both displacements are modeled as independent Gaussian

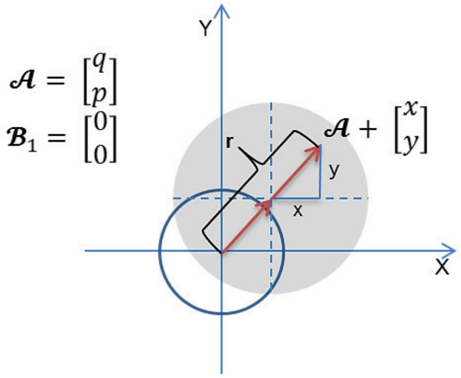

Figure 4.1: A general setup of Fig. 2.2a.

random variable i.e. $x \sim \mathcal{N}(\mu_x, \sigma_x)$ and $y \sim \mathcal{N}(\mu_y, \sigma_y)$. Then the distance between the center of the beam footprint and the center of the ith aperture can be expressed as

$$r = \left\| \mathcal{A} - \mathcal{B}_i + \begin{bmatrix} x \\ \\ y \end{bmatrix} \right\| = \left\| \begin{bmatrix} \hat{x} \\ \\ \hat{y} \end{bmatrix} \right\|. \tag{4.1}$$

It follows that the attenuation due to geometric spread and pointing errors can be approximated by 2.16 where $r_i = \sqrt{\hat{x}^2 + \hat{y}^2}$ such that $\hat{x} \sim \mathcal{N}(\hat{\mu}_x, \sigma_x^2)$ and $\hat{y} \sim \mathcal{N}(\hat{\mu}_y, \sigma_y^2)$, $\hat{\mu}_x = \mu_x + q - u_i$, $\hat{\mu}_y = \mu_y + p - v_i$,

4.4 Asymptotic Ergodic Capacity

In the high SNR regime, the channel capacity can be easily derived by utilizing the nth moment of the effective receive SNR as in (3.42). The nth moment of the electrical SNR is given as

$$\mathbb{E}[\gamma^n] = \left(\frac{\eta^r}{N_0} \right)^n \mathbb{E}[I^{rn}] \,, \tag{4.2}$$

such that the nth moment of the irradiance, assuming I_a and I_p being statistically independent processes, can be written as

$$\mathbb{E}[I^n] = \mathbb{E}[I_a^n]\mathbb{E}[I_p^n] = A_0^n \mathbb{E}[I_a^n]\mathcal{M}_{r^2}\left(-\frac{2n}{w_{z_{eq}}^2}\right) , \tag{4.3}$$

where $\mathcal{M}_{r^2}$ is defined in (2.19). Inserting (4.3) into (4.2) and following up from (3.42), the asymptotic capacity can be further expressed as

$$\overline{C} \underset{\mu\gg 1}{\approxeq} \mathcal{W} - r\log(\mathbb{E}[I_a]) + \frac{\partial}{\partial n}\mathbb{E}[I_a^{rn}]\bigg|_{n=0} , \tag{4.4}$$

such that

$$\mathcal{W} = \log\left(\frac{\delta\mu A_0^r}{\mathbb{E}[I_p]^r}\right) - \frac{2r}{w_{z_{eq}}}\mathcal{M}_{r^2}'(0) . \tag{4.5}$$

Hence, (4.4) is generic meaning that it is applicable to describe any turbulence by inserting the moments of I_a which can follow many distributions as seen in Sec. 2. Moreover, $\mathcal{M}_{r^2}$ can take multiple forms depending on the misalignment. Beam misalignment can be categorized into two types namely, bidirectional and unidirectional. The bidirectional misalignment occurs in both horizontal and vertical directions and r can follow different distributions such as Beckmann, Rayleigh, and Rician. On the other hand, the unidirectional misalignment only happens in one direction, either horizontal or vertical. In this case, r can only follows the one-sided Gaussian distribution. Therefore, $\mathcal{W}$ can take several forms as listed in Table 4.2 according to the specific pointing error model adopted. For example, for the most general case, $\mathcal{W}$ becomes

$$\mathcal{W} = \log\left(\left[\frac{(1+\xi_x^2)(1+\xi_y^2)}{\xi_x^2\xi_y^2}\right]^{\frac{r}{2}}\delta\mu\right) - \frac{r}{2\xi_x^2} - \frac{r}{2\xi_y^2} - \frac{2r}{w_{z_{eq}}^2}\left(\frac{\hat{\mu}_x^2}{1+\xi_x^2} + \frac{\hat{\mu}_y^2}{1+\xi_y^2}\right) . \tag{4.6}$$

4.4.1 Bi-Directional Misalignment

Here, we list the results of asymptotic ergodic capacity of FSO system over weak and strong turbulence under pointing errors along both directions (i.e. elevation and horizontal). The most general case of the pointing error is when the boresight and jitter are taken into account. Taking the first derivative of (2.4), (2.10), and (2.19) and substituting it in (4.4) and after doing some simple manipulations the following results is reached

$$\begin{aligned}\overline{C}|_{\Gamma\Gamma} \underset{\overline{\gamma}\gg 1}{\approxeq} & \log\left(\left[\frac{(1+\xi_x^2)(1+\xi_y^2)}{\xi_x^2\xi_y^2}\right]^{\frac{r}{2}}\delta\mu\right) - \frac{r}{2\xi_x^2} - \frac{r}{2\xi_y^2} - \frac{2r}{w_{z_{eq}}^2}\left(\frac{\hat{\mu}_x^2}{1+\xi_x^2} + \frac{\hat{\mu}_y^2}{1+\xi_y^2}\right) \\ & - r\log(\alpha\beta) + r\psi(\alpha) + r\psi(\beta), \qquad (4.7)\\ \overline{C}|_{\mathrm{LN}} \underset{\overline{\gamma}\gg 1}{\approxeq} & \log\left(\left[\frac{(1+\xi_x^2)(1+\xi_y^2)}{\xi_x^2\xi_y^2}\right]^{\frac{r}{2}}\delta\mu\right) - \frac{r}{2\xi_x^2} - \frac{r}{2\xi_y^2} - \frac{2r}{w_{z_{eq}}^2}\left(\frac{\hat{\mu}_x^2}{1+\xi_x^2} + \frac{\hat{\mu}_y^2}{1+\xi_y^2}\right) \\ & - 2r\sigma_X^2. \qquad (4.8)\end{aligned}$$

This result is generic and can specialize to different cases according to the pointing error impairments model. For example, for zero-boresight and identical jitter in both displacement directions (i.e. $\mu_x = \mu_y = 0$ and $\xi_x = \xi_y = \xi$), the general result reduces to

$$\overline{C}|_{\Gamma\Gamma} \underset{\overline{\gamma}\gg 1}{\approxeq} \log\left(\left[\frac{1+\xi^2}{\xi^2}\right]^{r}\delta\mu\right) - \frac{r}{\xi^2} - r\log(\alpha\beta) + r\psi(\alpha) + r\psi(\beta), \qquad (4.9)$$

$$\overline{C}|_{\mathrm{LN}} \underset{\overline{\gamma}\gg 1}{\approxeq} \log\left(\left[\frac{1+\xi^2}{\xi^2}\right]^{r}\delta\mu\right) - \frac{r}{\xi^2} - 2r\sigma_X^2. \qquad (4.10)$$

Table 4.2: Different forms of $\mathcal{W}$ depends mainly on the pointing error model considered.

Pointing Errors Model	$\mathcal{W}$
Beckmann ($\hat{\mu}_x \neq \hat{\mu}_y$ and $\xi_x \neq \xi_y$)	$\log\left(\left[\frac{(1+\xi_x^2)(1+\xi_y^2)}{\xi_x^2\xi_y^2}\right]^{\frac{r}{2}}\delta\mu\right) - \frac{r}{2\xi_x^2} - \frac{r}{2\xi_y^2} - \frac{2r}{w_{zeq}^2}\left(\frac{\hat{\mu}_x^2}{1+\xi_x^2} + \frac{\hat{\mu}_y^2}{1+\xi_y^2}\right)$
Rayleigh ($\hat{\mu}_x = \hat{\mu}_y = 0$ and $\xi_x = \xi_y = \xi$)	$\log\left(\left[\frac{1+\xi^2}{\xi^2}\right]^{r}\delta\mu\right) - \frac{r}{\xi^2}$
Rician ($\hat{\mu}_x + \hat{\mu}_y \neq 0$ and $\xi_x = \xi_y = \xi$)	$\log\left(\left[\frac{1+\xi^2}{\xi^2}\right]^{r}\delta\mu\right) - \frac{r}{\xi^2} - \frac{2rs^2}{w_{zeq}^2} + \frac{2rs^2\xi^2}{w_{zeq}^2(1+\xi^2)}$
Hoyt ($\hat{\mu}_x = \hat{\mu}_y = 0$ and $\xi_x \neq \xi_y$)	$\log\left(\left[\frac{1+\xi_x^2}{\xi_x^2}\right]^{\frac{r}{2}}\left[\frac{1+\xi_y^2}{\xi_y^2}\right]^{\frac{r}{2}}\delta\mu\right) - \frac{r}{2\xi_x^2} - \frac{r}{2\xi_y^2}$
Gaussian ($\hat{\mu}_x = 0$, $\xi_x = \xi$, and $\xi_y = \infty$)	$\log\left(\left[\frac{1+\xi^2}{\xi^2}\right]^{\frac{r}{2}}\delta\mu\right) - \frac{r}{2\xi^2}$
Shifted Gaussian ($\hat{\mu}_x = \mu_p$, $\xi_x = \xi$, and $\xi_y = \infty$)	$\log\left(\left[\frac{1+\xi^2}{\xi^2}\right]^{\frac{r}{2}}\delta\mu\right) - \frac{r}{2\xi^2} - \frac{4r\mu_p^2}{w_{zeq}^2} + \frac{2r\mu_p^2(1+2\xi^2)}{w_{zeq}^2(1+\xi^2)}$
No pointing errors	$\log(\delta\mu)$

On the other hand, when nonzero-boresight component is taken into account (i.e. $\mu_x \neq \mu_y$ and $\xi_x = \xi_y = \xi$), then (4.7) and (4.8) reduce to

$$\begin{aligned} \overline{C}|_{\Gamma\Gamma} \underset{\overline{\gamma}\gg 1}{\approxeq} & \log\left(\left[\frac{1+\xi^2}{\xi^2}\right]^{r}\delta\mu\right) - \frac{r}{\xi^2} - \frac{2rs^2}{w_{z_{eq}}^2} + \frac{2rs^2\xi^2}{w_{z_{eq}}^2(1+\xi^2)} - r\log(\alpha\beta) \\ & + r\psi(\alpha) + r\psi(\beta), \qquad (4.11) \\ \overline{C}|_{\mathrm{LN}} \underset{\overline{\gamma}\gg 1}{\approxeq} & \log\left(\left[\frac{1+\xi^2}{\xi^2}\right]^{r}\delta\mu\right) - \frac{r}{\xi^2} - \frac{2rs^2}{w_{z_{eq}}^2} + \frac{2rs^2\xi^2}{w_{z_{eq}}^2(1+\xi^2)} - 2r\sigma_X^2. \qquad (4.12) \end{aligned}$$

It is important to note that when $s = 0$, both (4.11) and (4.12) reduces to (4.9) and (4.10). When zero boresight but non-identical jitter for the two directions of the displacement are assumed (i.e. $\mu_x = \mu_y = 0$ and $\xi_x \neq \xi_y$), (4.7) becomes

$$\overline{C}|_{\Gamma\Gamma} \underset{\overline{\gamma}\gg 1}{\approxeq} \log\left(\left[\frac{1+\xi_x^2}{\xi_x^2}\right]^{\frac{r}{2}}\left[\frac{1+\xi_y^2}{\xi_y^2}\right]^{\frac{r}{2}}\delta\mu\right) - \frac{r}{2\xi_x^2} - \frac{r}{2\xi_y^2} - r\log(\alpha\beta) + r\psi(\alpha) + r\psi(\beta), \qquad (4.13)$$

$$\overline{C}|_{\mathrm{LN}} \underset{\overline{\gamma}\gg 1}{\approxeq} \log\left(\left[\frac{1+\xi_x^2}{\xi_x^2}\right]^{\frac{r}{2}}\left[\frac{1+\xi_y^2}{\xi_y^2}\right]^{\frac{r}{2}}\delta\mu\right) - \frac{r}{2\xi_x^2} - \frac{r}{2\xi_y^2} - 2r\sigma_X^2. \qquad (4.14)$$

4.4.2 Uni-Directional Misalignment

In this section, we consider the pointing errors along one direction either the elevation or the horizontal and we derive the asymptotic ergodic capacity accordingly by utilizing (4.4). For the zero boresight case (i.e. $\mu_x = \mu_y = 0$, $\xi_x = \xi$, and $\xi_y = 0$), we can obtain the result by utilizing (4.4), (2.31), and (2.10) as

$$\overline{C}|_{\Gamma\Gamma} \underset{\overline{\gamma}\gg 1}{\approxeq} \log\left(\left[\frac{1+\xi^2}{\xi^2}\right]^{\frac{r}{2}}\delta\mu\right) - \frac{r}{2\xi^2} - r\log(\alpha\beta) + r\psi(\alpha) + r\psi(\beta), \qquad (4.15)$$

$$\overline{C}|_{\mathrm{LN}} \underset{\overline{\gamma}\gg 1}{\approxeq} \log\left(\left[\frac{1+\xi^2}{\xi^2}\right]^{\frac{r}{2}}\delta\mu\right) - \frac{r}{2\xi^2} - 2r\sigma_X^2. \qquad (4.16)$$

It is meaningful to say that (4.13) and (4.14) reduces to (4.15) and (4.16), respectively if either ξ_x or ξ_y tends to infinity (i.e. zero pointing errors effect). In addition, if boresight is considered (i.e. $\mu_x = \mu_y = \mu$, $\xi_x = \xi$, and $\xi_y = 0$), we reach to the following result by utilizing (2.33)

$$\overline{C}|_{\Gamma\Gamma} \underset{\overline{\gamma}\gg 1}{\approxeq} \log\left(\left[\frac{1+\xi^2}{\xi^2}\right]^{\frac{r}{2}}\delta\mu\right) - \frac{r}{2\xi^2} - \frac{4r\mu_p^2}{w_{z_{eq}}^2} + \frac{2r\mu_p^2(1+2\xi^2)}{w_{z_{eq}}^2(1+\xi^2)} - r\log(\alpha\beta) + r\psi(\alpha) + r\psi(\beta), \tag{4.17}$$

$$\overline{C}|_{\mathrm{LN}} \underset{\overline{\gamma}\gg 1}{\approxeq} \log\left(\left[\frac{1+\xi^2}{\xi^2}\right]^{\frac{r}{2}}\delta\mu\right) - \frac{r}{2\xi^2} - \frac{4r\mu_p^2}{w_{z_{eq}}^2} + \frac{2r\mu_p^2(1+2\xi^2)}{w_{z_{eq}}^2(1+\xi^2)} - 2r\sigma_X^2. \tag{4.18}$$

4.5 Numerical Examples

In this section, we validate and evaluate our analytical expressions of the channel capacity for the single link FSO system over Log-Normal and ΓΓ channels with generalized pointing error model. It is important to mention that Monte-Carlo computer based simulations are utilized to obtain all exact results. In each plot, we specify all parameters considered in the simulation i.e. the beamwaist, w_0, phase front F_0, the distance z, aperture radius a, refractive index C_n^2, jitter variances σ_x^2 σ_y^2 and boresight mean μ_x and μ_y. First, we compare between the single link and dual-aperture FSO systems for different distances, z, as shown in Fig. 4.2. It is expected that the diversity link can enhance the capacity when the turbulence conditions get severe since the distance is directly proportional to the Rytov variance (i.e. as distance increases, more turbulence eddies are added). Also, our asymptotic results are tight at high SNR. However, as the channel gets more turbulent, the convergence of the asymptotic results to the exact ones happen at larger SNR. In Fig. 4.3 we plot the ergodic capacity of a single link versus the average electrical SNR over weak turbulence modeled as Log-normal fading channel. Assuming no-boresight, we consider different scenarios of jitter variance i.e. high pointing error effect is presented by high values of σ_x^2 and σ_y^2. Clearly, highly varying beam due to winds or other factor results in performance degradation. Interestingly, our asymptotic analytical results show an

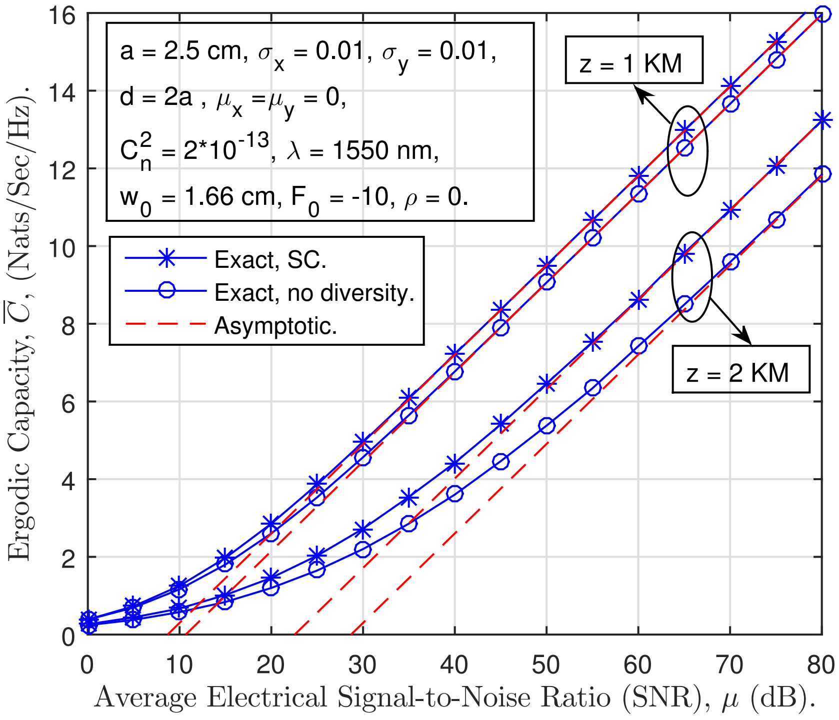

Figure 4.2: Comparison between the channel capacity of a single aperture and dual-aperture FSO system.

excellent match with the exact ones generated by Monte-Carlo computer based simulation. Next, we show the effect of beam waist at the transmitter on the capacity of the link in Fig. 4.4. First thing to observe is that our asymptotic results converge well to the ones generated by Monte-Carlo simulation. A wide beam delivers the best result as it is robust to the pointing errors, in contrast to narrow beams. Lastly, for the single link, we compare between unidirectional and bidirectional misalignments over Gamma-Gamma turbulence in Fig. 4.5. Clearly, for low jitter variance i.e. high values of ξ, both directions of misalignment have the same effect of the channel capacity. In contrast with high jitter variance case, channel capacity is less affected by the unidirectional misalignment.

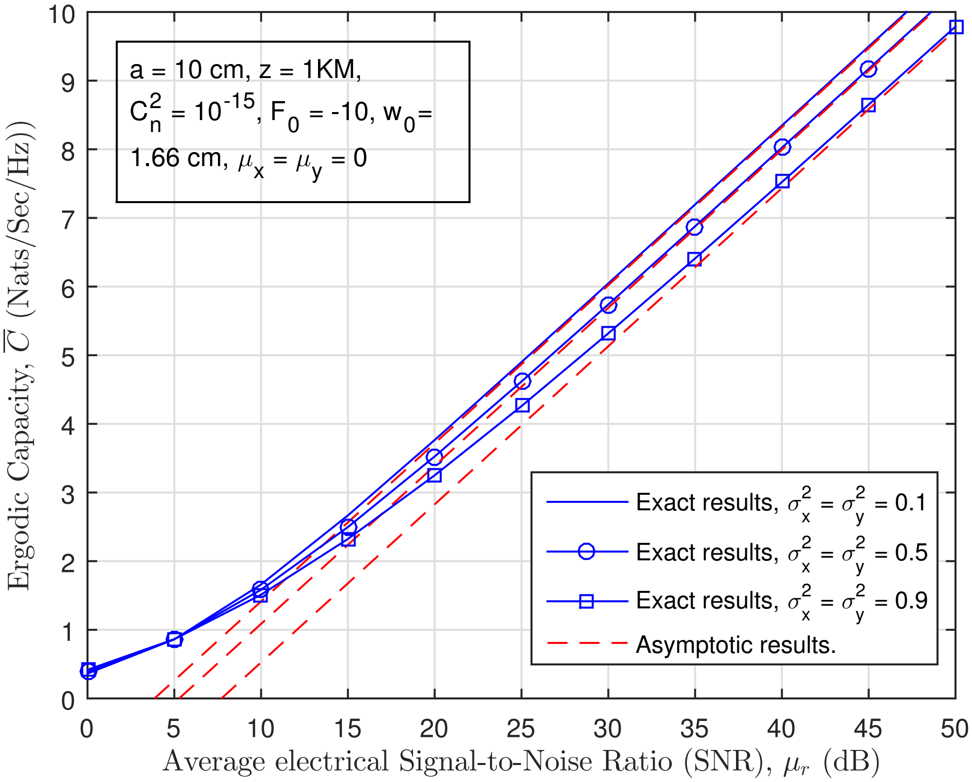

Figure 4.3: The effect of jitter variance on the capacity of a single link over Log-Normal turbulence.

4.6 Conclusion

In this chapter, closed-form asymptotic expressions of the FSO channel capacity were derived subject to generalized pointing error impairments. The results are generic and novel in the sense that they account for a variety of turbulence models and misalignment scenarios. In specific, we calculated the asymptotic ergodic capacity of FSO systems operating over the log-normal and Gamma-Gamma channels subject to generalized pointing error impairments. However, our formula can be applied to any turbulence channel such as K-distributed, double Weibull, double Generalized Gamma and $\mathcal{M}$ channels. Numerical results, validated by computer simulations, show that our asymptotic results can accurately predict the performance of FSO system in the high SNR regime.

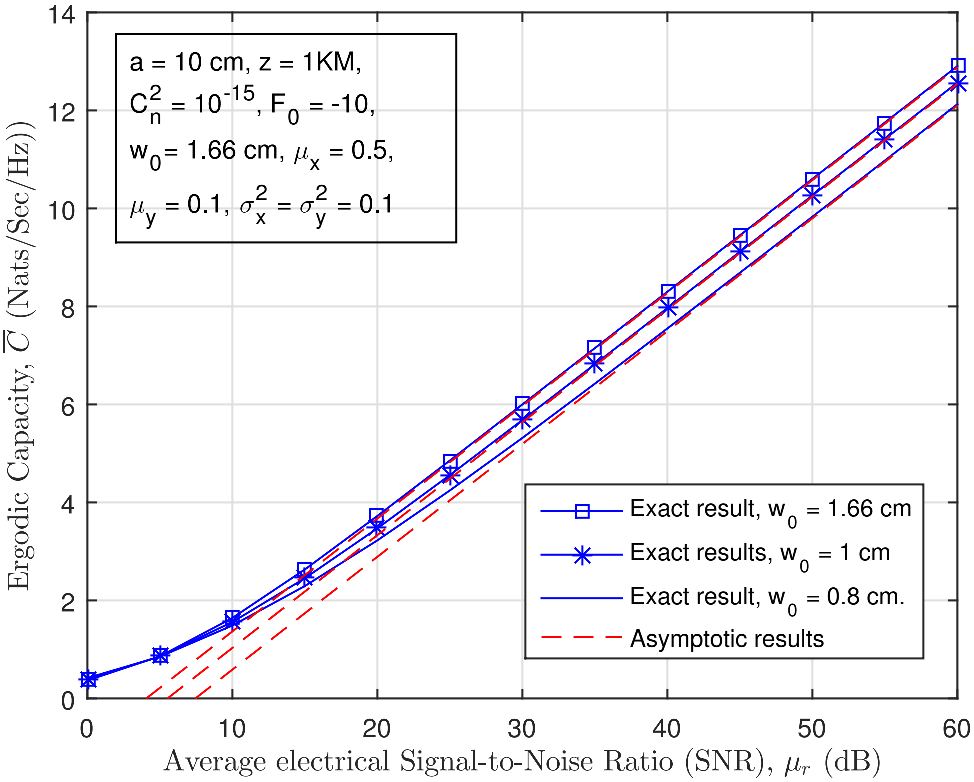

Figure 4.4: The effect of beam waist at the transmitter on the capacity over Log-Normal turbulence under boresight error.

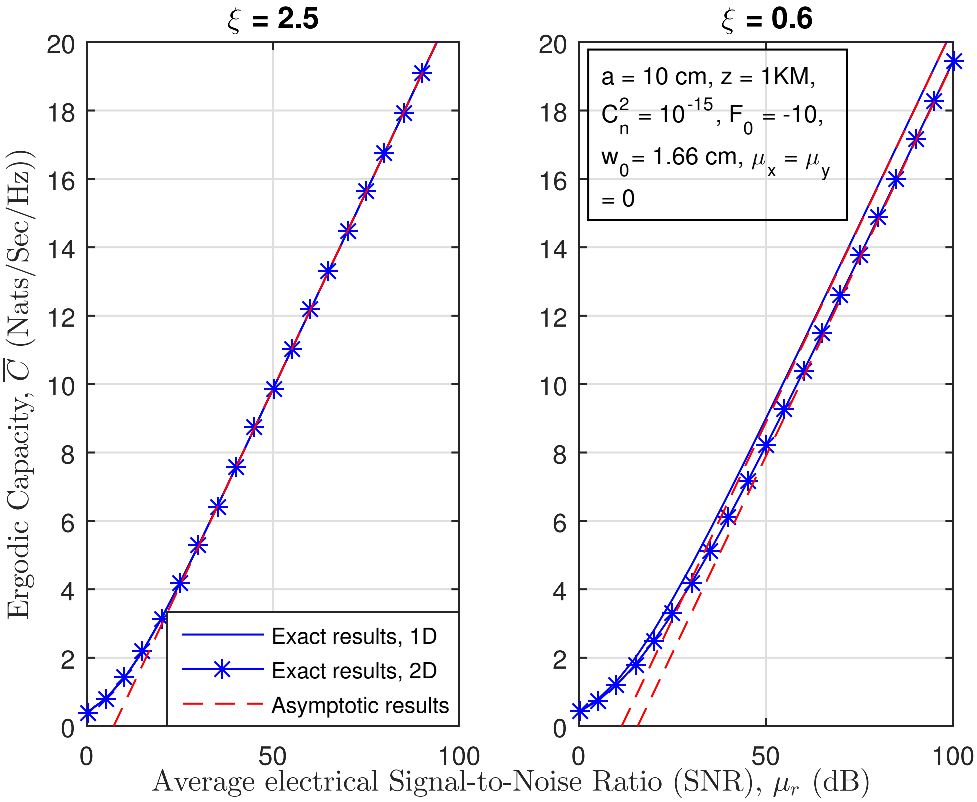

Figure 4.5: Comparison between unidirectional and bidirectional misalignment over Gamma-Gamma turbulence.

Chapter 5

On the Channel Capacity of Dual-Receive FSO Link over Correlated Weak Atmospheric Channels

5.1 Introduction

As widely adopted in RF, spatial diversity, in which multiple transmitters and/or multiple receivers are employed, is usually utilized to suppress the effect of channel fading. Similarly, this technique can efficiently mitigate scintillation according to some reported work in the literature [54, 75]. However, when considering diversity links and due to system design, it is crucial to take into account the correlation of the underlying channels since the spacing between beams or apertures cannot always ensure uncorrelated signals [76]. Furthermore, identifying the statistical model of the received irradiance that accounts for both scintillation and pointing error facilitate the performance analysis of FSO systems, especially in diversity links. Finding the combined effect of pointing errors and turbulence becomes more complicated for spatial diversity systems [42, 50, 77, 78].

Due to the complexity of obtaining closed-form expressions of any of the performance measures, the interest to investigate the asymptotic limit at high SNR has been raised. In this chapter, the results derived in Chapter 4 are extended to obtain the channel capacity of FSO systems with diversity reception. In particular, we aim to develop closed-form asymptotic expressions of the capacity of dual-branch correlated FSO channels operating over weak turbulence considering general model of the pointing error.

5.2 System Model

In this work, we consider dual-branch single-input multiple-output (SIMO) configurations of the FSO system with two types of detection techniques, heterodyne and IM/DD. Data transmission is affected by path loss, atmospheric turbulence conditions, pointing errors, and AWGN. As such, the received vector $\mathbf{y} = [y_1 \ y_2]^T$, with $(.)^T$ is the transpose operator, is given by

$$\mathbf{y} = \eta \mathbf{I_a} \mathbf{I_p} x + \boldsymbol{\omega} \,, \tag{5.1}$$

where $\mathbf{I_a} = \mathrm{diag}(I_1 \, , I_2)$ is a 2×2 diagonal matrix reflects the turbulence-induced fading such that I_i represents the irradiance received at the ith aperture, $\mathbf{I_p} = [I_{p_1} \ I_{p_2}]^T$ is the 2×1 pointing error matrix consists of independent random variables where each component represents the misalignment between the center of the beam footprint and the center of the ith aperture, and $x \in \{0, 2P_t\}$ is the OOK modulated transmitted signal with P_t being average transmitted optical power. The vector $\boldsymbol{\omega} = [\omega_1 \ \omega_2]^T$ is a noise vector of independent components modeled as white and Gaussian distributed RVs. The received irradiance captured by each aperture is assumed to be following a Log-Normal distribution with PDF equals to (2.3). Furthermore, it is important to note that I_i's are not necessarily independent random variables. The spatial matrix R can be of the form

$$R = \begin{bmatrix} 1 & \rho \\ \rho & 1 \end{bmatrix} , \tag{5.2}$$

where ρ is the correlation between I_1 and I_2 that is a function of the separation distance, d, and the coherence length [79, 80], given by

$$\rho = \exp\left[-\left(\frac{d}{\rho_o(z)}\right)^{\frac{-3}{5}}\right], \tag{5.3}$$

where $\rho_o(z) = (1.46C_n^2k^2z)^{(-3/5)}$ is the coherence length of a plane wave propagation[1]. It is clear from the expression that the links are correlated when the spacing between apertures is less than the coherence length of the beam. The electrical SNR of the ith branch can be defined as

$$\gamma_i = \frac{(\eta I_i I_{p_i})^r}{N_0}. \tag{5.4}$$

The pointing error components at each aperture, I_{p_1} and I_{p_2}, mainly depend on the distance r_i. As observed from 5.1, the beam is originally pointing at $\mathcal{A} = [0\ 0]^T$ while the apertures are placed in $\mathcal{B}_1 = [\frac{d}{2}\ 0]^T$ and $\mathcal{B}_2 = [-\frac{d}{2}\ 0]^T$ such that d is the separation distance between the centers of the apertures. Note that due to building

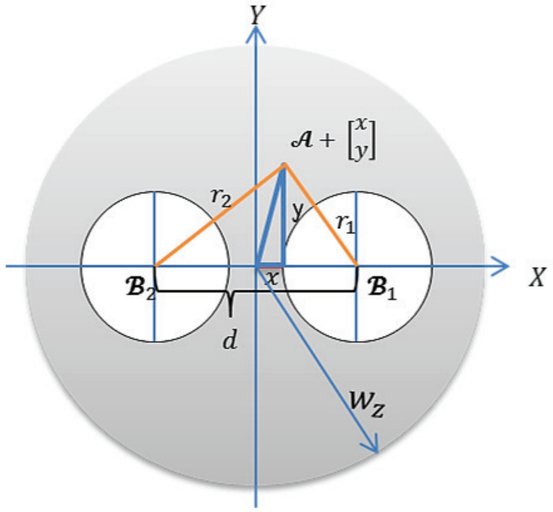

Figure 5.1: Beam foot-print of the dual-aperture FSO system.

---

[1] Physically, the coherence parameter is the measure of light coherence across each transverse plane along the propagation path [81]. The coherence length of a spherical wave propagation is equal to $\rho_o(z) = (0.55C_n^2k^2z)^{(-3/5)}$ [16, Eq. (65)].

sway or other factors, the center of the beam moved to a random location $\mathcal{A}+[x\ y]^T$. Then, the distance to the center of the ith aperture can be given as (4.1)

$$r_1 = \sqrt{\left(\frac{d}{2}-x\right)^2 + y^2}, \tag{5.5}$$

$$r_2 = \sqrt{\left(\frac{d}{2}+x\right)^2 + y^2}. \tag{5.6}$$

The displacements r_1 and r_2 are related as

$$r_2^2 = r_1^2 + 2dx. \tag{5.7}$$

At the receive end, two signals are captured. In order to detect the transmitted signal, They are combined using two well-known techniques namely, selection combining (SC) and switch-and-stay combining (SSC).

5.2.1 Selection-Combining

In this technique, the branch with the larger instantaneous SNR is selected and therefore the output SNR can be written as

$$\gamma_{SC} = \max(\gamma_1, \gamma_2), \tag{5.8}$$

where γ_i is defined in Eq. (5.4). Thus, Eq. 5.8 can be rewritten as

$$\gamma_{SC} = \max\left(\frac{\eta I_1^r I_{p_1}^r}{N_0}, \frac{\eta I_2^r I_{p_2}^r}{N_0}\right) = \frac{\eta}{N_0}\max\left(I_1 I_{p_1}, I_2 I_{p_2}\right)^r. \tag{5.9}$$

Inserting the definition of I_{p_1} and I_{p_2} (2.16), (5.9) can be rewritten as

$$\gamma_{SC} = \frac{\eta}{N_0}\max\left(I_1 A_0 \exp\left(\frac{-2r_1^2}{w_{z_{eq}}^2}\right), I_2 A_0 \exp\left(\frac{-2r_2^2}{w_{z_{eq}}^2}\right)\right)^r. \tag{5.10}$$

Utilizing the relationship between r_1 and r_2 in (5.7), the definition of γ_{SC} can be further expanded to

$$
\begin{aligned}
\gamma_{SC} &= \frac{\eta}{N_0} \max\left(I_1 A_0 \exp\left(\frac{-2r_1^2}{w_{z_{eq}}^2} \right), I_2 A_0 \exp\left(\frac{-2(r_1^2 + 2dx)}{w_{z_{eq}}^2} \right) \right)^r, \\
&= \frac{\eta}{N_0} \left(A_0 \exp\left(\frac{-2r_1^2}{w_{z_{eq}}^2} \right) \right)^r \max\left(I_1, I_2 \exp\left(\frac{-4dx}{w_{z_{eq}}^2} \right) \right)^r, \\
&= \frac{\eta}{N_0} I_{p_1} \max\left(I_1, \hat{I}_2 \right)^r = \frac{\eta}{N_0} I_{p_1}^r I_{SC}^r \ , \qquad (5.11)
\end{aligned}
$$

where $\hat{I}_2 = \exp\left(2X_2 - \frac{4d}{w_{z_{eq}}^2} x \right)$ leading to $\hat{I}_2 \sim \ln\mathcal{N}(-2\sigma_{x_2}^2 - \lambda_1, 4\sigma_{x_2}^2 + \lambda_2^2)$ such that $\lambda_1 = \frac{4d\mu_x}{w_{z_{eq}}^2}$ and $\lambda_2 = \frac{4d\sigma_x}{w_{z_{eq}}^2}$. Furthermore, the nth moment of γ_{SC} can be expressed as

$$
\mathbb{E}[\gamma_{SC}^n] = \frac{\mathbb{E}[I_{p_1}^{rn}]\mathbb{E}[I_{SC}^{rn}]}{\mathbb{E}[I_{p_1}]^{rn}\mathbb{E}[I_{SC}]^{rn}} \mu_{SC}^n, \qquad (5.12)
$$

where $\mathbb{E}[I_{p_1}^n]$ can be derived using (2.18), and $\mathbb{E}[I_{SC}^n]$ can be expressed as

$$
\begin{aligned}
\mathbb{E}[I_{SC}^n] = \exp&\left(\frac{1}{2} n^2 \kappa - n \left(\lambda_1 + 2\sigma_{x_2}^2 \right) \right) Q\left(\frac{\zeta - n\kappa \left(1 - \rho\phi \right)}{\mathcal{P}_1} \right) \\
&+ \exp\left(2n^2 \sigma_{x_1}^2 - 2n\sigma_{x_1}^2 \right) Q\left(\frac{-\zeta - 4n\sigma_{x_1}^2 \left(1 - \rho\phi^{-1} \right)}{\mathcal{P}_1} \right), \qquad (5.13)
\end{aligned}
$$

where $\zeta = \lambda_1 - 2\sigma_{x_1}^2 + 2\sigma_{x_2}^2$, $\kappa = \lambda_2^2 + 4\sigma_{x_2}^2$, $\phi = \frac{2\sigma_{x_1}}{\sqrt{\kappa}}$, and $\mathcal{P}_1^2 = f(2\sigma_{x_1}, \sqrt{\kappa}, -\rho)$ such that $f(a, b, c) = a^2 + b^2 + 2abc$.

5.2.2 Switch-and-Stay Combining

In this combining technique, the first branch is by default considered for signal detection. However, if the SNR of first branch falls belows a certain threshold, the receiver shifts to the second branch to detect the signal. In fact, the SNR at the output of a dual-branch SSC receiver, γ_{SSC}, can be expressed as [1, 82]

$$\gamma_{SSC} = \begin{cases} \gamma_1 \ , \quad \gamma_1 \geq \gamma_t \\ \\ \gamma_2 \ , \quad \gamma_1 < \gamma_t \end{cases} = \begin{cases} \frac{\eta I_1^r I_{p_1}^r}{N_0} \quad I_1 I_{p_1} \geq I_t \\ \\ \frac{\eta I_2^r I_{p_2}^r}{N_0} \quad I_1 I_{p_1} < I_t \end{cases} \tag{5.14}$$

where γ_t is the switching threshold below which the receiver switches to the other diversity branch and $I_t = \sqrt[r]{\frac{N_0 \gamma_t}{\eta}}$. Following similar analysis in Sec. 5.2.1 taking turbulence and pointing errors into consideration, we have $\gamma_{SSC} = \frac{\eta}{N_0} I_{p_1}^r I_{SSC}^r$, where I_{SSC}^r is given by

$$I_{SSC} = \begin{cases} I_1 \ , \quad I_{p_1} I_1 \geq I_t \\ \\ \hat{I}_2 \ , \quad I_{p_1} I_1 < I_t \end{cases} \tag{5.15}$$

Then, the nth moment of the γ_{SSC} can be expressed as

$$\mathbb{E}[\gamma_{SSC}^n] = \frac{\mathbb{E}[I_{p_1}^{rn}]\mathbb{E}[I_{SSC}^n]}{\mathbb{E}[I_{p_1}]^{rn}\mathbb{E}[I_{SSC}]^n} \mu_{SSC}^n, \tag{5.16}$$

where the moments of I_{SSC} can be derived by utilizing earlier results in [83] as

$$\begin{aligned} \mathbb{E}(I_{SSC}^n) = {} & \varepsilon_1 \exp\left(2n^2\sigma_{x_1}^2 - 2n\sigma_{x_1}^2\right) \left(Q\left(2n\rho\sigma_{x_1} - \mathcal{K}_1\right) + Q(\mathcal{K}_1 - 2n\sigma_{x_1})\right) \\ & + \gamma_t^n \ \varepsilon_2 \ \exp\left(\frac{\kappa n^2}{2} - n\mathcal{K}_2\right) \left(Q\left(\frac{\kappa n \rho - \mathcal{K}_2}{\sqrt{\kappa}}\right) + Q\left(\frac{-\kappa n + \mathcal{K}_2}{\sqrt{\kappa}}\right)\right). \end{aligned} \tag{5.17}$$

such that

$$\mathcal{K}_1 = \frac{2\sigma_{x_1}^2 + \log(\gamma_t)}{2\sigma_{x_1}}, \tag{5.18}$$

$$\mathcal{K}_2 = \lambda_1 + 2\sigma_{x_2}^2 + \log(\gamma_t)\ , \tag{5.19}$$

$$\varepsilon_1 = \frac{Q\left(-\mathcal{K}_1\right)}{Q\left(-\mathcal{K}_1\right) + Q\left(-\frac{\mathcal{K}_2}{\sqrt{\kappa}}\right)}\ , \tag{5.20}$$

$$\varepsilon_2 = \frac{Q\left(-\frac{\mathcal{K}_2}{\sqrt{\kappa}}\right)}{Q\left(-\mathcal{K}_1\right) + Q\left(-\frac{\mathcal{K}_2}{\sqrt{\kappa}}\right)}\ . \tag{5.21}$$

5.3 Ergodic capacity

Based on (3.42), the asymptotic capacity of a dual branch FSO system with SC can be written as shown in Eq. (5.22)

$$\begin{aligned}\overline{C}|_{SC} \underset{\mu \gg 1}{\approxeq} & \mathcal{W} + \frac{r}{\sqrt{2\pi}} \exp\left(\frac{-\zeta^2}{2\mathcal{P}_1^2}\right) \sqrt{\lambda_2^2 + 4\lambda_2(\sigma_{x_2} - \rho\sigma_{x_1}) + 4\mathcal{P}_2} - 2r\sigma_{x_1}^2 - r\zeta Q\left(\frac{\zeta}{\mathcal{P}_1}\right) \\ & - r\log\left[Q\left(\frac{-\zeta - 4\sigma_{x_1}^2(1-\rho\phi^{-1})}{\mathcal{P}_1}\right) + \exp\left(-(\zeta + 2\sigma_{x_1}^2) + \frac{1}{2}\kappa^2\right) Q\left(\frac{\zeta - \kappa(1-\rho\phi)}{\mathcal{P}_1}\right)\right].\end{aligned} \tag{5.22}$$

where $\mathcal{P}_2 = f(\sigma_{x_1}, \sigma_{x_2}, -\rho)$. Since the moment of the irradiance I_{SSC} is available, we can directly apply (3.42) to get the asymptotic capacity for SSC case as in Eq. (5.23).

$$\begin{aligned}\overline{C}|_{\mathrm{SSC}} \underset{\mu \gg 1}{\approxeq} & \mathcal{W} + \frac{r(1-\rho)}{\sqrt{\pi}} \left(\sqrt{2}\varepsilon_1\sigma_{x_1}\ \exp\left(\frac{-\mathcal{K}_1^2}{2}\right) + \frac{\varepsilon_2\sqrt{\kappa}}{\sqrt{2\pi}}\ \exp\left(\frac{-\mathcal{K}_2^2}{2\kappa}\right)\right) \\ & - r\left(\varepsilon_1\sigma_{x_1}^2 + \varepsilon_2\sigma_{x_2}^2 + \frac{1}{2}\varepsilon_2\lambda_1\right) - r\log\Bigg[\varepsilon_1 Q\left(-2\sigma_{x_1} + \sigma_{x_1}\mathcal{K}_1\right) + \varepsilon_1 Q\left(\frac{2\rho\sigma_{x_1}^2 - \mathcal{K}_1}{\sigma_{x_1}}\right) \\ & + \varepsilon_2\ \exp\left(\frac{\lambda_2^2 - 2\lambda_1}{2}\right)\left(Q\left(\frac{\rho\kappa - \mathcal{K}_2}{\sqrt{\kappa}}\right) + Q\left(\frac{-\kappa + \mathcal{K}_2}{\sqrt{\kappa}}\right)\right)\Bigg].\end{aligned} \tag{5.23}$$

5.4 Numerical Examples

In this section, we validate and evaluate our analytical expressions of the channel capacity for the dual-aperture FSO system over correlated Log-Normal channels. It is important to mention that Monte-Carlo computer based simulations are utilized to obtain all exact results. In each plot, we specify all parameters considered in the simulation i.e. the beamwaist, w_0, phase front F_0, the distance z, aperture radius a, refractive index C_n^2, jitter variances σ_x^2 σ_y^2 and boresight mean μ_x and μ_y.

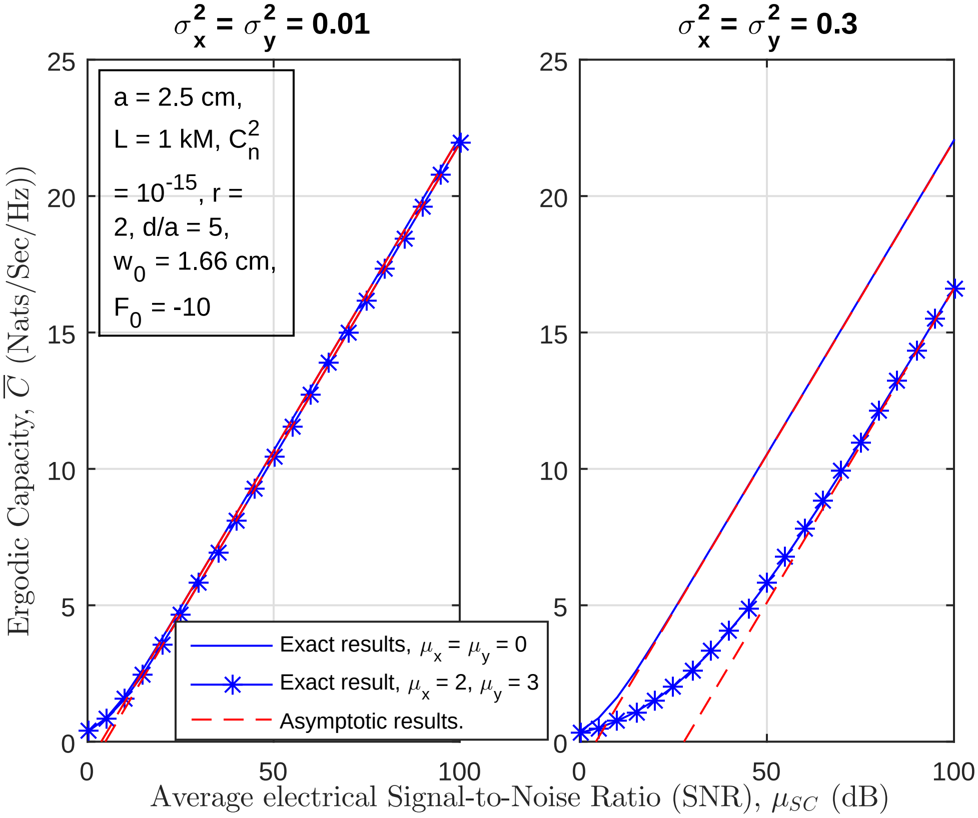

Figure 5.2: The effect of boresight and jitter variance on the channel capacity of dual-branch FSO link.

First, we show the effect of boresight on the channel capacity of selection combined FSO link with two scenarios of jitter variance and beam waist in Fig. 5.2 and Fig. 5.3, respectively. We can conclude that low varying beam and wide beam are more resistant to the boresight. The main purpose of diversity is to overcome scintillation.

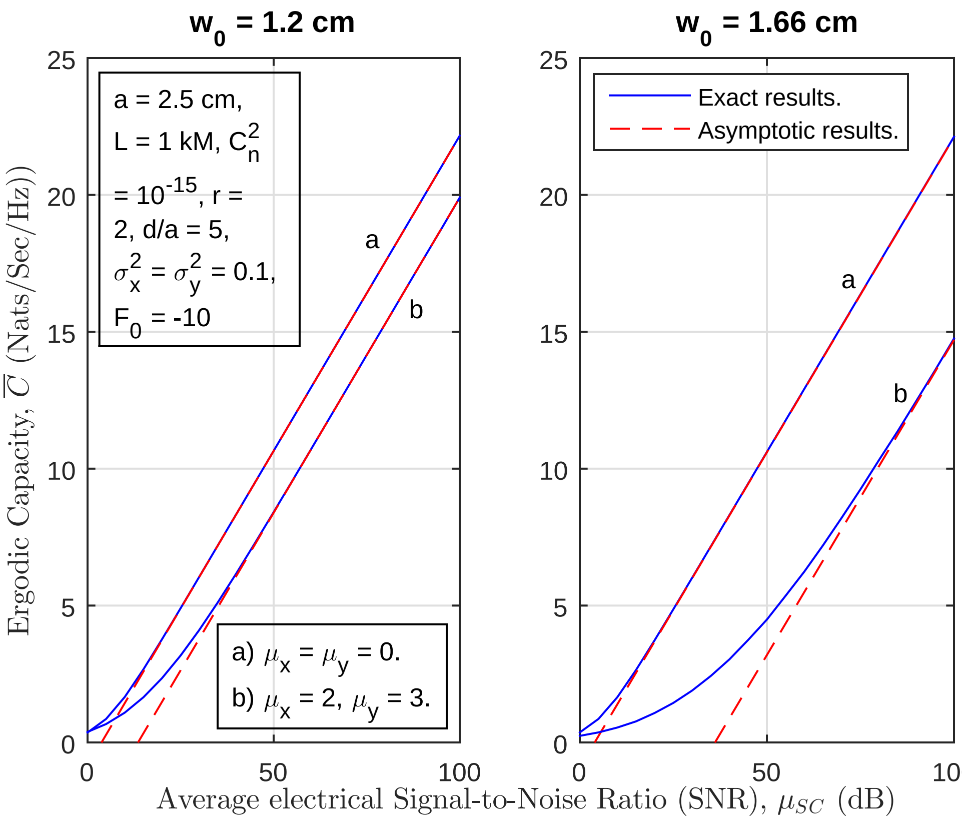

Figure 5.3: The effect of boresight and beam waist on the channel capacity of dual-branch FSO link.

It can also help suppressing the effect of beam boresight error. From our observation in Fig. 5.4, with small boresight error, the distance does not make any difference to the channel capacity. On the other hand, larger boresight, spacing distance can be helpful in diminishing the effect of boresight. Finally, we show in Fig. 5.5 the effect of the pointing error on the channel capacity if SSC are employed to combine the signal at the receive side. Here, we consider only unidirectional misalignment, so we can obtain the optimal threshold $\gamma_t = \exp(-2\sigma_X^2)$. It is clear that even with the misalignment being in one direction, performance degradation is expected.

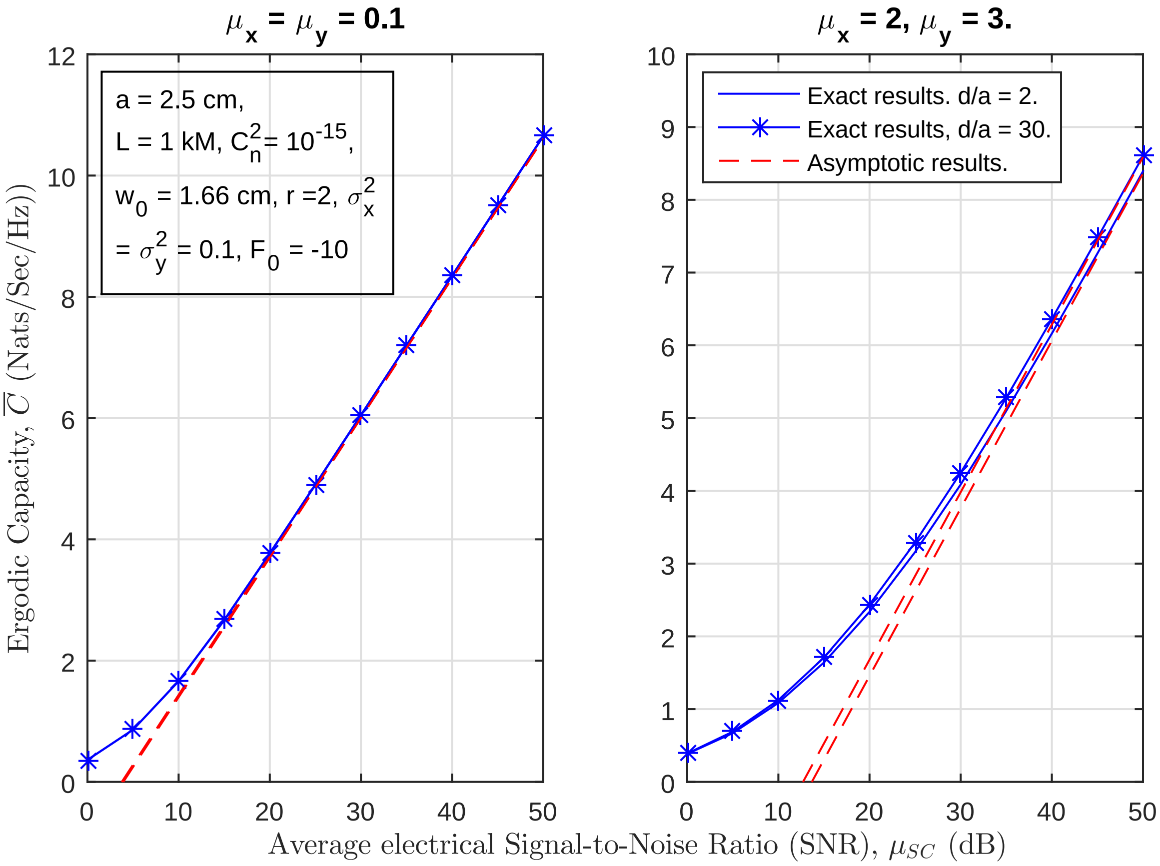

Figure 5.4: The effect of distance and boresight on the channel capacity of dual-branch FSO link.

5.5 Conclusion

In this chapter, we have successfully derived the asymptotic capacity of dual-aperture FSO systems over correlated Log-Normal channels based on two combining technique and under a general pointing error model. Numerical examples, validated by computer simulations, were utilized to show the effect of boresight error, beam waist, separation distance, and the jitter variance on the link capacity. Finally, the numerical examples demonstrated that our asymptotic results can accurately predict the performance of FSO systems in the high SNR regime.

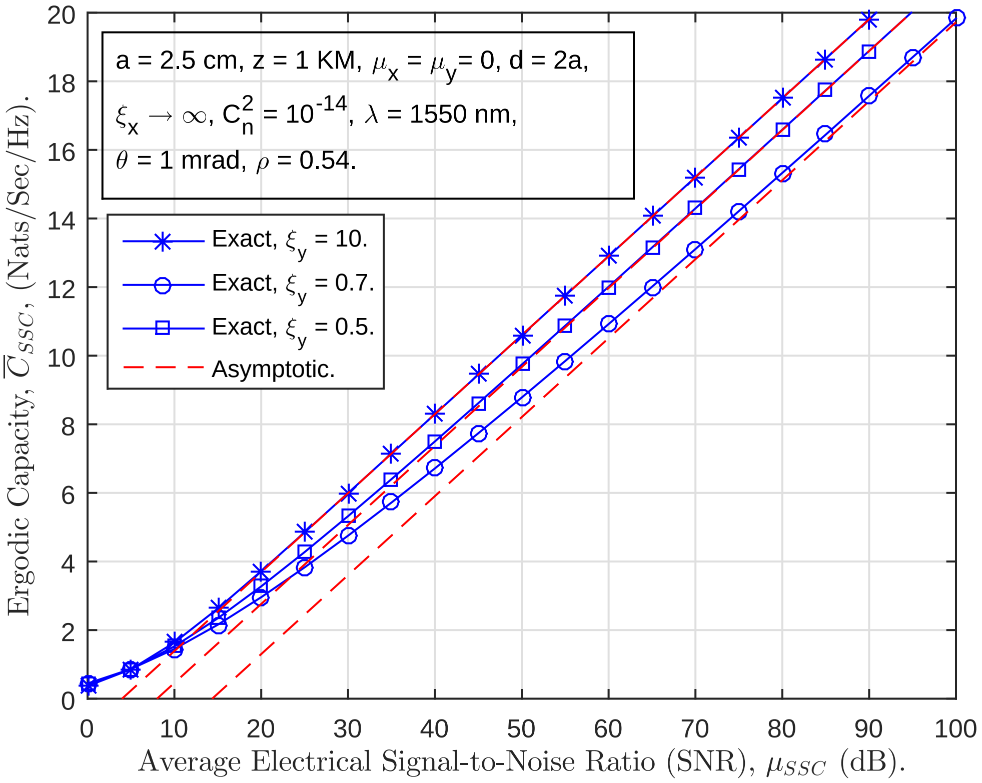

Figure 5.5: Unidirectional misalignment and corresponding channel capacity for the dual-aperture FSO system.

Chapter 6

Performance of Multichannel Reception over Generalized Atmospheric Channels

6.1 Introduction

Diversity, in which multiple copies of the same data is transmitted to the receiver such that each copy experiences different path/channel, has shown a great deal in mitigating fading effects in RF systems in addition to improving both performance and capacity [1, 84, 85]. For diversity combining techniques, SC is one of the most efficient and simple combining schemes. In SC, the receiver aims to process the branch with maximum SNR. Diversity schemes in FSO systems was first introduced by Ibrahim [86] followed by great number of research instigating diversity over weak and strong turbulence conditions. Some investigated the spatial diversity and combining techniques of correlated and independent log-normal turbulence channels [75, 87–89]. Also, spatial diversity was studied over K-distributed channels for different combining schemes in [54]. Moreover, SC over Gamma-Gamma under the impact of pointing errors has been investigated [90].

Double generalized gamma channel model for free-space optical communication systems developed by [32] covers a very wide range of turbulence conditions and makes it generic to describe the FSO channel. Also, pointing errors was integrated to this model to better show the impact of pointing error impairments on the FSO system [38]. Hence, in this chapter, the dual-branch FSO selection combining scheme operating on such channels is investigated to show diversity enhancement on the system performance and capacity.

In particular, we first express the statistical properties of the maximum of double Generalized Gamma random variable under the impact of pointing errors in terms of H-function and G-function. The statistical properties include finding the CDF, PDF, MGF, and the moments in closed-form. Then, these results are exploited to evaluate performance measures such as the average BER and the ergodic capacity of the FSO system.

6.2 System Model

In this chapter, we consider two independent not necessarily identical FSO branches over double GG turbulence and subject to pointing error impairments. The signal at the receive end is then combined for detection. The system model analysis explained further is suitable for any detection technique.

6.2.1 Selection Combining

Among different combining techniques, selection combining is utilized to mix the two received signals. In other words, the end-to-end SNR of the system can be expressed similar to (5.8) as

$$\gamma_{\mathrm{M}} = \max(\gamma_a, \gamma_b), \tag{6.1}$$

such that γ_a and γ_b are independent not necessarily identically distributed (i.n.i.d) modified double GG[1] RVs whose PDF and CDF is listed in (3.10) and (3.13), respectively. It is important to note that by setting the follwoing parameters $\sigma_i = \lambda_i = \Omega_i = 1$, $\beta_{1i} = \alpha_i$, $\beta_{2i} = \beta_i$, $h_i = \frac{\xi_i^2}{\xi_i^2+1}$, $\xi_i >> 1$ then $h_i = 1$, $C_i = \left(\frac{\alpha_i\beta_i}{r_i^2}\right)^{r_i}$, $u_i = 3r_i$, $v_i = 1$, $\kappa_{3i} = \Delta(r_i : \xi_i^2 + 1)$, $\kappa_{4i} = \Delta(r_i : \xi_i^2), \Delta(r_i : \alpha_i), \Delta(r_i : \beta_i)$, double GG reduces

---

[1] Modified double GG RV term refers to the joint effect of turbulence and pointing errors. In other words, the irradiance becomes a mixture of two independent processes and is written as $I = I_a I_p$ where I_a is modeled as double generalized Gamma RV whose PDF is expressed in (2.15) and I_p is the pointing error RV whose PDF can be found in (2.22). The PDF of I has been derived in (2.36).

to the case of ΓΓ turbulence perturbed by pointing errors [90].

6.2.2 Statistical Properties

For a complete performance analysis of the system considered in this chapter, identifying the statistical characteristics of the end-to-end SNR, γ_M, is crucial.

6.2.2.1 Cumulative Distribution Function

The CDF of the maximum of two random variables can be written as

$$F_{\gamma_{\mathrm{M}}}(\gamma) = \Pr\left(\gamma_a \leq \gamma \text{ and } \gamma_b \leq \gamma\right). \tag{6.2}$$

Since the branches are separated enough to make the random variables independent, then (6.2) turns to be

$$\begin{aligned} F_{\gamma_{\mathrm{M}}}(\gamma) &= \Pr\left(\gamma_a \leq \gamma\right) \Pr\left(\gamma_b \leq \gamma\right), \\ &= F_{\gamma_b}(\gamma) F_{\gamma_b}(\gamma). \end{aligned} \tag{6.3}$$

Then, the CDF of γ_M can be easily derived as

$$F_{\gamma_{\mathrm{M}}}(\gamma) = A_{3a} A_{3b} \mathrm{G}_{r_a+1,u_a+1}^{u_a,1}\left(C_a \left(\frac{\gamma}{\mu_{r_a,a}}\right)^{v_a} \middle| \begin{matrix} 1, \kappa_{3a} \\ \kappa_{4a}, 0 \end{matrix} \right) \mathrm{G}_{r_b+1,u_b+1}^{u_b,1}\left(C_b \left(\frac{\gamma}{\mu_{r_b,b}}\right)^{v_b} \middle| \begin{matrix} 1, \kappa_{3b} \\ \kappa_{4b}, 0 \end{matrix} \right), \tag{6.4}$$

where $A_{3i} = \frac{\xi_i^2 \sigma_i^{\beta_{1i}-\frac{1}{2}} \lambda_i^{\beta_{2i}-\frac{1}{2}} (2\pi)^{1-\frac{r_i(\lambda_i+\sigma_i)}{2}} r_i^{\beta_{1i}+\beta_{2i}-2}}{\alpha_{2i}\lambda_i \Gamma(\beta_{1i})\Gamma(\beta_{2i})}$. For the case of Gamma-Gamma turbulence model, we have $A_{3i} = \frac{\xi_i^2 r_i^{\alpha_1+\beta_1-2}}{\Gamma(\alpha_i)\Gamma(\beta_i)(2\pi)^{r_i-1}}$.

Moreover, an asymptotic expression can be obtained via the expansion of the

Meijer's G-function in (3.14) as $C_i(\frac{\gamma}{\mu_{r_i,i}})^{v_i} \rightarrow 0$ (i.e high SNR regime) as

$$\tilde{F}_{\gamma_{\mathrm{M}}}(\gamma) \underset{\mu_{r_i,i}>>1}{\approxeq} A_{3a}A_{3b} \sum_{k=1}^{u_a}\sum_{x=1}^{u_b} \left(\frac{\gamma^{v_a}C_a}{\mu_{r_a,a}^{v_a}}\right)^{\kappa_{4a,k}} \left(\frac{\gamma^{v_b}C_b}{\mu_{r_b,b}^{v_b}}\right)^{\kappa_{4b,x}}$$
$$\times \frac{\prod_{l=1;l\neq k}^{u_a}\Gamma(\kappa_{4a,l}-\kappa_{4a,k})\prod_{l=1;l\neq x}^{u_b}\Gamma(\kappa_{4b,l}-\kappa_{4b,x})}{\kappa_{4a,k}\kappa_{4b,x}\prod_{l=1}^{r_a}\Gamma(\kappa_{3a,l}-\kappa_{4a,k})\prod_{l=1}^{r_b}\Gamma(\kappa_{3b,l}-\kappa_{4b,k})}. \tag{6.5}$$

The asymptotic expression in (6.5) is simple and is in terms of elementary functions that can be evaluated using any computer software.

6.2.2.2 Probability Density Function

The PDF is then obtained by differentiating (6.4) with respect to γ yielding

$$f_{\gamma_{\mathrm{M}}}(\gamma) = \frac{A_{3a}A_{3b}}{\gamma}\left(v_b \mathrm{G}_{r_b,u_b}^{u_b,0}\left(C_b\left(\frac{\gamma}{\mu_{r_b,b}}\right)^{v_b} \middle| \begin{matrix}\kappa_{3b}\\ \kappa_{4b}\end{matrix}\right) \mathrm{G}_{r_a+1,u_a+1}^{u_a,1}\left(C_a\left(\frac{\gamma}{\mu_{r_a,a}}\right)^{v_a} \middle| \begin{matrix}1,\kappa_{3a}\\ \kappa_{4a},0\end{matrix}\right)\right.$$
$$\left. + v_a \mathrm{G}_{r_a,u_a}^{u_a,0}\left(C_a\left(\frac{\gamma}{\mu_{r_a,a}}\right)^{v_a} \middle| \begin{matrix}\kappa_{3a}\\ \kappa_{4a}\end{matrix}\right) \mathrm{G}_{r_b+1,u_b+1}^{u_b,1}\left(C_b\left(\frac{\gamma}{\mu_{r_b,b}}\right)^{v_b} \middle| \begin{matrix}1,\kappa_{3b}\\ \kappa_{4b},0\end{matrix}\right)\right). \tag{6.6}$$

This derived PDF was verified via Monte-Carlo simulations as shown in Fig. 6.1.

An asymptotic expression of the PDF can be obtained by the same way done in (6.5) for the CDF. In other words, by using the expansion of the Meijer's G-function, we can reach to an asymptotic result as

$$\tilde{f}_{\gamma_{\mathrm{M}}}(\gamma) \underset{\mu_{r_i,i}>>1}{\approxeq} A_{3a}A_{3b} \sum_{k=1}^{u_a}\sum_{x=1}^{u_b} \left(\frac{C_a}{\mu_{r_a,a}^{v_a}}\right)^{\kappa_{4a,k}} \left(\frac{C_b}{{\mu_{r_b,b}}^{v_b}}\right)^{\kappa_{4b,x}} \left(\frac{v_b}{\kappa_{4a,k}}+\frac{v_a}{\kappa_{4b,x}}\right)$$
$$\times \frac{\prod_{l=1;l\neq x}^{u_b}\Gamma(\kappa_{4b,l}-\kappa_{4b,x})\prod_{l=1;l\neq k}^{u_a}\Gamma(\kappa_{4a,l}-\kappa_{4a,k})}{\prod_{l=1}^{r_b}\Gamma(\kappa_{3b,l}-\kappa_{4b,x})\prod_{l=1}^{r_a}\Gamma(\kappa_{3a,l}-\kappa_{4a,k})}\gamma^{v_a\kappa_{4a,k}+v_b\kappa_{4b,x}-1} \tag{6.7}$$

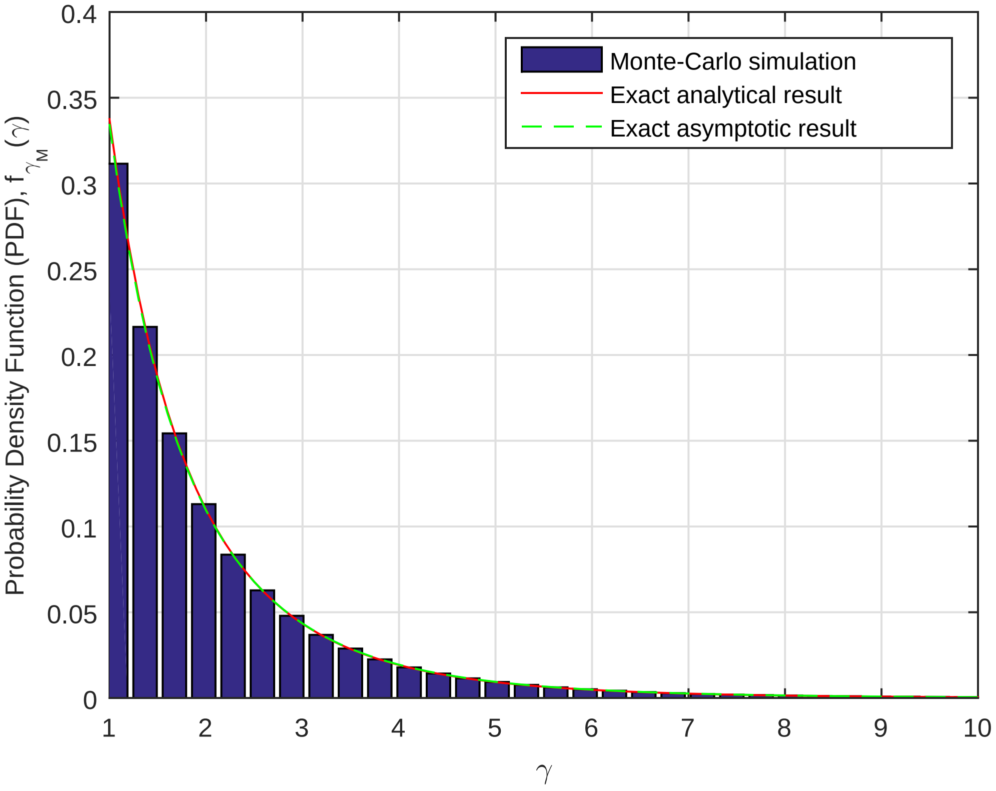

Figure 6.1: PDF validation for the maximum of two double GG variates

6.2.2.3 Moment Generating Function

In this section, the MGF of γ_M is derived in exact and asymptotic approach. First, the CDF in (6.4) is expressed in terms of the Fox's H-function[2] using the property [44, Eq. (07.34.26.0008.01)]

$$\frac{1}{C}\mathrm{G}_{p,q}^{m,n}\left(z^{1/C}\middle|\begin{matrix}\mathbf{a}\\ \mathbf{b}\end{matrix}\right) = \mathrm{H}_{p,q}^{m,n}\left(z\middle|\begin{matrix}(a,C)\\ (b,C)\end{matrix}\right). \tag{6.8}$$

---

[2] Fox's H-function is a special function and defined in Appendix A. The function can be easily valuated using MATHEMATICA® [91]

As such, the CDF in (6.4) can be rewritten as

$$F_{\gamma_{\mathrm{M}}}(\gamma) = \frac{A_{3a}A_{3b}}{v_a v_b}\,\mathrm{H}^{u_a,1}_{r_a+1,u_a+1}\left(\frac{C_a^{1/va}\gamma}{\mu_{r_a,a}}\left|\begin{matrix}(\kappa_{5a},1/va)\\ \\ (\kappa_{6a},1/va)\end{matrix}\right.\right)\mathrm{H}^{u_b,1}_{r_b+1,u_b+1}\left(\frac{C_b^{1/vb}\gamma}{\mu_{r_b,b}}\left|\begin{matrix}(\kappa_{5b},1/vb)\\ \\ (\kappa_{6b},1/vb)\end{matrix}\right.\right), \tag{6.9}$$

where $\kappa_{5i} = 1, \kappa_{3i}$ and $\kappa_{6i} = \kappa_{4i}, 0$. Afterward, (6.9) is inserted in (3.17) and with applying the identity [92, Eq. (2.2)] to obtain

$$\mathcal{M}_{\gamma_{\mathrm{M}}}(s) = \frac{A_{3a}A_{3b}}{v_a v_b}\,\mathbf{H}\left[\begin{array}{c|c|c}\begin{pmatrix}0,1\\ \\ 1,0\end{pmatrix} & \begin{array}{c}(0;1,1)\\ \\ (-;-,-)\end{array} & \\ \begin{pmatrix}u_a,1\\ \\ r_a+1,u_a+1\end{pmatrix} & \begin{array}{c}(\kappa_{5a},[v_a^{-1}])\\ \\ (\kappa_{6a},[v_a^{-1}])\end{array} & \frac{C_a^{1/v_a}}{s\mu_{r_a,a}} \\ & & \frac{C_b^{1/v_b}}{s\mu_{r_b,b}} \\ \begin{pmatrix}u_b,1\\ \\ r_b+1,u_b+1\end{pmatrix} & \begin{array}{c}(\kappa_{5b},[v_b^{-1}])\\ \\ (\kappa_{6b},[v_b^{-1}])\end{array} & \end{array}\right], \tag{6.10}$$

where $\mathbf{H}[.]$ is the bivariate H-function defined in the appendix A based on [92].

Simplified expression can be obtained if solving the integral in (3.17) but using the asymptotic CDF (6.5) to reach to the following result

$$\begin{aligned}\tilde{\mathcal{M}}_{\gamma_{\mathrm{M}}}(s) \underset{\mu_{r_i,i}>>1}{\approxeq} & A_{3a}A_{3b}\sum_{k=1}^{u_a}\sum_{x=1}^{u_b}\left(\frac{C_a}{\mu_{r_a,a}^{v_a}}\right)^{\kappa_{4a,k}}\left(\frac{C_b}{\mu_{r_b,b}^{v_b}}\right)^{\kappa_{4b,x}}\Gamma(v_a\kappa_{4a,k}+v_b\kappa_{4b,x}+1)\\ \times & \frac{\prod_{l=1;l\neq k}^{u_a}\Gamma(\kappa_{4a,l}-\kappa_{4a,k})\prod_{l=1;l\neq x}^{u_b}\Gamma(\kappa_{4b,l}-\kappa_{4b,x})}{\kappa_{4a,k}\kappa_{4b,x}\prod_{l=1}^{r_a}\Gamma(\kappa_{3a,l}-\kappa_{4a,k})\prod_{l=1}^{r_b}\Gamma(\kappa_{3b,l}-\kappa_{4b,k})}s^{-(v_a\kappa_{4a,k}+v_b\kappa_{4b,x})}.\end{aligned} \tag{6.11}$$

By setting $\sigma_i = \lambda_i = \Omega_i = 1$, $\beta_{1i} = \alpha_i$, $\beta_{2i} = \beta_i$, $h_i = \frac{\xi_i^2}{\xi_i^2+1}$, $\xi_i >> 1$ then $h_i = 1$, $C_i = \left(\frac{\alpha_i\beta_i}{r_i^2}\right)^{r_i}$, $u_i = 3r_i$, $v_i = 1$, $\kappa_{3i} = \Delta(r_i : \xi_i^2 + 1)$, $\kappa_{4i} = \Delta(r_i : \xi_i^2), \Delta(r_i : \alpha_i), \Delta(r_i : \beta_i)$ we have the special case of Gamma-Gamma turbulence perturbed by pointing errors [90]. Setting the special parameters for the Gamma-Gamma case, the MGF can be expressed as

$$\mathcal{M}^{*}_{\gamma_{\mathrm{M}}}(s) = A_{3a}A_{3b}\,\mathrm{G}^{1,0:3r_a,1:3r_b,1}_{1,0:r_a+1,3r_a+1:r_b+1,3r_b+1}\left[\begin{array}{c|c|c|c} 1 & \kappa_{5a} & \kappa_{5b} & \\ & & & \frac{C_a}{s\mu_{r_a,a}}, \frac{C_b}{s\mu_{r_b,b}} \\ - & \kappa_{6a} & \kappa_{6b} & \end{array}\right], \tag{6.12}$$

where $\mathrm{G}^{-,-:-,-:-,-}_{-,-:-,-:-,-}[.]$ is the extended generalized bivariate Meijer's G-function (EGB-MGF) defined in the appendix (A).

6.2.2.4 Moments

The moments of a random variable is defined in (3.20). For γ_M specifically, it can be easily found by first placing (6.6) in (3.20) and utilizing equation [93, Eq. (1.7)], we obtain the following

$$\begin{aligned}\mathbb{E}[\gamma^n_{\mathrm{M}}] = A_{3a}A_{3b}\Bigg[\left(\frac{\mu_{r_a,a}}{C_a^{1/v_a}}\right)^n v_b\;\mathrm{H}^{u_b+1,u_a}_{u_a+r_b+1,u_b+r_a+1}\left(\left(\frac{C_b^{1/v_b}\mu_{r_a,a}}{C_a^{1/v_a}\mu_{r_b,b}}\right)^{v_av_b}\middle|\begin{matrix}(\kappa_{7a},v_b),(\kappa_{3b},v_a)\\ \\ (\kappa_{4b},v_a),(\kappa_{8a},v_b)\end{matrix}\right)\\ + \left(\frac{\mu_{r_b,b}}{C_b^{1/v_b}}\right)^n v_a\;\mathrm{H}^{u_a+1,u_b}_{u_b+r_a+1,u_a+r_b+1}\left(\left(\frac{C_a^{1/v_a}\mu_{r_b,b}}{C_b^{1/v_b}\mu_{r_a,a}}\right)^{v_av_b}\middle|\begin{matrix}(\kappa_{7b},v_a),(\kappa_{3a},v_b)\\ \\ (\kappa_{4a},v_b),(\kappa_{8b},v_a)\end{matrix}\right)\Bigg].\end{aligned} \tag{6.13}$$

where $\kappa_{7i} = 1 - \kappa_{6i} - \frac{n}{v_i}$ and $\kappa_{8i} = 1 - \kappa_{5i} - \frac{n}{v_i}$. For Gamma-Gamma case, (6.13) simplifies to

$$\begin{aligned}\mathbb{E}[\gamma^n_{\mathrm{M}}]^{*} = A_{3a}A_{3b}\Bigg[\left(\frac{\mu_{r_a,a}}{C_a}\right)^n \mathrm{G}^{3r_b+1,3r_a}_{3r_a+r_b+1,3r_b+r_a+1}\left(\frac{C_b\mu_{r_a,a}}{C_a\mu_{r_b,b}}\middle|\begin{matrix}\kappa_{7a},\kappa_{3b}\\ \\ \kappa_{4b},\kappa_{8a}\end{matrix}\right)\\ + \left(\frac{\mu_{r_b,b}}{C_b}\right)^n \times\mathrm{G}^{3r_a+1,3r_b}_{3r_b+r_a+1,3r_a+r_b+1}\left(\frac{C_a\mu_{r_b,b}}{C_b\mu_{r_a,a}}\middle|\begin{matrix}\kappa_{7b},\kappa_{3a}\\ \\ \kappa_{4a},\kappa_{8b}\end{matrix}\right)\Bigg].\end{aligned} \tag{6.14}$$

6.2.3 Performance Analysis Measures

Based on the results obtained in Section 6.2.2, the performance of the selection combining scheme over dual-branch FSO links is studied.

6.2.3.1 Outage Probability

The outage probability is simply derived by substituting (6.4) into (3.22).

6.2.3.2 Average Bit Error Rate

To find the average BER of the system, (6.4) is inserted into (3.28) then the identity [92, Eq. (2.2)] is utilized. Then, the result can be written as

$$\overline{P}_{\mathrm{SC}} = \frac{A_{3a}A_{3b}}{2\Gamma(p)v_a v_b}\mathbf{H}\left[\begin{array}{c|c|c} \begin{pmatrix} 0,1 \\ \\ 1,0 \end{pmatrix} & \begin{array}{c} (1-p;1,1) \\ \\ (-;-,-) \end{array} & \\ \begin{pmatrix} u_a,1 \\ \\ r_a+1,u_a+1 \end{pmatrix} & \begin{array}{c} (\kappa_{5a},[v_a^{-1}]) \\ \\ (\kappa_{6a},[v_a^{-1}]) \end{array} & \begin{array}{c} \frac{C_a^{1/v_a}}{q\mu_{r_a,a}} \\ \\ \frac{C_b^{1/v_b}}{q\mu_{r_b,b}} \end{array} \\ \begin{pmatrix} u_b,1 \\ \\ r_b+1,u_b+1 \end{pmatrix} & \begin{array}{c} (\kappa_{5b},[v_b^{-1}]) \\ \\ (\kappa_{6b},[v_b^{-1}]) \end{array} & \end{array}\right], \tag{6.15}$$

where p and q indicate different modulation schemes parameters in [1, Table 8.1] .

An asymptotic expression of $\overline{P}_{\mathrm{SC}}$ at high SNR can be derived as

$$\overline{P}_{SC} \underset{\mu_{r_i,i}>>1}{\approxeq} \frac{q^p}{2\Gamma(p)} \int_0^\infty \exp(-q\gamma)\ \gamma^{p-1}\tilde{F}_{\gamma_M}(\gamma)\ d\gamma, \tag{6.16}$$

where $\tilde{F}_{\gamma_M}$ is the asymptotic CDF of γ_M and defined in (6.5). Solving the integrals leads to the following

$$\begin{aligned}\overline{P}_{\mathrm{SC}} \underset{\mu_{r_i,i}>>1}{\approxeq} & \frac{A_{3a}A_{3b}}{2\Gamma(p)}\sum_{k=1}^{u_a}\sum_{x=1}^{u_b}\left(\frac{C_a}{\mu_{r_a,a}^{v_a}}\right)^{\kappa_{4a,k}}\left(\frac{C_b}{\mu_{r_b,b}^{v_b}}\right)^{\kappa_{4b,x}}\Gamma(v_a\kappa_{4a,k}+v_b\kappa_{4b,x}+p)\\ \times & \frac{\prod_{l=1;l\neq k}^{u_a}\Gamma\big(\kappa_{4a,l}-\kappa_{4a,k}\big)\prod_{l=1;l\neq x}^{u_b}\Gamma\big(\kappa_{4b,l}-\kappa_{4b,x}\big)}{\kappa_{4a,k}\ \kappa_{4b,x}\prod_{l=1}^{r_a}\Gamma\big(\kappa_{3a,l}-\kappa_{4a,k}\big)\prod_{l=1}^{r_b}\Gamma\big(\kappa_{3b,l}-\kappa_{4b,k}\big)}\, q^{-(v_a\kappa_{4a,k}+v_b\kappa_{4b,x})}. \end{aligned} \tag{6.17}$$

Above expression can facilitate extracting the diversity and coding gain of the system. First, the formula (6.17) can be rewritten in the form of (3.31). Upon our observation, this is possible if the absolute difference between $\{\frac{\xi_i^2}{v_i r_i}, \frac{\beta_{1i}}{r_i\sigma_i}, \frac{\beta_{2i}}{r_i\lambda_i}\} \in \kappa_{4i}$ is significance. If so, then the summation in (6.17) reduces to a single dominant term results from the min $\left(\frac{\xi_i^2}{v_i r_i}, \frac{\beta_{1i}}{r_i\sigma_i}, \frac{\beta_{2i}}{r_i\lambda_i}\right)$. In this case, the diversity and coding gain can be written as

$$\begin{aligned} G_d &= v_a\kappa_{4a,k}+v_b\kappa_{4b,x},\\ G_c &= q\left(\frac{A_{3a}A_{3b}{C_a}^{\kappa_{4a,k}}{C_b}^{\kappa_{4b,x}}\Gamma(v_a\kappa_{4a,k}+v_b\kappa_{4b,x}+p)}{2\Gamma(p)\kappa_{4a,k}\ \kappa_{4b,x}}\right.\\ &\quad\left.\times\frac{\prod_{l=1;l\neq k}^{u_a}\Gamma\big(\kappa_{4a,l}-\kappa_{4a,k}\big)\prod_{l=1;l\neq x}^{u_b}\Gamma\big(\kappa_{4b,l}-\kappa_{4b,x}\big)}{\prod_{l=1}^{r_a}\Gamma\big(\kappa_{3a,l}-\kappa_{4a,k}\big)\prod_{l=1}^{r_b}\Gamma\big(\kappa_{3b,l}-\kappa_{4b,k}\big)}\right)^{-1/G_d}, \end{aligned} \tag{6.18}$$

where $k \in \{1, r_a+1, r_a+r_a\sigma_a+1\}$ and $x \in \{1, r_b+1, r_b+r_b\sigma_b+1\}$.

For the Gamma-Gamma case, the result reduces to

$$\overline{P}_{\mathrm{SC}}^{*} = \frac{A_{3a}A_{3b}}{2\Gamma(p)}\mathrm{G}_{1,0:r_a+1,3r_a+1:r_b+1,3r_b+1}^{1,0:3r_a,1:3r_b,1}\left[\begin{array}{c|c|c|c} p & \kappa_{5a} & \kappa_{5b} & \\ & & & \frac{C_a}{q\mu_{r_a,a}}, \frac{C_b}{q\mu_{r_b,b}} \\ - & \kappa_{6a} & \kappa_{6b} & \end{array}\right]. \tag{6.19}$$

6.2.3.3 Ergodic Capacity

The ergodic capacity of FSO systems is defined in (3.36). To find the the channel capacity for the selection combining scheme, first (3.37) is expressed in terms of the

H-function as

$$\ln(1+x) = \mathrm{G}_{2,2}^{1,2}\left(x \,\middle|\, \begin{matrix}1,1\\ 1,0\end{matrix}\right) = \mathrm{H}_{2,2}^{1,2}\left(x \,\middle|\, \begin{matrix}(1,1),(1,1)\\ (1,1),(0,1)\end{matrix}\right). \tag{6.20}$$

Afterward $\overline{C}_{\mathrm{SC}}$ is obtained by using (3.36) along with the identities and [92, Eq. (2.3)] yielding

$$\begin{aligned}\overline{C}_{\mathrm{SC}} = \frac{A_{3a}A_{3b}}{v_a v_b \ln(2)} \times \Bigg(& v_b\mathbf{H}\left[\begin{matrix}\begin{pmatrix}0,u_b\\ u_b,r_b\end{pmatrix}\\ \begin{pmatrix}1,2\\ 2,2\end{pmatrix}\\ \begin{pmatrix}u_a,1\\ r_a+1,u_a+1\end{pmatrix}\end{matrix}\,\middle|\,\begin{matrix}(1-\kappa_{4b};[v_b^{-1}],[v_b^{-1}])\\ (1-\kappa_{3b};[v_b^{-1}],[v_b^{-1}])\\ (1,1;1,1)\\ (1,0;1,1)\\ (\kappa_{5a},[v_a^{-1}])\\ (\kappa_{6a},[v_a^{-1}])\end{matrix}\,\middle|\,\begin{matrix}\frac{c\mu_{r_b,b}}{C_b^{1/v_b}}\\ \\ \frac{C_a^{1/v_a}\mu_{r_b,b}}{C_b^{1/v_b}\mu_{r_a,a}}\end{matrix}\right]\\ & + v_a\mathbf{H}\left[\begin{matrix}\begin{pmatrix}0,u_a\\ u_a,r_a\end{pmatrix}\\ \begin{pmatrix}1,2\\ 2,2\end{pmatrix}\\ \begin{pmatrix}u_b,1\\ r_b+1,u_b+1\end{pmatrix}\end{matrix}\,\middle|\,\begin{matrix}(1-\kappa_{4a};[v_a^{-1}],[v_a^{-1}])\\ (1-\kappa_{3a};[v_a^{-1}],[v_a^{-1}])\\ (1,1;1,1)\\ (1,0;1,1)\\ (\kappa_{5b},[v_b^{-1}])\\ (\kappa_{6b},[v_b^{-1}])\end{matrix}\,\middle|\,\begin{matrix}\frac{c\mu_{r_a,a}}{C_a^{1/v_a}}\\ \\ \frac{C_b^{1/v_b}\mu_{r_a,a}}{C_a^{1/v_a}\mu_{r_b,b}}\end{matrix}\right]\Bigg).\end{aligned} \tag{6.21}$$

For the Gamma-Gamma case, the expression is reduced to

$$\begin{aligned}\overline{C}_{\mathrm{SC}}^{*} = \frac{A_{3a}A_{3b}}{\ln(2)} \times \Bigg(& \mathrm{G}_{3r_b,r_b:r_a+1,3r_a+1:2,2}^{3r_b,0:3r_a,1:1,2}\left[\begin{matrix}\kappa_{4b}\\ \kappa_{3b}\end{matrix}\middle|\begin{matrix}\kappa_{5a}\\ \kappa_{6a}\end{matrix}\middle|\begin{matrix}1,1\\ 1,0\end{matrix}\middle|\frac{C_a\mu_{r_b,b}}{C_b\mu_{r_a,a}}, \frac{c\mu_{r_b,b}}{C_b}\right]\\ & + \mathrm{G}_{3r_a,r_a:r_b+1,3r_b+1:2,2}^{3r_a,0:3r_b,1:1,2}\left[\begin{matrix}\kappa_{4a}\\ \kappa_{3a}\end{matrix}\middle|\begin{matrix}\kappa_{5b}\\ \kappa_{6b}\end{matrix}\middle|\begin{matrix}1,1\\ 1,0\end{matrix}\middle|\frac{B_b\mu_{r_a,a}}{B_a\mu_{r_b,b}}, \frac{c\mu_{r_a,a}}{B_a}\right]\Bigg).\end{aligned} \tag{6.22}$$

6.3 Numerical Analysis

In this section, we verify and validate our analytical results of hybrid FSO communication systems[3] using computer-based simulations.

First, we investigate the BER performance of dual-branch FSO/FSO ($r_a = r_b \in \{1, 2\}$) and RF/FSO ($r_a = 1$ and $r_b \in \{1, 2\}$) SC systems under DPSK modulation in which $p = 1$ and $q = 1$. In this work, we consider two scenarios of atmospheric turbulence conditions, strong (consider the following set of parameters: $\alpha_{1,i} = 1.8621$, $\alpha_{2,i} = 1$, $\beta_{1,i} = 0.5$, $\beta_{2,i} = 1.8$, $\Omega_{1,i} = 1.5074$, and $\Omega_{2,i} = 0.9280$ such that $\lambda_i = 17$ and $\sigma_i = 9$) and moderate (consider the following set of parameters:$\alpha_{1,i} = 2.1690$, $\alpha_{2,i} = 1$, $\beta_{1,i} = 0.55$, $\beta_{2,i} = 2.35$, $\Omega_{1,i} = 1.5793$, and $\Omega_{2,i} = 0.9671$ where $\lambda_i = 28$ and $\sigma_i = 13$).

Starting with Fig. 6.2 to show the impact of pointing errors on the performance of single FSO link and dual-branch SC of FSO/FSO and RF/FSO. We can notice instantly that SC helps to improve the performance comparing to the single link with expense of utilizing more hardware at the receive side. Also, dual-branch RF/FSO SC performance better than symmetric branches FSO/FSO. This encourages the integration of RF into FSO systems or vice verse. Regarding the asymptotic results, they converge fast to exact ones even for low SNR (i.e starting at 30 dB). Interestingly, the asymptotic results representing of all terms in the summation matches perfectly the exact results which give our expression more value instead of using special functions. In the same fashion, two dominants terms asymptotic results provide better match than single dominant term.

Moreover, Fig. 6.3 shows the impact of the turbulence conditions on the performance of FSO systems. Clearly, they lead to some degradation. Again, the asymptotic results including all terms in the summation provide an excellent match with

---

[3] Hybrid systems are defined as systems in which RF and FSO technologies are employed to enhance the communication link.

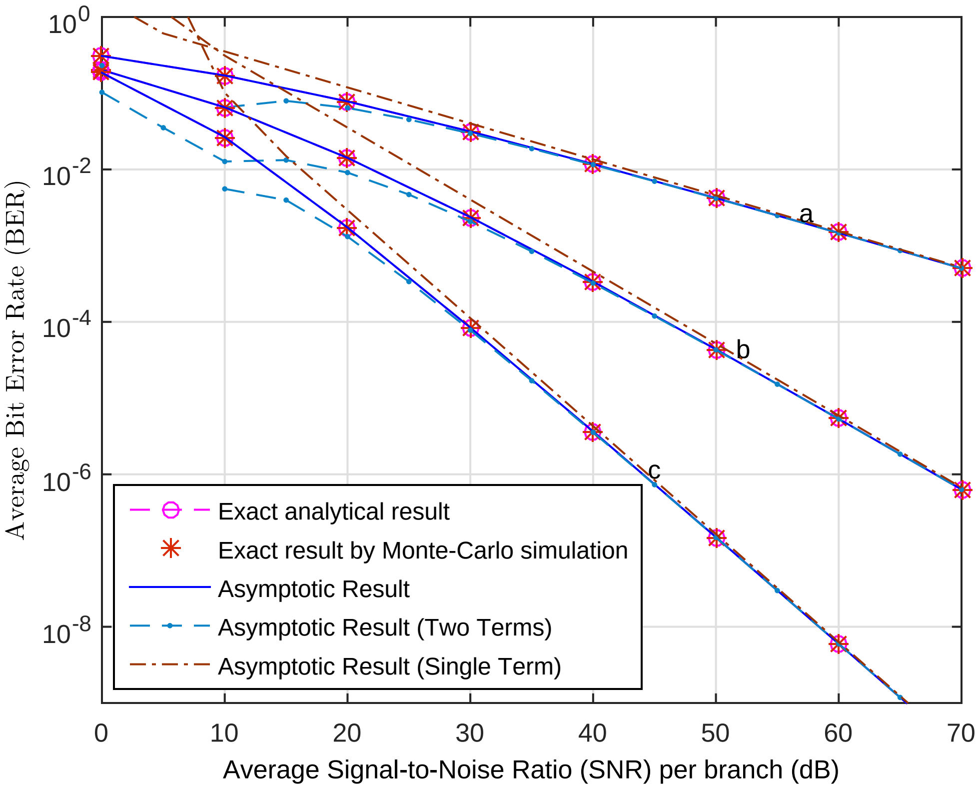

Figure 6.2: The impact of pointing error ($\xi = 1.2$) on the average BER of DPSK over (a) single FSO link, (b) dual-branch FSO/FSO and (c) RF/FSO SC in strong turbulence conditions.

the exact result. It is noticeable that for strong conditions the asymptotic expressions including single dominant terms is better than for the moderate conditions and that is due to the fact that the differences between $\{\frac{\xi_i^2}{v_i r_i}, \frac{\beta_{1i}}{r_i \sigma_i}, \frac{\beta_{2i}}{r_i \lambda_i}\}$, $i \in \{a, b\}$, for moderate conditions is not significant.

Lastly, we evaluate another performance metric that is the ergodic capacity of dual-branch SC FSO/FSO and RF/FSO SC as shown in Fig. 6.4. Generally, SC systems provides higher data rate than a single link system. Also, we can notice that behavior of RF/FSO and FSO/FSO capacity are not in big difference in contrast with BER.

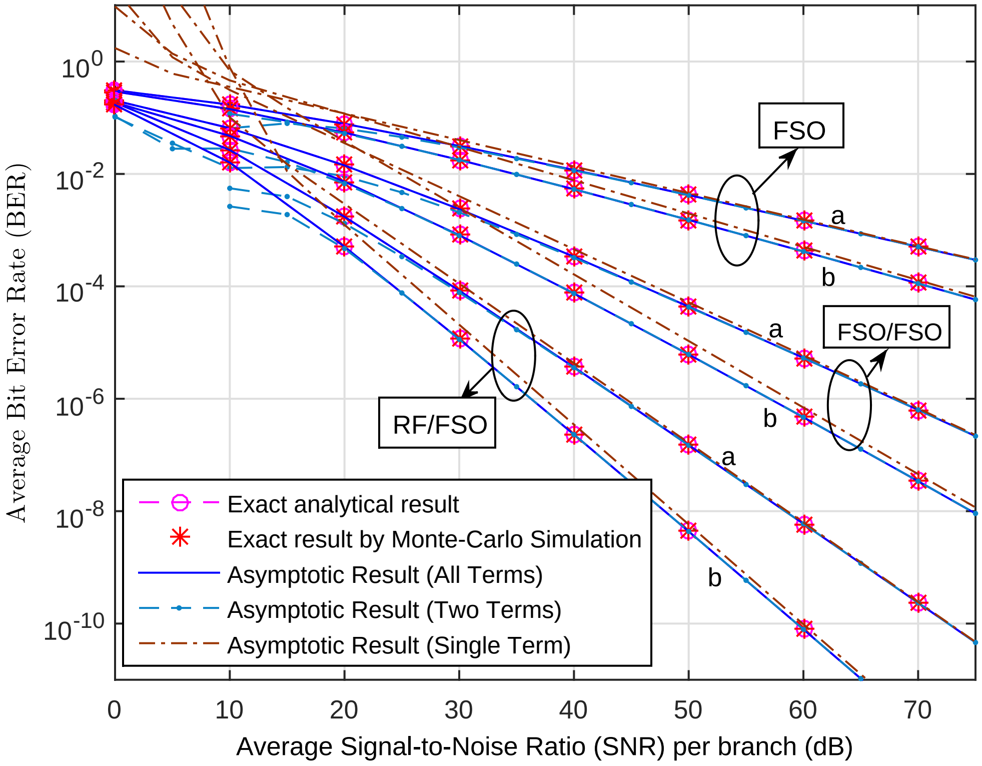

Figure 6.3: The effect of turbulence conditions ((a) Strong turbulence and (b) Moderate conditions) on the average BER of DPSK over single FSO link, dual-branch FSO/FSO and RF/FSO SC with severe pointing error, $\xi = 1.2$

6.4 Conclusion

Closed-form expressions for the CDF, the PDF, the MGF, and the moments of the maximum of two modified double generalized gamma variates were obtained. Based on that, we derived analytical exact and asymptotic expressions for the average bit error rate and the ergodic capacity of dual-branch hybrid FSO SC systems. In addition, Monte-Carlo computer simulations were carried out to validate our results.

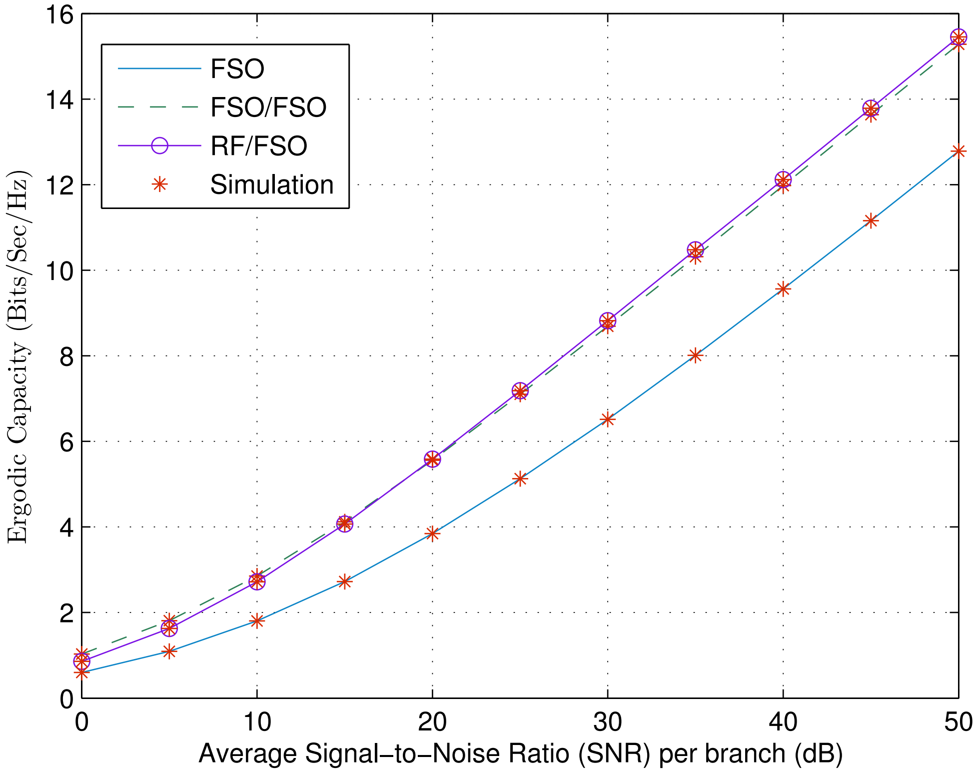

Figure 6.4: Ergodic capacity of single FSO link, dual-branch FSO/FSO, RF/FSO SC in strong turbulence conditions and under severe pointing errors, $\xi = 1.2$.

Chapter 7

Performance of FSO Dual-Hop Relaying Systems

7.1 Introduction

Improving the performance and enhancing the capacity has been the motivation of any newly developed scheme. For instance, relaying technology over the last decade has received a great deal of interest as it enhances the capacity of the system in addition to providing a wider coverage. The basic idea behind relaying is that a relay node is positioned in the way between transmitter and receiver to support direct data transmission. In other words, the dual-hop (DH) relay system consists of three main nodes namely, a source (S) that intends to transmit the signal, a relay (R) node that aims to cooperate in sending the signal to the end node, and the destination (D) that is the receiver.

Relaying can take several modes depending on the requirements of the implementations. For example, the system can be symmetric and asymmetric (i.e. symmetric system is when source-relay (S$\sim$R) and relay-destination (R$\sim$D) links fall under the same fading model). Asymmetric link is more practical and can be expected in a real-life environment as the received signals can be transmitted via different communication systems. In addition, the main task of the intermediate entity in the dual-hop system is to cooperate in transmitting the signal to the receiver. The cooperation can be classified into two techniques namely, amplified-and-forward (AF) and decode-and-forward (DF). The AF is particularly investigated in this work. In AF technique, the relay hears the signal from the source, amplifies it and transmits it again in order to reach the destination. The amplification is usually associated with a gain which can be either fixed or variable.

Multiple research works have been reported to analyze the relay system on both symmetric and asymmetric links [94–97]. Moreover, relaying over FSO system was introduced and then followed by several research work concerning symmetric multi-hop FSO systems over K-distributed, Gaussian and Gamma-Gamma turbulence channel [98–100]. On the other hand, several studies have been conducted to analyze asymmetric fixed and variable gain FSO relay systems as such integrating RF links in FSO systems. Specifically, assuming that RF and FSO links are, respectively, subject to Rayleigh and Gamma-Gamma or M-distributed turbulence channels [101–103]. Analyzing variable gain relay system analytically might not be tractable and mathematically not feasible. Throughout the years, the end-to-end SNR has been upper bounded by the minimum SNR among the sublinks [104] and harmonic mean of the each link SNR [105]. Few research work have been reported focusing on variable gain FSO relay systems over Gamma-Gamma with pointing errors [90, 106, 107].

7.2 Outline

In this chapter, we consider both symmetric and asymmetric dual-hop FSO link. For the symmetric link, we assume that both FSO links experience double GG fading model and under the effect of pointing error. On other hand, when asymmetric link is investigated, it is assumed that the S$\sim$ R link is operated via RF and experience Rayleigh fading [56, 101] while the R$\sim$D link is an FSO link and experience double GG fading.

7.3 RF-FSO Fixed Gain Dual-Hop Transmission Systems

7.3.1 Channel and System Model

In this section, we consider asymmetric fixed gain dual-hop system in which the RF link (S∼R) experiences Rayleigh fading whose SNR can be modeled by an exponential distribution with a PDF given as [1]

$$f_{\gamma_1}(\gamma_1) = \frac{1}{\overline{\gamma}_1} \exp\left(-\frac{\gamma_1}{\overline{\gamma}_1}\right), \tag{7.1}$$

such that $\overline{\gamma}_1$ is the average SNR. On the other hand, the FSO link (R∼D) is assumed to experience turbulence induced fading with the impact of pointing errors whose SNR PDF $f_{\gamma_2 1}(\gamma_2)$is given in (3.10). As a result, the end-to-end SNR, γ of the dual-hop fixed gain transmission system cane be given as [56, 101, 108]

$$\gamma = \frac{\gamma_1 \gamma_2}{\gamma_2 + G}, \tag{7.2}$$

such that G is a fixed relay gain.

7.3.2 Statistical Properties

In this section, we derive the statistics of the end-to-end SNR, γ.

7.3.2.1 Cumulative Distribution Function

The CDF of γ is defined as [108]

$$\begin{aligned} F_\gamma(\gamma) &= \Pr\left[\frac{\gamma_1 \gamma_2}{\gamma_2 + G} < \gamma\right], \\ &= \int_0^\infty \Pr\left[\frac{\gamma_1 \gamma_2}{\gamma_2 + G} < \gamma \,\middle|\, \gamma_2\right] f_{\gamma_2}(\gamma_2)\, d\gamma_2, \\ &= 1 - \exp\left(-\frac{\gamma}{\overline{\gamma}_1}\right) \int_0^\infty \exp\left(-\frac{\gamma\, G}{\overline{\gamma}_1 \gamma_2}\right) f_{\gamma_2}(\gamma_2)\, d\gamma_2. \end{aligned} \tag{7.3}$$

Utilizing [44, Eq. (07.34.03.0228.01)] along with [43, Eq. (9.31.2)] to express the exponential function in terms of the Meijer's G-function as

$$\exp\left(-\frac{\gamma\, G}{\overline{\gamma}_1\gamma_2}\right) = \mathrm{G}_{1,0}^{0,1}\left(\frac{\overline{\gamma}_1\gamma_2}{\gamma\, G}\middle|\begin{matrix}1\\ -\end{matrix}\right), \tag{7.4}$$

and then applying it on [44, Eq. (07.34.21.0013.01)], the CDF of γ can be expressed as

$$F_\gamma(\gamma) = 1 - A_3 \exp\left(-\frac{\gamma}{\overline{\gamma}_1}\right) \mathrm{G}_{r,u+v}^{u+v,0}\left(C\left(\frac{\gamma\, G}{v\mu_{2,r}\overline{\gamma}_1}\right)^v \middle|\begin{matrix}\kappa_3\\ \kappa_4, \Delta(v:0)\end{matrix}\right), \tag{7.5}$$

where

$$A_3 = \frac{\xi^2\sigma^{\beta_1-1/2}\lambda^{\beta_2-1/2}(2\pi)^{\frac{3-r(\lambda+\sigma)-\alpha_2\lambda}{2}} r^{\beta_1+\beta_2-2}}{\sqrt{\alpha_2\lambda}\Gamma(\beta_1)\Gamma(\beta_2)}. \tag{7.6}$$

The CDF can be expressed at high SNR as

$$F_\gamma(\gamma) \underset{\mu_r\gg 1}{\approxeq} 1 - A_3 \exp\left(-\frac{\gamma}{\overline{\gamma}_1}\right) \sum_{k=1}^{u+v}\left[C^{-1}\left(\frac{v\mu_{2,r}\overline{\gamma}_1}{\gamma\, G}\right)^v\right]^{-\kappa_{8,k}} \frac{\prod_{l=1,l\neq k}^{u+v}\Gamma\left(\kappa_{8,l}-\kappa_{8,k}\right)}{\prod_{l=1}^{r}\Gamma\left(\kappa_{3,l}-\kappa_{8,k}\right)}, \tag{7.7}$$

where $\kappa_8 = \kappa_4, \Delta(v:0)$. In the case of the relay link, the dominant terms for (7.7) and for the asymptotic expressions derived ahead are dominated by the summation of two terms. The first term corresponds to $\min\left(\frac{\xi^2}{rv}, \frac{\beta_1}{r\sigma}, \frac{\beta_2}{r\lambda}, \frac{\epsilon}{v}\right)$ while the second term corresponds to $\frac{\epsilon+v-1}{v}$ that is the $(u+v)^{th}$ term in κ_8.

7.3.2.2 Probability Density Function

The PDF is obtained by differentiating (7.5) with respect to γ, using the product rule, and then utilizing [44, Eq. (07.34.20.0002.01)] as

$$f_\gamma(\gamma) = \exp\left(-\frac{\gamma}{\overline{\gamma}_1}\right)\left(\frac{A_3}{\overline{\gamma}_1}\mathrm{G}^{u+v,0}_{r,u+v}\left(C\left(\frac{\gamma\, G}{v\mu_{2,r}\overline{\gamma}_1}\right)^v \middle| \begin{matrix} \kappa_3 \\ \kappa_4, \Delta(v:0) \end{matrix}\right)\right.$$
$$\left. -\frac{A_3 v}{\gamma}\mathrm{G}^{u+v,1}_{r+1,m+n+1}\left(C\left(\frac{\gamma\, G}{v\mu_{2,r}\overline{\gamma}_1}\right)^v \middle| \begin{matrix} 0, \kappa_3 \\ \kappa_4, \Delta(v:0), 1 \end{matrix}\right)\right). \qquad (7.8)$$

7.3.2.3 Moment Generating Function

Substituting (7.5) in (3.17) and utilizing [44, Eq. (07.34.21.0088.01)], the MGF can be expressed as

$$\mathcal{M}_\gamma(s) = 1 - \frac{s\xi^2\sigma^{\beta_1-1/2}\lambda^{\beta_2-1/2}(2\pi)^{\frac{4-r(\lambda+\sigma)-2\alpha_2\lambda}{2}}r^{\beta_1+\beta_2-2}}{(1/\overline{\gamma}_1+s)\Gamma(\beta_1)\Gamma(\beta_2)}$$
$$\times\, \mathrm{G}^{u+v,v}_{r+v,u+v}\left(C\left(\frac{G}{(1/\overline{\gamma}_1+s)\mu_{2,r}\overline{\gamma}_1}\right)^v \middle| \begin{matrix} \Delta(v:0), \kappa_3 \\ \kappa_4, \Delta(v:0) \end{matrix}\right). \qquad (7.9)$$

Using the asymptotic expansion of the Meijer's G-function (3.14), the MGF can be approximated at **high SNR** with

$$\mathcal{M}_\gamma(s) \underset{\mu_r \gg 1}{\approxeq} 1 - \frac{\sigma^{\beta_1-1/2}\lambda^{\beta_2-1/2}(2\pi)^{\frac{4-r(\lambda+\sigma)-2\alpha_2\lambda}{2}}r^{\beta_1+\beta_2-2}}{\xi^{-2}s^{-1}(1/\overline{\gamma}_1+s)\Gamma(\beta_1)\Gamma(\beta_2)}$$
$$\times \sum_{k=1}^{u+v}\left[C^{-1}\left(\frac{(1/\overline{\gamma}_1+s)\mu_{2,r}\overline{\gamma}_1}{G}\right)^v\right]^{-\kappa_{8,k}} \frac{\prod_{l=1,l\neq k}^{u+v}\Gamma\left(\kappa_{8,l}-\kappa_{8,k}\right)\prod_{l=1}^{v}\Gamma\left(\{\Delta(v:1)\}_l+\kappa_{8,k}\right)}{\prod_{l=1}^{r}\Gamma\left(\kappa_{3,l}-\kappa_{8,k}\right)}.$$
$$(7.10)$$

7.3.2.4 Moments

The moments is defined as (3.20) can be expressed in terms of the complementary CDF, $F_{\gamma}^{c}(\gamma) = 1 - F_{\gamma}(\gamma)$ as

$$\mathbb{E}[\gamma^n] \triangleq n \int_0^{\infty} \gamma^{n-1} F_{\gamma}^{c}(\gamma) d\gamma. \tag{7.11}$$

By using this definition (7.11) and placing the complementary of (7.5) into it, we obtain the moments after utilizing [44, Eq. (07.34.21.0088.01)] as

$$\mathbb{E}[\gamma^n] = \frac{\overline{\gamma}_1^n n \xi^2 \sigma^{\beta_1 - 1/2} \lambda^{\beta_2 - 1/2} (2\pi)^{\frac{4 - r(\lambda+\sigma) - 2\alpha_2 \lambda}{2}} r^{\beta_1 + \beta_2 - 2}}{(\alpha_2 \lambda)^{1-n} \Gamma(\beta_1) \Gamma(\beta_2)} \mathrm{G}_{r+v, u+v}^{u+v, v} \left(C \left(\frac{G}{\mu_{2,r}} \right)^{v} \middle| \begin{matrix} \Delta(v : 1-n), \kappa_3 \\ \kappa_4, \Delta(v : 0) \end{matrix} \right). \tag{7.12}$$

Using again the asymptotic expansion of the Meijer's function (3.14), we can express (7.12) asymptotically at high SNR as

$$\begin{aligned} \mathbb{E}[\gamma^n] \underset{\mu_r \gg 1}{\approxeq} & \frac{\overline{\gamma}_1^n n \xi^2 \sigma^{\beta_1 - 1/2} \lambda^{\beta_2 - 1/2} (2\pi)^{\frac{4 - r(\lambda+\sigma) - 2\alpha_2 \lambda}{2}} r^{\beta_1 + \beta_2 - 2}}{(\alpha_2 \lambda)^{1-n} \Gamma(\beta_1) \Gamma(\beta_2)} \sum_{k=1}^{u+v} \left[C^{-1} \left(\frac{\mu_{2,r}}{G} \right)^{v} \right]^{-\kappa_{8,k}} \\ & \times \frac{\prod_{l=1, l \neq k}^{u+v} \Gamma\left(\kappa_{8,l} - \kappa_{8,k}\right) \prod_{l=1}^{v} \Gamma\left(\{\Delta(v : n)\}_l + \kappa_{8,k}\right)}{\prod_{l=1}^{r} \Gamma\left(\kappa_{3,l} - \kappa_{8,k}\right)}. \end{aligned} \tag{7.13}$$

7.3.3 Performance Metrics

In this section, we evaluate the performance measures of the dual-hop RF-FSO relay transmission system.

7.3.3.1 Outage Probability

The outage probability is obtained by substituting (7.5) into (3.22).

7.3.3.2 Average Bit Error Rate

Placing (7.5) into (3.28) and utilizing [44, Eq. (07.34.21.0088.01)], we obtain $\overline{P}_b$ as

$$\begin{aligned}\overline{P}_b = {} & \frac{1}{2} - \frac{q^p \xi^2 \sigma^{\beta_1-1/2} \lambda^{\beta_2-1/2} (2\pi)^{\frac{4-r(\lambda+\sigma)-2\alpha_2\lambda}{2}} r^{\beta_1+\beta_2-2}}{2(\alpha_2\lambda)^{1-p}(1/\overline{\gamma}_1+q)^p \Gamma(\beta_1)\Gamma(\beta_2)\Gamma(p)} \\ & \times \mathrm{G}^{u+v,v}_{r+v,u+v}\left(C\left(\frac{G}{(1/\overline{\gamma}_1+q)\mu_{2,r}\overline{\gamma}_1}\right)^v \middle| \begin{matrix} \Delta(v:1-p),\kappa_3 \\ \kappa_4,\Delta(v:0) \end{matrix} \right).\end{aligned} \tag{7.14}$$

$\overline{P}_b$ can be expressed at **high SNR** as

$$\begin{aligned}\overline{P}_b \underset{\mu_r \gg 1}{\approxeq} {} & \frac{1}{2} - \frac{q^p \xi^2 \sigma^{\beta_1-1/2} \lambda^{\beta_2-1/2} (2\pi)^{\frac{4-r(\lambda+\sigma)-2\alpha_2\lambda}{2}} r^{\beta_1+\beta_2-2}}{2(\alpha_2\lambda)^{1-p}(1/\overline{\gamma}_1+q)^p \Gamma(\beta_1)\Gamma(\beta_2)\Gamma(p)} \\ & \times \sum_{k=1}^{u+v} \left[C^{-1} \left(\frac{(1/\overline{\gamma}_1+q)\mu_{2,r}\overline{\gamma}_1}{G} \right)^v \right]^{-\kappa_{8,k}} \\ & \times \frac{\prod_{l=1,l\neq k}^{u+v} \Gamma\left(\kappa_{8,l}-\kappa_{8,k}\right) \prod_{l=1}^{v} \Gamma\left(\{\Delta(v:p)\}_l + \kappa_{8,k}\right)}{\prod_{l=1}^{r} \Gamma\left(\kappa_{3,l}-\kappa_{8,k}\right)}.\end{aligned} \tag{7.15}$$

7.3.3.3 Ergodic Capacity

The ergodic capacity in (3.36) can be expressed in terms of the complementary CDF [109, Eq. (15)] as

$$\overline{C} = \int_0^\infty \frac{1}{\ln(2)} (1+\delta\gamma)^{-1} F_\gamma^c(\gamma) d\gamma. \tag{7.16}$$

We utilize the identities [44, Eq. (07.34.03.0271.01), Eq. (07.34.03.0228.01)] to express $(1+\delta\gamma)^{-1}$ and $\exp(\gamma/\overline{\gamma}_1)$ in terms of the Meijer's G-function, respectively. Next, to solve the integral with the product of three G-functions, we transformed each term into the Fox H-function [110] using [44, Eq. (07.34.26.0008.01)] and then we use the identity [92, Eq. (2.3)] to obtain $\overline{C}$ in terms of the H-function of two variables [92, Eq.

(1.1)]

$$\overline{C} = \frac{A_3 \delta \overline{\gamma}_1}{\ln(2) v} \mathrm{H}^{0,1:1,1:u+v,0}_{1,0:1,1:r,u+v} \left[\begin{array}{c|c|c|c} (0;1,1) & (0,1) & (\kappa_3,[(v)^{-1}]_r) & \\ & & & \delta\overline{\gamma}_1, \frac{GC^{1/v}}{v\mu_{2,r}},, \\ - & (0,1) & (\kappa_8,[(v)^{-1}]_{u+v}) & \end{array} \right] \tag{7.17}$$

where $[x]_i = x, x, \ldots x$, comprising of i terms and $\mathrm{H}^{-,-:-,-:-,-}_{-,-:-,-:-,-}[.]$ is another form of the bivariate H-function.

In addition, we can obtain an asymptotic expression of the ergodic capacity utilizing the expansion of the Meijer's G-function. In other words, exploiting the asymptotic expression of the CDF in (7.7) to be then inserted in (7.16) leading to

$$\begin{aligned} \overline{C} \underset{\mu_r \gg 1}{\approxeq} & \frac{A_3}{\ln(2)} \exp\left(\frac{1}{\delta\overline{\gamma}_1}\right) \sum_{k=1}^{u+v} C^{\kappa_{8,k}} \left(\frac{G}{v\delta\overline{\gamma}_1\mu_{2,r}}\right)^{v\kappa_{8,k}} \mathbf{\Gamma}(-v\kappa_{8,k}, 1/\delta\overline{\gamma}) \\ & \times \frac{\prod_{l=1, l\neq k}^{u+v} \Gamma\left(\kappa_{8,l} - \kappa_{8,k}\right) \Gamma(1+\kappa_{8,k})}{\prod_{l=1}^{r} \Gamma\left(\kappa_{3,l} - \kappa_{8,k}\right)}, \end{aligned} \tag{7.18}$$

where $\mathbf{\Gamma}(.,.)$ is the upper incomplete Gamma function.

7.4 FSO-FSO Variable Gain Dual-Hop Transmission Systems

7.4.1 System Model

In this section, we present the performance analysis of symmetric dual-hop FSO variable gain relay transmission system over double GG fading and under the impact of pointing error. The end-to-end SNR of the system is known to be given by

$$\gamma = \frac{\gamma_1 \gamma_2}{1 + \gamma_1 + \gamma_2}, \tag{7.19}$$

where γ_1 and γ_2 corresponds to the SNR of S$\sim$R and R$\sim$D links, respectively. The definition of the SNR in (7.19) is mathematically not easy to handle. Therefore, it is typically approximated by [104]

$$\gamma_m \simeq \min(\gamma_1, \gamma_2), \tag{7.20}$$

such that the statistics if γ_1 and γ_2 can be found in Sec. 3.3.

7.4.2 Statistical Properties

In this section, we list the statistical properties of the minimum of two modified double generalized gamma random variables, γ_{m}.

7.4.2.1 Cumulative Distribution Function

The CDF of the minimum of two random variables is given by

$$\begin{aligned} F_{\gamma_{\mathrm{m}}}(\gamma) &= 1 - \Pr(\min(\gamma_1, \gamma_2) > \gamma) \\ &= 1 - \Pr\left(\gamma_1 > \gamma \text{ and } \gamma_2 > \gamma\right) \\ &= 1 - \Pr\left(\gamma_1 > \gamma\right)\Pr\left(\gamma_2 > \gamma\right) \\ &= 1 - \left(1 - \Pr\left(\gamma_1 < \gamma\right)\right)\Pr\left(1 - \left(\gamma_2 < \gamma\right)\right) \\ &= 1 - \left(1 - F_{\gamma_1}(\gamma)\right)\left(1 - F_{\gamma_2}(\gamma)\right) \\ &= F_{\gamma_1}(\gamma) + F_{\gamma_2}(\gamma) - F_{\gamma_1}(\gamma)F_{\gamma_2}(\gamma), \end{aligned} \tag{7.21}$$

under the assumption that γ_1 and γ_2 are i.n.i.d. Substituting (3.13) in (7.21), the follwoing result is obtained

$$F_{\gamma_{\mathrm{m}}}(\gamma) = A_{3a}\mathrm{G}^{u_a,1}_{r_a+1,u_a+1}\left(C_a\left(\frac{\gamma}{\mu_{r_a,a}}\right)^{v_a}\middle|\begin{matrix}1,\kappa_{3a}\\ \\ \kappa_{4a},0\end{matrix}\right) + A_{3b}\mathrm{G}^{u_b,1}_{r_b+1,u_b+1}\left(C_b\left(\frac{\gamma}{\mu_{r_b,b}}\right)^{v_b}\middle|\begin{matrix}1,\kappa_{3b}\\ \\ \kappa_{4b},0\end{matrix}\right)$$
$$- A_{3a}A_{3b}\mathrm{G}^{u_a,1}_{r_a+1,u_a+1}\left(C_a\left(\frac{\gamma}{\mu_{r_a,a}}\right)^{v_a}\middle|\begin{matrix}1,\kappa_{3a}\\ \\ \kappa_{4a},0\end{matrix}\right)\mathrm{G}^{u_b,1}_{r_b+1,u_b+1}\left(C_b\left(\frac{\gamma}{\mu_{r_b,b}}\right)^{v_b}\middle|\begin{matrix}1,\kappa_{3b}\\ \\ \kappa_{4b},0\end{matrix}\right). \tag{7.22}$$

In addition, an asymptotic expression can be obtained via the expansion of the Meijer's G function as

$$\tilde{F}_{\gamma_{\mathrm{m}}}(\gamma) \underset{\mu_{r_i,i}>>1}{\approxeq} A_{3a}\sum_{k=1}^{u_a}\left(\frac{\gamma^{v_a}C_a}{\mu^{v_a}_{r_a,a}}\right)^{\kappa_{4a,k}}\frac{\prod_{l=1;l\neq k}^{u_a}\Gamma(\kappa_{4a,l}-\kappa_{4a,k})}{\kappa_{4a,k}\prod_{l=1}^{r_a}\Gamma(\kappa_{3a,l}-\kappa_{4a,k})}$$
$$+ A_{3b}\sum_{x=1}^{u_b}\left(\frac{\gamma^{v_b}C_b}{\mu^{v_b}_{r_b,b}}\right)^{\kappa_{4b,x}}\frac{\prod_{l=1;l\neq x}^{u_b}\Gamma(\kappa_{4b,l}-\kappa_{4b,x})}{\kappa_{4b,x}\prod_{l=1}^{r_b}\Gamma(\kappa_{3b,l}-\kappa_{4b,x})} - \tilde{F}_{\gamma_{\mathrm{M}}}(\gamma), \tag{7.23}$$

where $\tilde{F}_{\gamma_{\mathrm{M}}}(\gamma)$ is defined in (6.5).

7.4.2.2 Probability Density Function

Differentiating (7.22) with respect to γ, a closed-form expression of the PDF of γ_{m} is obtained as

$$f_{\gamma_{\mathrm{m}}}(\gamma) = \frac{A_{3a}}{\gamma}v_a\mathrm{G}^{u_a,0}_{r_a,u_a}\left(C_a\left(\frac{\gamma}{\mu_{r_a,a}}\right)^{v_a}\middle|\begin{matrix}\kappa_{3a}\\ \\ \kappa_{4a}\end{matrix}\right) + \frac{A_{3b}}{\gamma}v_b\mathrm{G}^{u_b,0}_{r_b,u_b}\left(C_b\left(\frac{\gamma}{\mu_{r_b,b}}\right)^{v_b}\middle|\begin{matrix}\kappa_{3b}\\ \\ \kappa_{4b}\end{matrix}\right) - f_{\gamma_M}(\gamma), \tag{7.24}$$

where $f_{\gamma_{\mathrm{M}}}(\gamma)$ is defined in (6.7). Monte-Carlo simulations were utilized to verify the PDF as in Fig. 7.1.

Similarly, an asymptotic expression of the PDF can be obtained when expanding

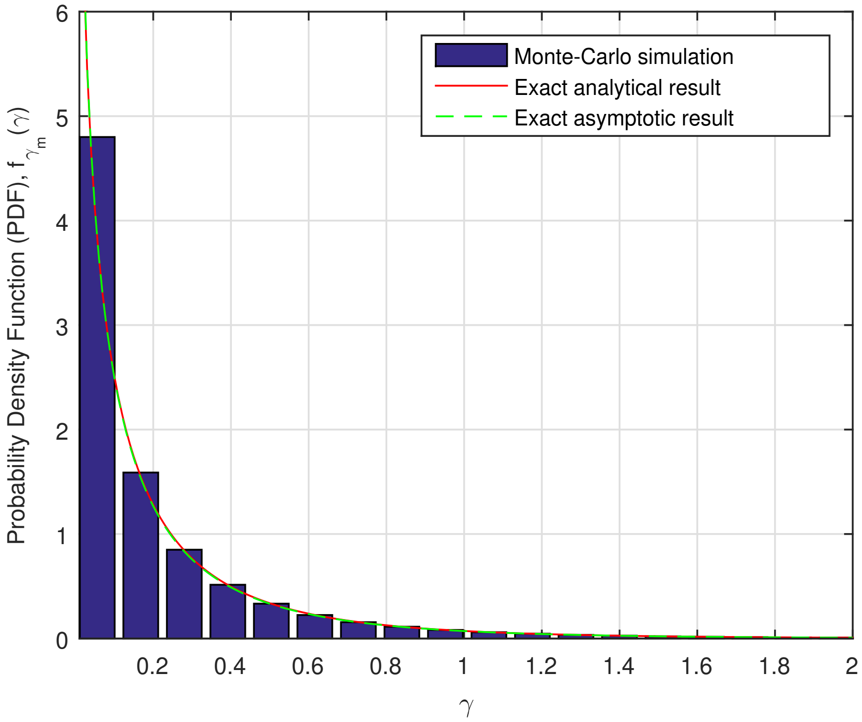

Figure 7.1: PDF validation for the minimum of two double GG variates

the Meijer's G-function leading to

$$\begin{aligned}\tilde{f}_{\gamma_{\mathrm{m}}}(\gamma) \underset{\mu_{r_i,i}>>1}{\approxeq} & A_{3a}v_a \sum_{k=1}^{u_a} \left(\frac{C_a}{\mu_{r_a,a}^{v_a}}\right)^{\kappa_{4a,k}} \frac{\prod_{l=1;l\neq k}^{u_a} \Gamma(\kappa_{4a,l}-\kappa_{4a,k})}{\prod_{l=1}^{r_a} \Gamma(\kappa_{3a,l}-\kappa_{4a,k})} \gamma^{v_a \kappa_{4a,k}-1} \\ & + A_{3b}v_b \sum_{x=1}^{u_b} \left(\frac{C_b}{\mu_{r_b,b}^{v_b}}\right)^{\kappa_{4b,x}} \frac{\prod_{l=1;l\neq x}^{u_b} \Gamma(\kappa_{4b,l}-\kappa_{4b,x})}{\prod_{l=1}^{r_b} \Gamma(\kappa_{3b,l}-\kappa_{4b,x})} \gamma^{v_b \kappa_{4b,x}-1} - \tilde{f}_{\gamma_{\mathrm{M}}}(\gamma), \qquad (7.25)\end{aligned}$$

where $\tilde{f}_{\gamma_{\mathrm{M}}}(\gamma)$ is defined in (6.7).

7.4.2.3 Moment Generating Function

Placing (7.22) in the definition of the MGF (3.17), and utilizing Eq. (6.10) and [44, Eq. (07.34.21.0088.01)], the MGF can be expressed as

$$\begin{aligned}\mathcal{M}_{\gamma_{\mathrm{m}}}(s) = {} & \frac{A_{3a}\sqrt{v_a}}{(2\pi)^{\frac{v_a-1}{2}}}\,\mathrm{G}^{u_a,v_a}_{r_a+v_a,u_a}\left(C_a\left(\frac{v_a}{s\mu_{r_a,a}}\right)^{v_a}\,\middle|\,\begin{matrix}\Delta(v_a,1),\kappa_{3a}\\ \kappa_{4a}\end{matrix}\right)\\ & + \frac{A_{3b}\sqrt{v_b}}{(2\pi)^{\frac{v_b-1}{2}}}\,\mathrm{G}^{u_b,v_b}_{r_b+v_b,u_b}\left(C_b\left(\frac{v_b}{s\mu_{r_b,b}}\right)^{v_b}\,\middle|\,\begin{matrix}\Delta(v_b,1),\kappa_{3b}\\ \kappa_{4b}\end{matrix}\right) - \mathcal{M}_{\gamma_{\mathrm{M}}}(s).\end{aligned} \tag{7.26}$$

More simplified expression for the MGF can be obtained if the expansion of the Meijer's G-function (3.14) was utilized as follows

$$\begin{aligned}\tilde{\mathcal{M}}_{\gamma_{\mathrm{m}}}(s) \underset{\mu_{r_i,i}>>1}{\approxeq} {} & A_{3a}v_a\sum_{k=1}^{u_a}\left(\frac{C_a}{(s\mu_{r_a,a})^{v_a}}\right)^{\kappa_{4a,k}}\frac{\Gamma(v_a\kappa_{4a,k})\prod_{l=1;l\neq k}^{u_a}\Gamma(\kappa_{4a,l}-\kappa_{4a,k})}{\prod_{l=1}^{r_a}\Gamma(\kappa_{3a,l}-\kappa_{4a,k})}\\ & + A_{3b}v_b\sum_{x=1}^{u_b}\left(\frac{C_b}{(s\mu_{r_b,b})^{v_b}}\right)^{\kappa_{4b,x}}\frac{\Gamma(v_b\kappa_{4b,x})\prod_{l=1;l\neq x}^{u_b}\Gamma(\kappa_{4b,l}-\kappa_{4b,x})}{\prod_{l=1}^{r_b}\Gamma(\kappa_{3b,l}-\kappa_{4b,x})} - \tilde{\mathcal{M}}_{\gamma_{\mathrm{M}}}(s),\end{aligned} \tag{7.27}$$

where $\tilde{\mathcal{M}}_{\gamma_{\mathrm{M}}}(s)$ is defined in (6.11). The MGF for Gamma-Gamma model can be obtained by setting the same parameters listed in Sec.

$$\begin{aligned}\mathcal{M}^{*}_{\gamma_{\mathrm{m}}}(s) = {} & A_{3a}\mathrm{G}^{3r_a,1}_{r_a+1,3r_a}\left(\frac{C_a}{s\mu_{r_a,a}}\,\middle|\,\begin{matrix}1,\kappa_{3a}\\ \kappa_{4a}\end{matrix}\right) + A_{3b}\,\mathrm{G}^{3r_b,1}_{r_b+1,3r_b}\left(\frac{C_b}{s\mu_{r_b,b}}\,\middle|\,\begin{matrix}1,\kappa_{3b}\\ \kappa_{4b}\end{matrix}\right)\\ & - A_{3a}A_{3b}\times\mathrm{G}^{1,0:3r_a,1:3r_b,1}_{1,0:r_a+1,3r_a+1:r_b+1,3r_b+1}\left[\begin{matrix}1\\ -\end{matrix}\middle|\begin{matrix}\kappa_{5a}\\ \kappa_{6a}\end{matrix}\middle|\begin{matrix}\kappa_{5b}\\ \kappa_{6b}\end{matrix}\middle|\frac{C_a}{s\mu_{r_a,a}},\frac{C_b}{s\mu_{r_b,b}}\right].\end{aligned} \tag{7.28}$$

7.4.2.4 Moments

Substituting (7.24) in the definition of the moments (3.20) and utilizing [44, Eq. (2.25.2.1)] and Eq. (6.13), the moments is obtained as

$$\mathbb{E}[\gamma_{\mathrm{m}}^{n}] = A_{3a}\left(\frac{\mu_{r_a,a}}{C_a^{1/v_a}}\right)^{n}\Gamma\left(\begin{matrix}\kappa_{4a}+\frac{n}{v_a}\\ \\ \kappa_{3a}+\frac{n}{v_a}\end{matrix}\right)+A_{3b}\left(\frac{\mu_{r_b,b}}{C_b^{1/v_b}}\right)^{n}\Gamma\left(\begin{matrix}\kappa_{4b}+\frac{n}{v_b}\\ \\ \kappa_{3b}+\frac{n}{v_b}\end{matrix}\right)-\mathbb{E}[\gamma_{\mathrm{M}}^{n}], \quad (7.29)$$

where $\mathbb{E}[\gamma_{\mathrm{M}}^{n}]$ is defined in (6.13) and $\Gamma\left(\begin{matrix}\mathbf{x}\\ \\ \mathbf{y}\end{matrix}\right)=\prod_{i=1}^{m}\Gamma(x_i)/\prod_{i=1}^{n}\Gamma(y_i)$ such that m and n are the lengths of x and y, respectively.

In the Gamma-Gamma case, (7.29) simplifies to

$$\begin{aligned}\mathbb{E}[\gamma_{m}^{n}]^{*} &= A_{3a}\left(\frac{\mu_{r_a,a}}{C_a^{1/v_a}}\right)^{n}\Gamma\left(\begin{matrix}\kappa_{4a}+n\\ \\ \kappa_{3a}+n\end{matrix}\right)+A_{3b}\left(\frac{\mu_{r_b,b}}{C_b^{1/v_b}}\right)^{n}\Gamma\left(\begin{matrix}\kappa_{4b}+n\\ \\ \kappa_{3b}+n\end{matrix}\right)\\ &- A_{3a}A_{3b}\left[\left(\frac{\mu_{r_a,a}}{C_a}\right)^{n}\mathrm{G}_{3r_a+r_b+1,3r_b+r_a+1}^{3r_b+1,3r_a}\left(\frac{C_b\mu_{r_a,a}}{C_a\mu_{r_b,b}}\left|\begin{matrix}\kappa_{7a},\kappa_{3b}\\ \\ \kappa_{4b},\kappa_{8a}\end{matrix}\right.\right)\right.\\ &+\left.\left(\frac{\mu_{r_b,b}}{C_b}\right)^{n}\mathrm{G}_{3r_b+r_a+1,3r_a+r_b+1}^{3r_a+1,3r_b}\left(\frac{C_a\mu_{r_b,b}}{C_b\mu_{r_a,a}}\left|\begin{matrix}\kappa_{7b},\kappa_{3a}\\ \\ \kappa_{4a},\kappa_{8b}\end{matrix}\right.\right)\right]. \quad (7.30)\end{aligned}$$

as found in [90, Eq. (16)].

7.4.3 Performance Measures

In this section, we present the performance analysis of a dual-hop FSO variable gain relay transmission systems.

7.4.3.1 Outage Probability

The outage probability of the system is obtained by substituting (7.22) into (3.22).

7.4.3.2 Average Bit Error Rate

$\overline{P}_b$ is obtained by placing (7.22) into (3.28), and utilizing (6.15) and [59, Eq. (20)] yielding

$$\overline{P}_b = \frac{A_{3a} v_a^{p-1/2}}{2\Gamma(p)(2\pi)^{\frac{v_a-1}{2}}} \mathrm{G}_{r_a+v_a+1,u_a+1}^{u_a,v_a+1}\left(C_a \left(\frac{v_a}{q\mu_{r_a,a}} \right)^{v_a} \middle| \begin{matrix} \Delta(v_a, 1-p), \kappa_{5a} \\ \kappa_{6a} \end{matrix} \right)$$

$$+ \frac{A_{3b} v_b^{p-1/2}}{2\Gamma(p)(2\pi)^{\frac{v_b-1}{2}}} \mathrm{G}_{r_b+v_b+1,u_b+1}^{u_b,v_b+1}\left(C_b \left(\frac{v_b}{q\mu_{r_b,b}} \right)^{v_b} \middle| \begin{matrix} \Delta(v_b, 1-p), \kappa_{5b} \\ \kappa_{6b} \end{matrix} \right) - \overline{P}_{\mathrm{SC}}. \qquad (7.31)$$

Furthermore, an asymptotic expression of the BER via Meijer's G-function expansion (3.14) is obtained by solving (6.16) as follows

$$\overline{P}_{DH} \underset{\mu_{r_i,i}>>1}{\approxeq} \frac{A_{3a}}{2\Gamma(p)} \sum_{k=1}^{u_a} \left(\frac{C_a}{(q\mu_{r_a,a})^{v_a}} \right)^{\kappa_{4a,k}} \frac{\Gamma(v_a\kappa_{4a,k}+p)\prod_{l=1;l\neq k}^{u_a}\Gamma(\kappa_{4a,l}-\kappa_{4a,k})}{\kappa_{4a,k}\prod_{l=1}^{r_a}\Gamma(\kappa_{3a,l}-\kappa_{4a,k})}$$

$$+ \frac{A_{3b}}{2\Gamma(p)} \sum_{x=1}^{u_b} \left(\frac{C_b}{q\mu_{r_b,b}{}^{v_b}} \right)^{\kappa_{4b,x}} \frac{\Gamma(v_b\kappa_{4b,x}+p)\prod_{l=1;l\neq x}^{u_b}\Gamma(\kappa_{4b,l}-\kappa_{4b,x})}{\kappa_{4b,x}\prod_{l=1}^{r_b}\Gamma(\kappa_{3b,l}-\kappa_{4b,x})} - \overline{P}_{SC}, \qquad (7.32)$$

where $\overline{P}_{SC}$ is defined in (6.15). In this case, diversity or coding can not be extracted due to the fact that the expression consists of 3 terms and can not be reduced to the form of (3.31).

For the case of Gamma-Gamma, we have

$$\overline{P}_{\mathrm{DH}}^{*} = \frac{A_{3a}}{2\Gamma(p)} \mathrm{G}_{r_a+2,3_a+1}^{3r_a,2}\left(\frac{C_a}{q\mu_{r_a,a}} \middle| \begin{matrix} 1-p, \kappa_{5a} \\ \kappa_{6a} \end{matrix} \right) + \frac{A_{3b}}{2\Gamma(p)} \mathrm{G}_{r_b+2,r_b u_b+1}^{3r_b,2}\left(\frac{C_b}{q\mu_{r_b,b}} \middle| \begin{matrix} 1-p, \kappa_{5b} \\ \kappa_{6b} \end{matrix} \right) - \overline{P}_{\mathrm{SC}}^{*}. \qquad (7.33)$$

7.4.3.3 Ergodic Capacity

Using (3.36), (3.37), along with the identities [111, Eq. (12)], and [44, Eq. (07.34.21.0011.01)], we obtain the ergodic capacity in closed- form as

$$\begin{aligned}\overline{C}_{\text{DH}} &= \frac{A_{3b}}{\ln(2)(2\pi)^{v_b-1}} \mathrm{G}_{r_b+2v_b,u_b+2v_b}^{u_b+2v_b,v_b}\left(\frac{C_b}{(\delta\mu_{r_b,b})^{v_b}}\,\middle|\,\begin{matrix}\kappa_{9b},\kappa_{3b}\\ \\ \kappa_{4b},\kappa_{10b}\end{matrix}\right)\\ &\quad+\frac{A_{3a}}{\ln(2)(2\pi)^{v_a-1}} \mathrm{G}_{r_a+2v_a,u_a+2v_a}^{u_a+2v_a,v_a}\left(\frac{C_a}{(\delta\mu_{r_a,a})^{v_a}}\,\middle|\,\begin{matrix}\kappa_{9a},\kappa_{3a}\\ \\ \kappa_{4a},\kappa_{10a}\end{matrix}\right)-\overline{C}_{\text{SC}}\,, \qquad (7.34)\end{aligned}$$

where $\kappa_{9i} = \Delta(v_i, 0), \Delta(v_i, 1)$ and $\kappa_{10i} = \Delta(v_i, 0), \Delta(v_i, 0)$.

For the special case of Gamma-Gamma, we have

$$\overline{C}^{*}_{\text{DH}} = \frac{A_{3b}}{\ln(2)} \mathrm{G}_{r_b+2,3r_b+2}^{3r_b+2,1}\left(\frac{C_b}{\delta\mu_{r_b,b}}\,\middle|\,\begin{matrix}0,1,\kappa_{3b}\\ \\ \kappa_{4b},0,0\end{matrix}\right)+\frac{A_{3a}}{\ln(2)} \mathrm{G}_{r_a+2,3r_a+2}^{3r_a+2,1}\left(\frac{C_a}{\delta\mu_{r_a,a}}\,\middle|\,\begin{matrix}0,1,\kappa_{3a}\\ \\ \kappa_{4a},0,0\end{matrix}\right)-\overline{C}^{*}_{\text{SC}}. \qquad (7.35)$$

7.5 Numerical Analysis

In this section, we validate our analytical results and compare it with computer-based Monte Carlo simulations. In fact, we present selected examples of the performance of the two proposed systems.

7.5.1 RF-FSO Fixed Gain Dual-Hop Transmission Systems

The outage probability of mixed RF-FSO dual-hop relay transmission system experiencing different turbulence conditions is presented in Figs. 7.2, 7.3, and 7.4 with varying ξ and r to show the impact of pointing errors and the detection technique. In Figs 7.2 and 7.3, the average SNR of the second link is fixed to $\mu_{r,2} = 27$ dB and the OP is evaluated with respect to the average SNR of the first link, $\overline{\gamma}_1$. It is observed

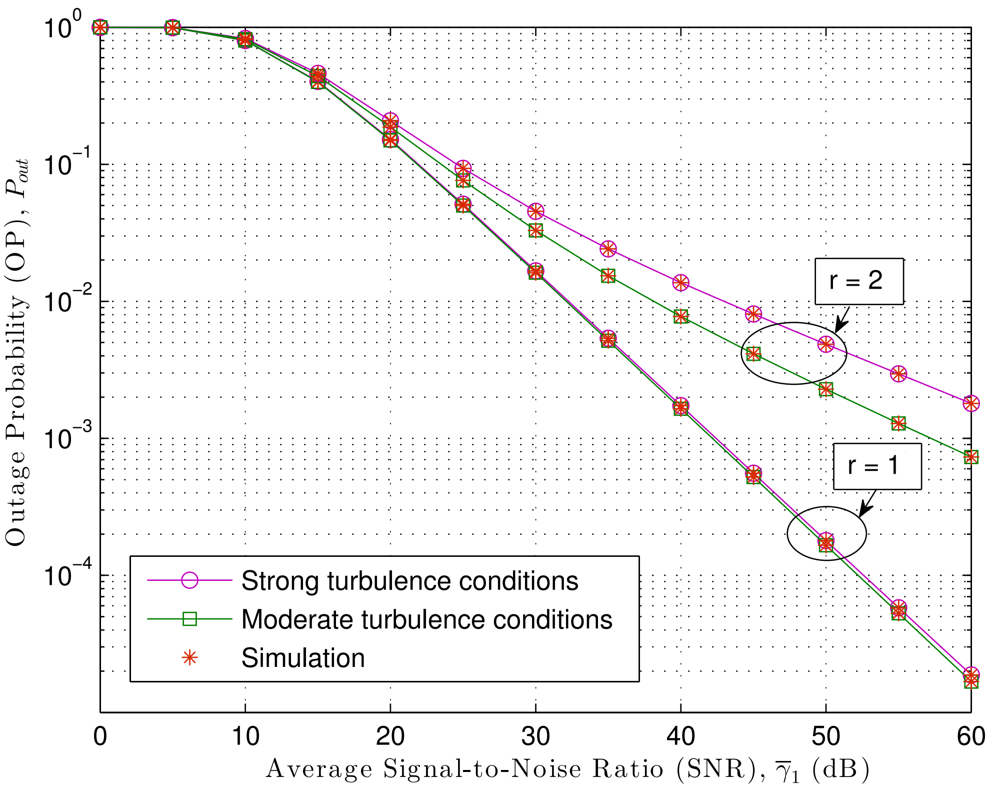

Figure 7.2: Outage probability of mixed RF-FSO system link under strong and moderate turbulence conditions for both detection techniques, heterodyne ($r = 1$) and IM/DD ($r = 2$) with $\xi = 1$.

that considering heterodyne detection for the FSO link leads to reduction in the OP of the system. Moreover, high effect of pointing errors results in higher outage of the system. In Fig. 7.4, however, the average SNR of the RF link is fixed as $\overline{\gamma}_1 \in \{20, 40\}$ dB and the average of the second link, $\mu_{2,2}$ is varied. It is shown that for lower $\overline{\gamma}_1$, the system saturates very fast and the asymptotic results converge fast as well.

Similarly, the average bit error rate performance under DBPSK modulation where $p = 1$ and $q = 1$ for RF-FSO dual hop relay was evaluated in Figs. 7.5, 7.6, and 7.7. More specifically, in Figs. 7.5 and 7.6, the BER is evaluated with respect to the first hop average SNR, $\overline{\gamma}_1$. As expected, utilizing heterodyne detection for the FSO link provides better error performance than if IM/DD is considered. Also, high pointing errors effect lowers the system performance. On the other hand, in Fig. 7.7, the BER

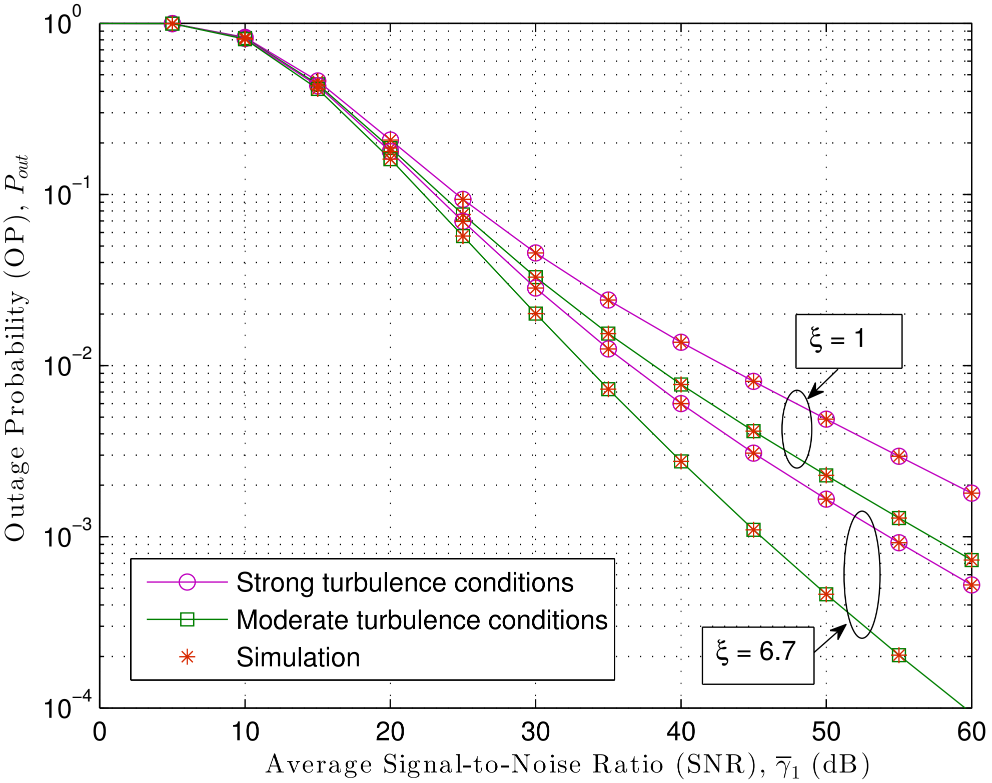

Figure 7.3: The impact of pointing errors on the outage probability of mixed FR-FSO relay link under strong and moderate turbulence conditions using IM/DD technique ($r = 2$) with varying pointing errors.

is evaluated with respect to $\mu_{2,2}$ along with asymptotic results. Similar to the OP, low values of $\overline{\gamma}_1$ leads to system saturation and better convergence for the asymptotic results (utilizing the dominant terms).

Furthermore, the ergodic capacity of mixed RF-FSO dual-hop system operating over double GG turbulence channel under the impact of pointing errors is evaluated in Figs. 7.8, 7.9, and 7.10. Specifically, in Figs. 7.8 and 7.9, the capacity is evaluated with respect to $\overline{\gamma_1}$. It is clear that heterodyne detection technique provides higher capacity than IM/DD. However, the capacity is still low when the pointing errors effect is high. Furthermore, in Fig. 7.10, we compare the capacity of the system for $\overline{\gamma}_1 = 20$ dB and $\overline{\gamma}_1 = 40$ dB. It is observed that higher $\overline{\gamma}_1$ yields better system capacity. Finally, in Figs. 7.8, 7.9, and 7.10, the asymptotic results based in all terms

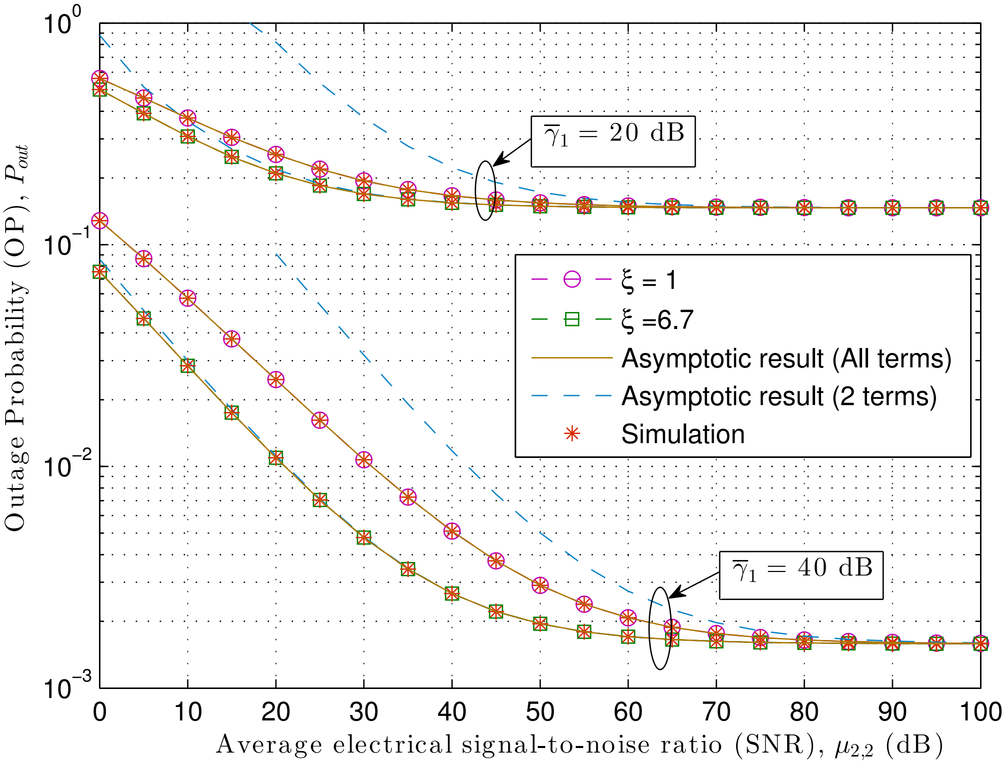

Figure 7.4: The impact of $\overline{\gamma}_1$ on the outage probability of mixed RF-FSO relay link under strong turbulence conditions using IM/DD technique ($r = 2$) with varying pointing errors.

as in Eq. (7.18) are presented. Interestingly, they perfectly agrees with the analytical results.

7.5.2 FSO-FSO Variable Gain Dual-Hop Transmission Systems

The BER over DPSK modulation and ergodic capacity of variable gain FSO relay systems Figs. 7.11 and 7.12. We had to compare the performance of a single FSO link that suffers both strong turbulence conditions and severe pointing errors with relay assisted link of RF-FSO and FSO-FSO experiencing moderate turbulence conditions with $\xi >> 1$. Clearly, relay links outperform the single link in addition to providing higher data rate. Moreover, the asymptotic analysis shows an excellent match with

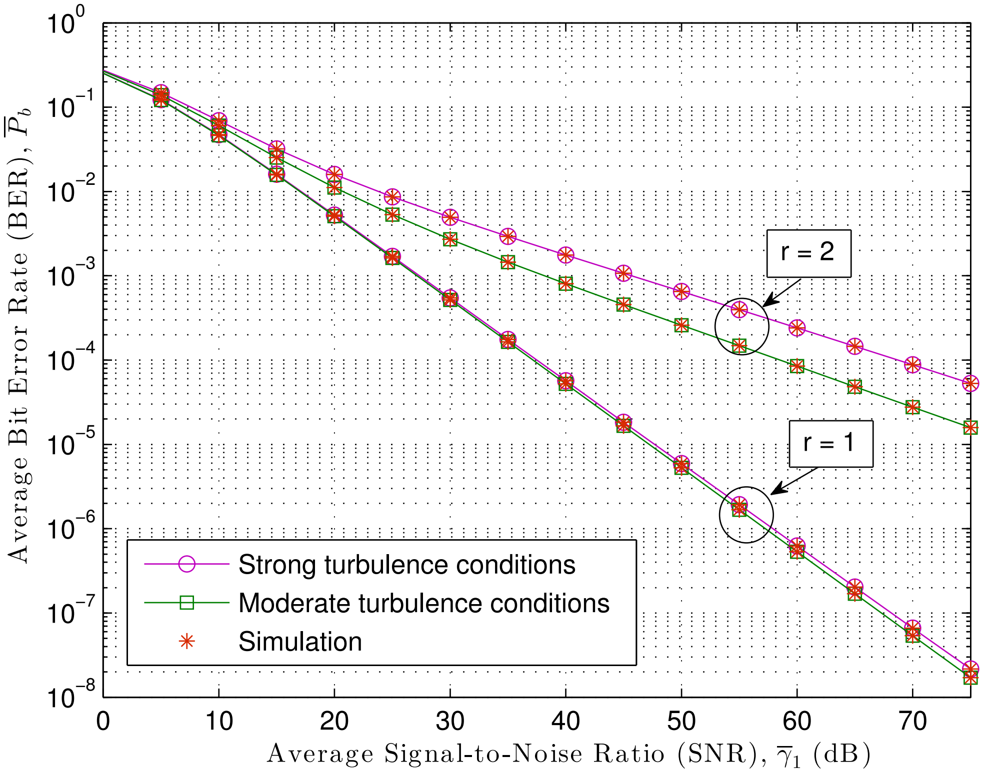

Figure 7.5: Average bit error rate of mixed RF-FSO relay link under strong and moderate turbulence conditions for both detection techniques, heterodyne ($r = 1$) and IM/DD ($r = 2$) with $\xi = 1$.

the exact results even for low SNR values (i.e starting at 20 dB).

7.6 Conclusion

Closed-form expressions for the CDF, the PDF, the MGF, and the moments of the end-to-end SNR of RF-FSO fixed gain and FSO-FSO variable gain dual-hop relaying systems were obtained. Furthermore, we developed analytical expressions for the average bit error rate and the ergodic capacity to evaluate the performance of both systems. Monte-Carlo computer simulations were carried out to validate our analytical results. Our results are expressed in terms of some special functions, however, relatively simple asymptotic limits at high SNR were provided. Finally, it can be concluded that relaying can be helpful in supporting FSO links.

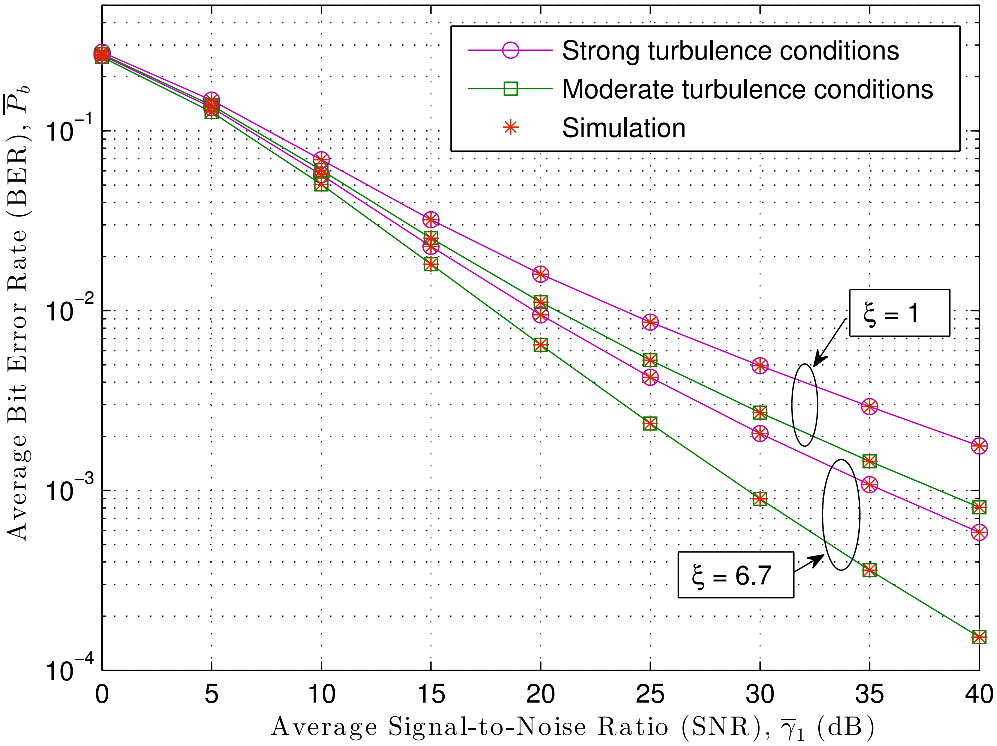

Figure 7.6: The impact of pointing errors on the average bit error rate of mixed RF-FSO relay link under strong and moderate turbulence conditions using IM/DD technique ($r = 2$) with varying pointing errors.

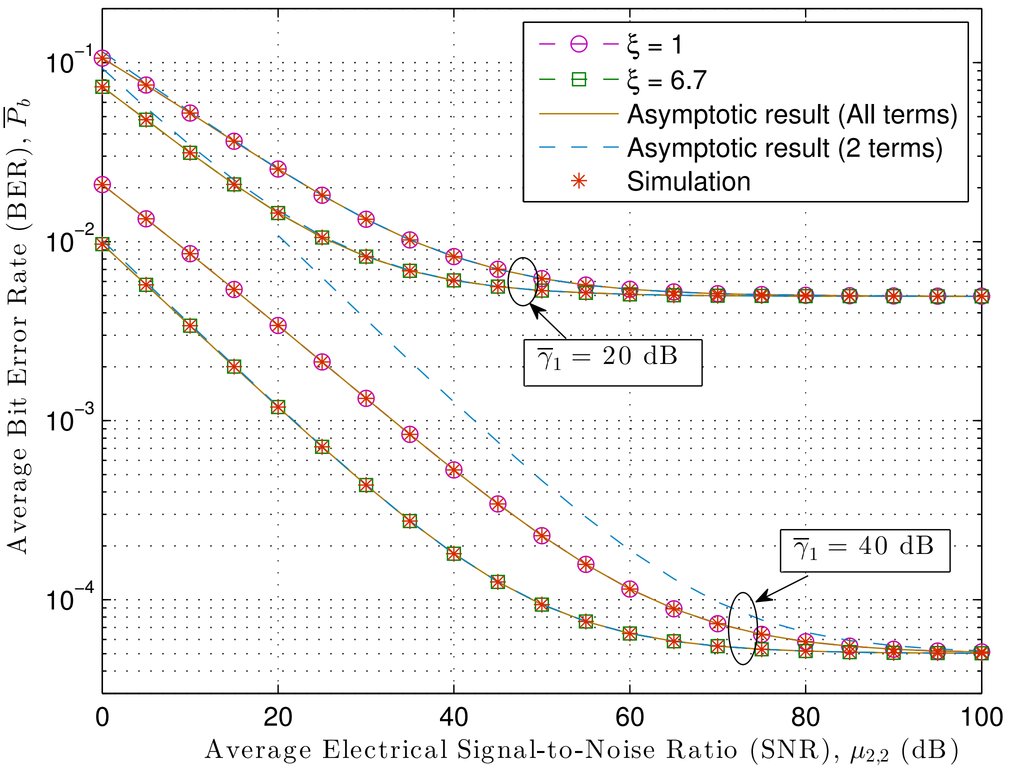

Figure 7.7: The impact of $\overline{\gamma}_1$ on the average bit error rate of mixed RF-FSO relay link under strong turbulence conditions using IM/DD technique ($r = 2$) with varying pointing errors.

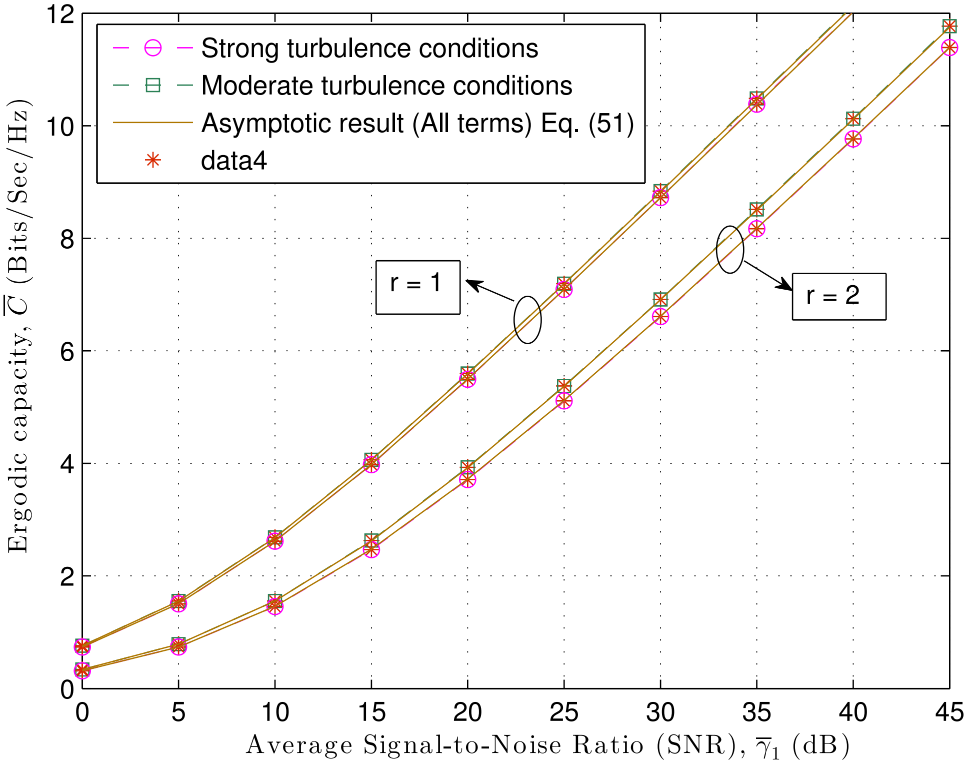

Figure 7.8: Ergodic capacity of mixed RF-FSO relay link under strong and moderate turbulence conditions for both detection techniques, heterodyne ($r = 1$) and IM/DD ($r = 2$) with $\xi = 1$.

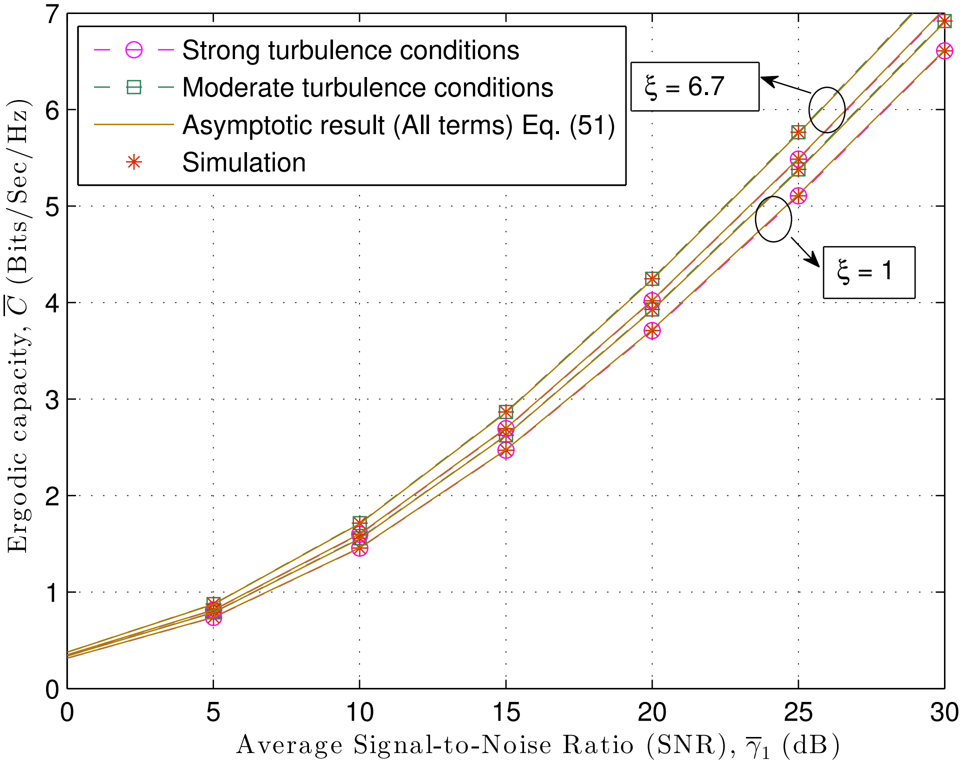

Figure 7.9: The impact of pointing errors on the ergodic capacity of mixed RF-FSO relay link under strong and moderate turbulence conditions using IM/DD technique ($r = 2$) with varying pointing errors.

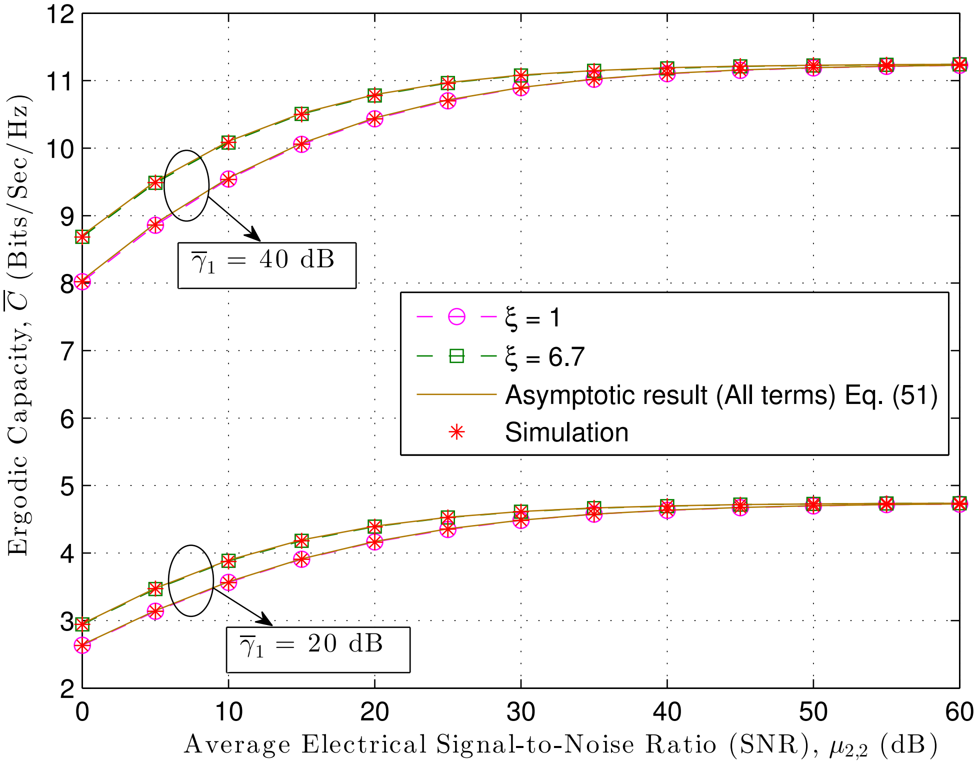

Figure 7.10: The impact of $\overline{\gamma}_1$ on the ergodic capacity of mixed RF-FSO relay link under strong turbulence conditions using IM/DD technique ($r = 2$) with varying pointing errors.

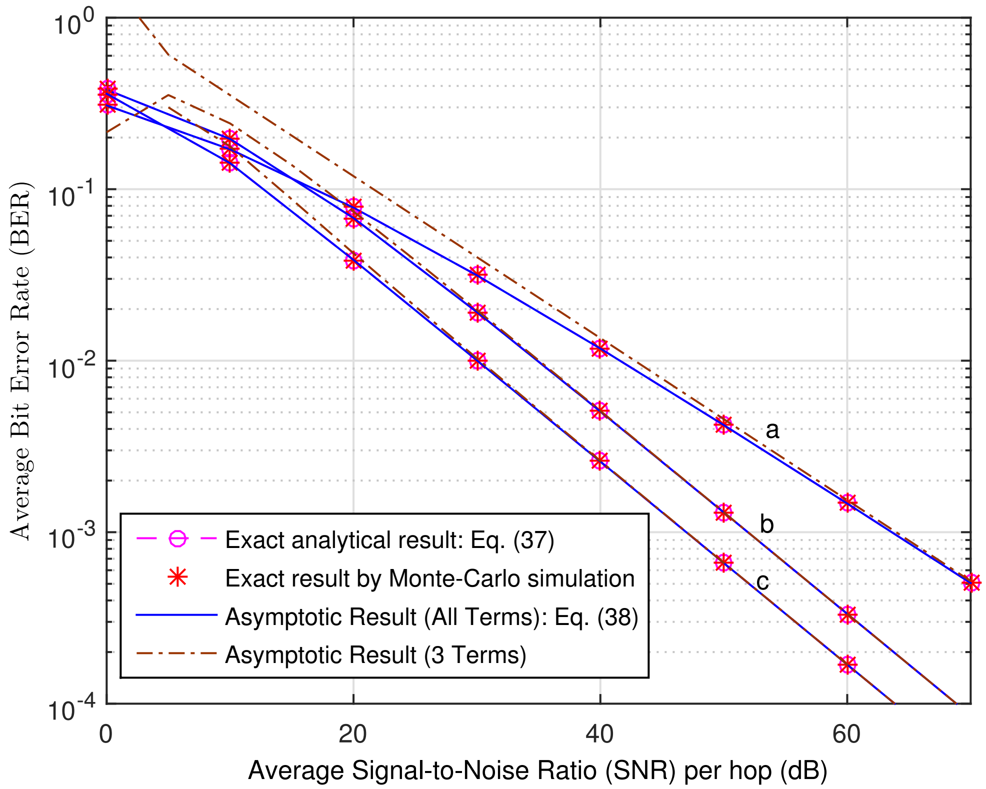

Figure 7.11: Average BER of DPSK over (a) single FSO link (b) dual-hop FSO-FSO (c) RF-FSO.

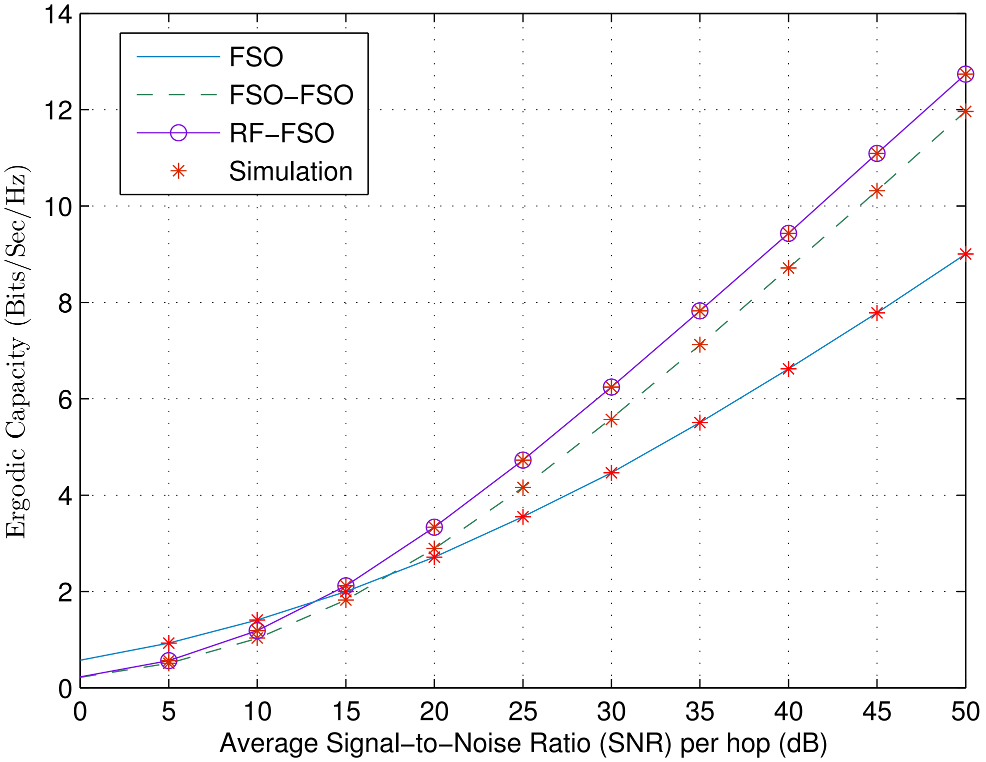

Figure 7.12: Ergodic capacity of single FSO link and dual-hop FSO-FSO and RF-FSO.

Chapter 8

Summary of Contributions and Future Work

8.1 Summary of Contributions

A general model for scintillation and misalignment is crucial in order to effectively analyze and assess FSO systems. In this thesis, first a general model for turbulence with the effect of pointing errors is provided in order to evaluate the major performance metrics in exact and asymptotic ways. Then, generalized model for misalignment was investigated to facilitate finding the asymptotic ergodic capacity of a single FSO link which agrees with the exact results at high SNR.

The next part of the thesis aims to examine several ways to mitigate the effect of scintillation and pointing errors. First, the performance analysis of selection combining diversity techniques is studied and it has been shown that it can effectively be used to overcome the scintillation. Finally, amplify-and-forward FSO relaying is investigated and it has shown great potential, especially with the integration of RF links.

8.2 Future Research Directions

This research work of this thesis can be extended in different directions. First, for the double generalized Gamma model, there is still a need to link the parameters of the distribution with the scintillation index to fully characterize the turbulence channel and to model real-life scenario. Second, the pointing error definition is an approximation which motivates research direction in the area of finding the exact definition in terms of the radial displacement. Third, closed-form statistics and performance metrics of a generalized channel model considering the Beckmann distribution can be further investigated.

Since the FSO channel can be considered as composite channel taking the large-scale and small-scale effects into consideration in addition the pointing errors effect, an approximation of either double generalized Gamma or Gamma-Gamma model will be further studied.

REFERENCES

[1] M. K. Simon and M.-S. Alouini, *Digital Communication over Fading Channels.* New York: Wiley, 2000.

[2] S. Hranilovic, *Wireless Optical Communication Systems.* Springer Science & Business Media, 2006.

[3] A. A. Huurdeman, *The Worldwide History of Telecommunications.* John Wiley & Sons, 2003.

[4] F. E. Goodwin, "A review of operational laser communication systems," *Proceedings of the IEEE*, vol. 58, no. 10, pp. 1746–1752, 1970.

[5] M. Uysal and H. Nouri, "Optical wireless communications an emerging technology," in *16th International Conference on Transparent Optical Networks (ICTON), 2014.* Graz, Austria: IEEE, 2014, pp. 1–7.

[6] S. Schmid, G. Corbellini, S. Mangold, and T. R. Gross, "Continuous synchronization for led-to-led visible light communication networks," in *3rd International Workshop in Optical Wireless Communications (IWOW), 2014*, Funchal, Portugal, Sep 2014, pp. 45–49.

[7] G. Cossu, A. M. Khalid, P. Choudhury, R. Corsini, and E. Ciaramella, "3.4 Gbit/s visible optical wireless transmission based on RGB LED," *Opt. Express*, vol. 20, no. 26, pp. B501–B506, Dec 2012.

[8] D. Tsonev, H. Chun, S. Rajbhandari, J. J. McKendry, S. Videv, E. Gu, M. Haji, S. Watson, A. E. Kelly, G. Faulkner *et al.*, "A 3-Gb/s single-LED OFDM-based wireless VLC link using a Gallium Nitride," *IEEE Photonics Technology Letters*, vol. 26, no. 7, pp. 637–640, April 2014.

[9] M. Zuckerberg, "Connecting the world from the sky," http://newsroom.fb.com/news/2014/03/connecting-the-world-from-the-sky/, published: 2014-03-28.

[10] http://esc.gsfc.nasa.gov/267/271.html, accessed: 2016-07-15.

[11] D. K. Borah, A. C. Boucouvalas, C. C. Davis, S. Hranilovic, and K. Yiannopoulos, "A review of communication-oriented optical wireless systems," *EURASIP*

Journal on Wireless Communications and Networking, vol. 2012, no. 1, pp. 1–28, March 2012.

[12] S. S. Muhammad, B. Flecker, E. Leitgeb, and M. Gebhart, "Characterization of fog attenuation in terrestrial free space optical links," *Optical Engineering*, vol. 46, no. 6, pp. 066 001–066 001, 2007.

[13] M. A. Khalighi and M. Uysal, "Survey on free space optical communication: A communication theory perspective," *IEEE Communications Surveys & Tutorials*, vol. 16, no. 4, pp. 2231–2258, June 2014.

[14] H. Willebrand and B. S. Ghuman, *Free Space Optics: Enabling Optical Connectivity in Todays Networks.* SAMS publishing, 2002.

[15] I. I. Kim, B. McArthur, and E. Korevaar, "Comparison of laser beam propagation at 785 nm and 1550 nm in fog and haze for optical wireless communications," in *proc. SPIE*, vol. 4214, Feb 2001, pp. 26–37.

[16] L. C. Andrews, R. L. Phillips, and C. Y. Hopen, *Laser Beam Scintillation with Applications.* SPIE press, 2001, vol. 99.

[17] M. Al-Habash, L. C. Andrews, and R. L. Phillips, "Mathematical model for the irradiance probability density function of a laser beam propagating through turbulent media," *Optical Engineering*, vol. 40, no. 8, pp. 1554–1562, Aug. 2001.

[18] L. C. Andrews and R. L. Phillips, *Laser Beam Propagation through Random Media.* SPIE press, 2005, vol. 152.

[19] R. Rui-Zhong, "Scintillation index of optical wave propagating in turbulent atmosphere," *Chinese Physics B*, vol. 18, no. 2, p. 581, 2009.

[20] A. Majumdar, *Advanced Free Space Optics (FSO): A Systems Approach*, ser. Springer Series in Optical Sciences. Springer New York, 2014.

[21] N. Perlot, *Characterization of Signal Fluctuations in Optical Communications with Intensity Modulation and Direct Detection Through the Turbulent Atmospheric Channel*, ser. Berichte aus der Kommunikationstechnik. Shaker, 2006.

[22] M. Niu, J. F. Holzman, and J. Cheng, *Terrestrial Coherent Free-Space Optical Communication Systems.* INTECH Open Access Publisher, 2012.

[23] D. J. T. Heatley, D. R. Wisely, I. Neild, and P. Cochrane, "Optical wireless: the story so far," *IEEE Communications Magazine*, vol. 36, no. 12, pp. 72–74, 79–82, Dec 1998.

[24] I. S. Ansari, H. AlQuwaiee, E. Zedini, and M.-S. Alouini, *Information Theoretical Limits of Free-Space Optical Links.* Cham: Springer International Publishing, 2016, pp. 171–208.

[25] E. Jakeman and P. Pusey, “Significance of K distributions in scattering experiments,” *Physical Review Letters*, vol. 40, no. 9, p. 546, Feb. 1978.

[26] L. Andrews and R. Phillips, “I–K distribution as a universal propagation model of laser beams in atmospheric turbulence,” *Journal of Optical Society of America (JOSA)*, vol. 2, no. 2, pp. 160–163, Feb. 1985.

[27] ——, “Mathematical genesis of the I-K distribution for random optical fields,” *Journal of the Optical Society of America A (JOSA A)*, vol. 3, no. 11, pp. 1912–1919, Nov 1986.

[28] J. H. Churnside and R. Frehlich, “Experimental evaluation of log-normally modulated rician and IK models of optical scintillation in the atmosphere,” *Journal of Optical Society of America (JOSA) A*, vol. 6, no. 11, pp. 1760–1766, Nov. 1989.

[29] J. H. Churnside and S. F. Clifford, “Log-normal Rician probability-density function of optical scintillations in the turbulent atmosphere,” *Journal of the Optical Society of America A (JOSA A)*, vol. 4, no. 10, pp. 1923–1930, Oct. 1987.

[30] R. Barrios and F. Dios, “Exponentiated weibull distribution family under aperture averaging for gaussian beam waves,” *Optics express*, vol. 20, no. 12, pp. 13 055–13 064, June 2012.

[31] R. J. Hill and R. G. Frehlich, “Probability distribution of irradiance for the onset of strong scintillation,” *Journal of Optical Society of America (JOSA) A*, vol. 14, no. 7, pp. 1530–1540, July 1997.

[32] M. A. Kashani, M. Uysal, and M. Kavehrad, “A novel statistical channel model for turbulence-induced fading in free-space optical systems,” *IEEE/OSA Journal of Lightwave Technology*, vol. 33, no. 11, pp. 2303–2312, March 2015.

[33] D. K. Borah and D. G. Voelz, “Pointing error effects on free-space optical communication links in the presence of atmospheric turbulence,” *IEEE/OSA Journal of Lightwave Technology*, vol. 27, no. 18, pp. 3965–3973, Sep. 2009.

[34] F. Yang, J. Cheng, and T. Tsiftsis, “Free-space optical communication with nonzero boresight pointing errors,” *IEEE Transactions on Communications,*, vol. 62, no. 2, pp. 713–725, Feb. 2014.

[35] A. Farid and S. Hranilovic, “Outage capacity optimization for free-space optical links with pointing errors,” *IEEE/OSA Journal of Lightwave Technology*, vol. 25, no. 7, pp. 1702–1710, July 2007.

[36] W. Gappmair, S. Hranilovic, and E. Leitgeb, “OOK performance for terrestrial FSO links in turbulent atmosphere with pointing errors modeled by Hoyt distributions,” *IEEE Communications Letters*, vol. 15, no. 8, pp. 875–877, 2011.

[37] I. S. Ansari, F. Yilmaz, and M.-S. Alouini, “A unified performance of free-space optical links over Gamma-Gamma turbulence channels with pointing errors,” in *Proceedings of IEEE 81st Vehicular Technology Conference (VTC Spring’ 2015)*, Glasgow, Scotland, May 2015.

[38] H. AlQuwaiee, I. Ansari, and M.-S. Alouini, “On the performance of free-space optical communication systems over double generalized Gamma channel,” *IEEE Journal on Selected Areas in Communications*, vol. 33, no. 9, pp. 1829–1840, May. 2015.

[39] I. Ansari, F. Yilmaz, and M.-S. Alouini, “Performance analysis of free-space optical links over Malaga ($\mathcal{M}$) turbulence channels with pointing errors,” *IEEE Transactions on Wireless Communications*, vol. PP, no. 99, pp. 1–1, Aug. 2015.

[40] W. Gappmair, “Further results on the capacity of free-space optical channels in turbulent atmosphere,” *IET Communications*, vol. 5, no. 9, pp. 1262–1267, June 2011.

[41] S. Karp, R. Gagliardi, S. Moran, and L. Stotts, *Optical Channels: Fibers, Clouds, Water, and the Atmosphere*, ser. Applications of Communications Theory. Springer US, 1988.

[42] S. M. Navidpour, M. Uysal, and M. Kavehrad, “BER performance of free-space optical transmission with spatial diversity,” *IEEE Transactions on Wireless Communications,*, vol. 6, no. 8, pp. 2813–2819, Aug. 2007.

[43] I. S. Gradshteyn and I. M. Ryzhik, “Table of Integrals, Series and Products,” *Academic Press, New York*, 2000.

[44] I. Wolfram, *Mathematica Edition: Version 8.0*. Champaign, Illinois: Wolfram Research Inc., 2010.

[45] E. Stacy, “A generalization of the Gamma distribution,” *The Annals of Mathematical Statistics*, vol. 33, no. 3, pp. 1187–1192, Sep. 1962.

[46] M. Kashani, M. Uysal, and M. Kavehrad, “A novel statistical model for turbulence-induced fading in free-space optical systems,” in *Proceedings of*

the 15th International Conference on Transparent Optical Networks (ICTON), Cartagena, Colombia, June 2013, pp. 1–5.

[47] F. Yilmaz and M.-S. Alouini, "A new simple model for composite fading channels: Second order statistics and channel capacity," in *Proceedings of the 7th International Symposium on Wireless Communication Systems (ISWCS)*, York, UK, Sep. 2010, pp. 676–680.

[48] ——, "A novel unified expression for the capacity and bit error probability of wireless communication systems over generalized fading channels," *IEEE Transactions on Communications*, vol. 60, no. 7, pp. 1862–1876, July 2012.

[49] A. Jurado-Navas, J. Garrido-Balsells, J. Paris, and A. Puerta-Notario, *Numerical Simulations of Physical and Engineering Processes*. Intech, September, 2011.

[50] A. Farid and S. Hranilovic, "Diversity gain and outage probability for MIMO free-space optical links with misalignment," *IEEE Transactions on Communications*, vol. 60, no. 2, pp. 479 – 487, Feb. 2012.

[51] P. Beckmann, "Statistical distribution of the amplitude and phase of a multiply scattered field," *Journal of research of the National Bureau of Standards-D.Radio propagation*, vol. 66D, no. 3, June 1962.

[52] H. Sandalidis, T. Tsiftsis, G. Karagiannidis, and M. Uysal, "BER performance of FSO links over strong atmospheric turbulence channels with pointing errors," *IEEE Communications Letters*, vol. 12, no. 1, pp. 44–46, Jan. 2008.

[53] H. Sandalidis, T. Tsiftsis, and G. Karagiannidis, "Optical wireless communications with heterodyne detection over turbulence channels with pointing errors," *IEEE/OSA Journal of Lightwave Technology*, vol. 27, no. 20, pp. 4440–4445, Oct. 2009.

[54] T. Tsiftsis, H. Sandalidis, G. Karagiannidis, and M. Uysal, "Optical wireless links with spatial diversity over strong atmospheric turbulence channels," *IEEE Transactions on Communications*, vol. 8, no. 2, pp. 951–957, Feb. 2009.

[55] M. Niu, J. Cheng, and J. Holzman, "Error rate performance comparison of coherent and subcarrier intensity modulated optical wireless communications," *IEEE/OSA Journal of Optical Communications and Networking*, vol. 5, no. 6, pp. 554–564, June 2013.

[56] I. S. Ansari, F. Yilmaz, and M.-S. Alouini, "Impact of pointing errors on the performance of mixed RF/FSO dual-hop transmission systems," *IEEE Wireless Communications Letters*, vol. 2, no. 3, pp. 351–354, June 2013.

[57] F. Yilmaz and M.-S. Alouini, "Novel asymptotic results on the high-order statistics of the channel capacity over generalized fading channels," in *Proceedings of IEEE 13th International Workshop on Signal Processing Advances in Wireless Communications (SPAWC' 2012)*, Cesme, Turkey, June 2012, pp. 389–393.

[58] A. Wojnar, "Union bounds on performance in Nakagami channels," *IEEE Transactions on Communications*, vol. 34, no. 1, pp. 22–24, Jan. 1986.

[59] I. S. Ansari, S. Al-Ahmadi, F. Yilmaz, M.-S. Alouini, and H. Yanikomeroglu, "A new formula for the BER of binary modulations with dual-branch selection over generalized-K composite fading channels," *IEEE Transactions on Communications*, vol. 59, no. 10, pp. 2654–2658, Oct. 2011.

[60] Z. Wang and G. Giannakis, "A simple and general parameterization quantifying performance in fading channels," *IEEE Transactions on Communications*, vol. 51, no. 8, pp. 1389–1398, Aug 2003.

[61] A. Chaaban, J. M. Morvan, and M. S. Alouini, "Free-space optical communications: Capacity bounds, approximations, and a new sphere-packing perspective," *IEEE Transactions on Communications*, vol. 64, no. 3, pp. 1176–1191, March 2016.

[62] A. Lapidoth, S. Moser, and M. Wigger, "On the capacity of free-space optical intensity channels," *IEEE Transactions on Information Theory*, vol. 55, no. 10, pp. 4449–4461, Oct 2009.

[63] S. Arnon, J. Barry, G. Karagiannidis, R. Schober, and M. Uysal, *Advanced Optical Wireless Communication Systems.* Cambridge University Press, 2012.

[64] X. Zhu and J. Kahn, "Free-space optical communication through atmospheric turbulence channels," *IEEE Transactions on Communications*, vol. 50, no. 8, pp. 1293–1300, Aug. 2002.

[65] T. Tsiftsis, "Performance of heterodyne wireless optical communication systems over Gamma-Gamma atmospheric turbulence channels," *Electronics Letters*, vol. 44, no. 5, pp. 372–373, Feb. 2008.

[66] H. Nistazakis, T. Tsiftsis, and G. Tombras, "Performance analysis of free-space optical communication systems over atmospheric turbulence channels," *IET Communications*, vol. 3, no. 8, pp. 1402–1409, Aug. 2009.

[67] A. Prokeš, “Modeling of atmospheric turbulence effect on terrestrial FSO link,” *Radio Eng*, vol. 18, no. 1, pp. 42–47, 2009.

[68] X. Tang, S. Rajbhandari, W. Popoola, Z. Ghassemlooy, E. Leitgeb, S. Muhammad, and G. Kandus, “Performance of BPSK subcarrier intensity modulation free-space optical communications using a Log-Normal atmospheric turbulence model,” in *2010 Symposium on Photonics and Optoelectronic (SOPO)*, Chengdu, China, June 2010, pp. 1–4.

[69] H. AlQuwaiee, H.-C. Yang, and M.-S. Alouini, “On the asymptotic ergodic capacity of FSO links with generalized pointing error model,” in *2015 IEEE International Conference on Communications, (ICC 2015)*, London, UK, June 2015, pp. 5072–5077.

[70] H. E. Nistazakis, T. A. Tsiftsis, and G. S. Tombras, “Performance analysis of free-space optical communication systems over atmospheric turbulence channels,” *IET communications*, vol. 3, no. 8, pp. 1402–1409, 2009.

[71] H. Sandalidis and T. Tsiftsis, “Outage probability and ergodic capacity of free-space optical links over strong turbulence,” *Electronics Letters*, vol. 44, no. 1, pp. 46–47, Jan 2008.

[72] K. P. Peppas, A. N. Stassinakis, G. K. Topalis, H. E. Nistazakis, and G. S. Tombras, “Average capacity of optical wireless communication systems over IK atmospheric turbulence channels,” *Journal of Optical Communications and Networking*, vol. 4, no. 12, pp. 1026–1032, Dec. 2012.

[73] H. Nistazakis, V. Assimakopoulos, and G. Tombras, “Performance estimation of free space optical links over negative exponential atmospheric turbulence channels,” *OPTIK-International Journal for Light and Electron Optics*, vol. 122, no. 24, pp. 2191–2194, Dec. 2011.

[74] C. Liu, Y. Yao, Y. Sun, and X. Zhao, “Average capacity for heterodyne FSO communication systems over gamma-gamma turbulence channels with pointing errors,” *Electronics letters*, vol. 46, no. 12, pp. 851–853, June 2010.

[75] E. J. Lee and V. W. S. Chan, “Part 1: optical communication over the clear turbulent atmospheric channel using diversity,” *IEEE Journal on Selected Areas in Communications*, vol. 22, no. 9, pp. 1896–1906, Nov 2004.

[76] G. Yang, M. A. Khalighi, S. Bourennane, and Z. Ghassemlooy, “Fading correlation and analytical performance evaluation of the space-diversity

free-space optical communications system," *Journal of Optics*, vol. 16, no. 3, p. 035403, Feb. 2014.

[77] H. Moradi, H. Refai, and P. LoPresti, "Switch-and-stay and switch-and-examine dual diversity for high-speed free-space optics links," *IET Optoelectronics*, vol. 6, no. 1, pp. 34–42, February 2012.

[78] M. Abaza, R. Mesleh, A. Mansour, and E.-H. M. Aggoune, "Diversity techniques for a free-space optical communication system in correlated Log-Normal channels," *Optical Engineering*, vol. 53, no. 1, pp. 016 102–016 102, Jan 2014.

[79] X. Zhu and J. M. Kahn, "Maximum-likelihood spatial-diversity reception on correlated turbulent free-space optical channels," in *IEEE Global Telecommunications Conference (GLOBECOM'00)*, vol. 2, San Francisco, CA, Dec. 2000, pp. 1237–1241.

[80] G. R. Osche, "Optical detection theory for laser applications," *Optical Detection Theory for Laser Applications, by Gregory R. Osche, pp. 424. ISBN 0-471-22411-1. Wiley-VCH, July 2002.*, vol. 1, 2002.

[81] J. C. Ricklin and F. M. Davidson, "Atmospheric turbulence effects on a partially coherent Gaussian beam: Implications for free-space laser communication," *J. Opt. Soc. Am. A*, vol. 19, no. 9, pp. 1794–1802, Sep 2002.

[82] M. Blanco and K. Zdunek, "Performance and optimization of switched diversity systems for the detection of signals with rayleigh fading," *IEEE Transactions on Communications*, vol. 27, no. 12, pp. 1887–1895, Dec 1979.

[83] M.-S. Alouini and M. K. Simon, "Dual diversity over correlated log-normal fading channels," *IEEE Transactions on Wireless Communications*, vol. 50, no. 12, pp. 1946–1959, Dec. 2002.

[84] H.-C. Yang, "New results on ordered statistics and analysis of minimum-selection generalized selection combining (GSC)," *IEEE Transactions on Wireless Communications*, vol. 5, no. 7, pp. 1876–1885, July 2006.

[85] Y.-C. Ko, M.-S. Alouini, and M. K. Simon, "Analysis and optimization of switched diversity systems," *IEEE Transactions on Vehicular Technology*, vol. 49, no. 5, pp. 1813–1831, Sep. 2000.

[86] A. Ibrahim, M.M.; Ibrahim, "Performance analysis of optical receivers with space diversity reception," *IEEE Transactions on Communications*, vol. 134, no. 6, pp. 369–372, Dec. 1996.

[87] E. J. Shin and V. W. Chan, “Optical communication over the turbulent atmospheric channel using spatial diversity,” in *Proceedings of IEEE Global Telecommunications Conference, 2002 (GLOBECOM’02)*, vol. 3, Nov. 2002, pp. 2055–2060.

[88] H. Moradi, M. Falahpour, H. H. Refai, and P. G. LoPresti, “A diversity combining approach for MIMO FSO nodes with misaligned receivers,” in *Proceedings of Global Telecommunications Conference (GLOBECOM’11)*, April. 2011, pp. 1–5.

[89] H. Kazemi and M. Uysal, “Performance analysis of MIMO free-space optical communication systems with selection combining,” in *Proceedings of the 21st Signal Processing and Communications Applications Conference (SIU)*, April. 2013, pp. 1–4.

[90] H. AlQuwaiee, I. S. Ansari, and M.-S. Alouini, “On the maximum and minimum of two modified Gamma-Gamma variates with applications,” in *Proceedings of IEEE Wireless Communications and Networking Conference (WCNC’ 2014)*, Apr. 2014, pp. 269–274.

[91] F. Yilmaz and M.-S. Alouini, “Product of the powers of generalized Nakagami-m variates and performance of cascaded fading channels,” in *Proceedings of IEEE Global Telecommunications Conference, (GLOBECOM’09)*, Nov 2009, pp. 1–8.

[92] P. Mittal and K. Gupta, “An integral involving generalized function of two variables,” *Proceedings of the Indian Academy of Sciences - Section A*, vol. 75, no. 3, pp. 117–123, Mar. 1972.

[93] K. Gupta and P. Mittal, “The H-function transform II,” *Journal of the Australian Mathematical Society*, vol. 12, no. 04, pp. 444–450, Nov. 1971.

[94] M. O. Hasna and M.-S. Alouini, “A performance study of dual-hop transmissions with fixed gain relays,” in *Proceedings of IEEE International Conference on Acoustics, Speech, and Signal Processing (ICASSP ’03)*, vol. 4, Apr. 2003, pp. IV–189–92.

[95] F. Yilmaz, O. Kucur, and M.-S. Alouini, “A novel framework on exact average symbol error probabilities of multihop transmission over amplify-and-forward relay fading channels,” in *Proceedings of the 7th International Symposium on Wireless Communication Systems (ISWCS)*, York, UK, Sep. 2010, pp. 546–550.

[96] Y. Zhu, Y. Xin, and P.-Y. Kam, “Outage probability of Rician fading relay channels,” in *Proceedings of Military Communications Conference (MILCOM)*, Sep. 2006, pp. 1–6.

[97] S. N. Datta, S. Chakrabarti, and R. Roy, “Error analysis of noncoherent FSK with variable gain relaying in dual-hop Nakagami-m relay fading channel,” in *Proceedings of International Conference on Signal Processing and Communications (SPCOM’ 2010)*, Bangalore, India, July 2010, pp. 1–5.

[98] T. Tsiftsis, H. Sandalidis, G. Karagiannidis, and N. Sagias, “Multihop free-space optical communications over strong turbulence channels,” in *Proceedings of IEEE International Conference on Communications, (ICC ’06)*, vol. 6, June 2006, pp. 2755–2759.

[99] G. Karagiannidis, N. Sagias, and T. Tsiftsis, “Closed-form statistics for the sum of squared Nakagami-m variates and its applications,” *IEEE Transactions on Communications*, vol. 54, no. 8, pp. 1353–1359, Aug. 2006.

[100] M. Safari and M. Uysal, “Relay-assisted free-space optical communication,” *IEEE Transactions on Wireless Communications*, vol. 7, no. 12, pp. 5441–5449, December 2008.

[101] E. Lee, J. Park, D. Han, and G. Yoon, “Performance analysis of the asymmetric dual-hop relay transmission with mixed RF/FSO links,” *IEEE Photonics Technology Letters,*, vol. 23, no. 21, pp. 1642–1644, Nov. 2011.

[102] I. S. Ansari, M.-S. Alouini, and F. Yilmaz, “On the performance of hybrid RF and RF/FSO fixed gain dual-hop transmission systems,” in *Proceedings of 2013 Saudi International Electronics, Communications and Photonics Conference (SIECPC)*, April 2013, pp. 1–6.

[103] H. Samimi and M. Uysal, “End-to-end performance of mixed RF/FSO transmission systems,” *IEEE/OSA Journal of Optical Communications and Networking*, vol. 5, no. 11, pp. 1139–1144, Nov 2013.

[104] S. Ikki and M. Ahmed, “Performance analysis of dual-hop relaying communications over generalized Gamma fading channels,” in *Global Telecommunications Conference (GLOBECOM ’07)*, Nov. 2007, pp. 3888–3893.

[105] M. Hasna and M.-S. Alouini, “End-to-end performance of transmission systems with relays over Rayleigh-fading channels,” *IEEE Transactions on Wireless Communications*, vol. 2, no. 6, pp. 1126–1131, Nov 2003.

[106] I. Ansari, F. Yilmaz, and M.-s. Alouini, "On the performance of mixed RF/FSO variable gain dual-hop transmission systems with pointing errors," in *Proceedings of 78th IEEE Vehicular Technology Conference (VTC Fall)*, Sept 2013, pp. 1–5.

[107] M. Aggarwal, P. Garg, and P. Puri, "Dual-hop optical wireless relaying over turbulence channels with pointing error impairments," *IEEE/OSA Journal of Lightwave Technology*, vol. 32, no. 9, pp. 1821–1828, May 2014.

[108] M. Hasna and M.-S. Alouini, "A performance study of dual-hop transmissions with fixed gain relays," *IEEE Transactions on Wireless Communications*, vol. 3, no. 6, pp. 1963–1968, Nov. 2004.

[109] A. Annamalai, R. Palat, and J. Matyjas, "Estimating ergodic capacity of cooperative analog relaying under different adaptive source transmission techniques," in *Proceedings of 2010 IEEE Sarnoff Symposium*, Princeton, NJ, USA, Apr. 2010, pp. 1–5.

[110] A. Mathai, R. K. Saxena, and H. J. Haubold, *The H-function: Theory and Applications*. Springer, 2010.

[111] S. Gupta, "Integrals involving products of G-function," *Proceedings of the National Academy of Sciences, India Section A: Physical Sciences*, vol. 39, no. 2, pp. 193–200, 1969.

[112] A. P. Prudnikov, Y. A. Brychkov, and O. I. Marichev, *Integrals and Series Volume 3: More Special Functions*, Integrals and Series ed. Gordon and Breach Science Publishers, 1986.

[113] K. Peppas, "A new formula for the average bit error probability of dual-hop amplify-and-forward relaying systems over generalized shadowed fading channels," *Wireless Communications Letters, IEEE*, vol. 1, no. 2, pp. 85–88, April 2012.

APPENDICES

A Special Functions

Meijer's G-function The Meijer's G-function can be defined as a line integrals in the complex plane as follows [112]

$$\mathrm{G}_{p,q}^{m,n}\left(z\,\middle|\,\begin{matrix}a_1,\dots,a_n,\dots,a_p\\ b_1,\dots,b_m,\dots,b_q\end{matrix}\right)=\frac{1}{2\pi i}\int_L\frac{\prod_{j=1}^{m}\Gamma(b_j-s)\prod_{j=1}^{n}\Gamma(1-a_j+s)}{\prod_{j=m+1}^{q}\Gamma(1-b_j+s)\prod_{j=n+1}^{p}\Gamma(a_j-s)}z^{-s}\,ds. \tag{A.1}$$

The definition of the Meijer's G-function is satisfied under some conditions as

- The variables m, n, p and q are integer numbers i.e. $0 \le m \le q$ and $0 \le n \le p$.
- $z \neq 0$.
- For $k = 1, 2, \dots, n$ and $j = 1, 2, \dots, m$, $a_k - b_j \neq 1, 2, 3, \dots$.

The Meijer's G-function can be simply evaluated using a built-in function in MATHEMATICA®.

Fox's H-function The Fox's H-function is considered as a generalized form of the Meijer's G-function that can be defined as

$$\begin{aligned}&\mathrm{H}_{p,q}^{m,n}\left(z\,\middle|\,\begin{matrix}(a_1,A_1),(a_2,A_2),\dots(a_n,A_n),\dots,(a_p,A_p)\\ (b_1,B_1),(b_2,B_2),\dots,(b_m,B_m),\dots,(b_q,B_p)\end{matrix}\right)\\ &=\int_L\frac{\prod_{j=1}^{m}\Gamma(b_j-B_js)\prod_{j=1}^{n}\Gamma(1-a_j+A_js)}{\prod_{j=m+1}^{q}\Gamma(1-b_j+B_js)\prod_{j=n+1}^{p}\Gamma(a_j-A_js)}z^{-s}\,ds.\end{aligned} \tag{A.2}$$

The Fox H-function can be evaluated using the MATHEMATICA® script available in [91, Appendix A]. Furthermore, the Fox H-function reduces to the Meijer's G-function when $A_j = B_k = C > 0$ for $j = 1, \dots, p$ and $k = 1, \dots, q$ as

$$\mathrm{H}_{p,q}^{m,n}\left(z \middle| \begin{matrix} (a_1, C), (a_2, C), \dots (a_n, C), \dots, (a_p, C) \\ (b_1, C), (b_2, C), \dots, (b_m, C), \dots, (b_q, C) \end{matrix}\right) = \frac{1}{C}\,\mathrm{G}_{p,q}^{m,n}\left(z^{1/C} \middle| \begin{matrix} a_1, \dots, a_n, \dots, a_p \\ b_1, \dots, b_m, \dots, b_q \end{matrix}\right). \tag{A.3}$$

Extended Generalized Bivariate Meijer's G-function A general form of the Meijer's G-function was defined as

$$\mathrm{G}_{p_1,q_1:p_2,q_2,p_3,q_3}^{m_1,0:n_2,m_2:n_3,m_3}\left[\begin{matrix}(\mathbf{a})\\(\mathbf{b})\end{matrix}\middle|\begin{matrix}(\mathbf{c})\\(\mathbf{d})\end{matrix}\middle|\begin{matrix}(\mathbf{e})\\(\mathbf{f})\end{matrix}\middle| x, y\right] = \frac{1}{(2\pi i)^2}\int_{L_1}\int_{L_2}\Phi(s+t)\Psi(s,t)x^s y^t\,ds\,dt, \tag{A.4}$$

where notation $(\mathbf{a})$, $(\mathbf{b})$ and $(\mathbf{d})$ stand for

$$(\mathbf{a}) = a_1, \dots, a_{m_1}, \dots, a_{p_1}, \tag{A.5}$$

$$(\mathbf{b}) = b_1, \dots, b_{q_1}, \tag{A.6}$$

$$(\mathbf{d}) = d_1, \dots, d_{n_1}, \dots, a_{q_1} \tag{A.7}$$

with similar interpretations for $(\mathbf{c})$, $(\mathbf{e})$, and $(\mathbf{f})$.

In A.4, L_1 and L_2 are suitable contour lines

$$\Phi(s+t) = \frac{\prod_{j=1}^{m_1}\Gamma(a_j+s+t)}{\prod_{j=m_1+1}^{p_1}\Gamma(1-a_j-s-t)\prod_{j=1}^{q_1}\Gamma(b_j+s+t)}, \tag{A.8}$$

$$\begin{aligned}\Psi(s,t) &= \frac{\prod_{j=1}^{m_2}\Gamma(1-c_j+s)\prod_{j=1}^{m_3}\Gamma(1-e_j+t)\prod_{j=1}^{n_2}\Gamma(d_j-s)}{\prod_{j=m_2+1}^{p_2}\Gamma(c_j-s)\prod_{j=m_3+2}^{p_3}\Gamma(e_j-t)} \\ &\times \frac{\prod_{j=1}^{n_3}\Gamma(f_j-t)}{\prod_{j=n_2+1}^{q_2}\Gamma(1-d_j+s)\prod_{j=n_3+1}^{q_3}\Gamma(1-f_j+t)}.\end{aligned} \tag{A.9}$$

The EGBMG function can be written in another presentation as [59, Table. I] and easily evaluated in MATHEMATICA® using the code given in [59, Table II].

H-function of Two Variables The bivariate H-function was first introduced in [92] and is defined as

$$\mathbf{H}\left[\begin{array}{c|c|c} \begin{pmatrix} 0, n_1 \\ \\ p_1, q_1 \end{pmatrix} & \begin{array}{c} (a_{p_1};\alpha_{p_1},A_{p_1}) \\ \\ (b_{q_1};\beta_{q_1},B_{q_1}) \end{array} & \\ \begin{pmatrix} m_2, n_2 \\ \\ p_2, q_2 \end{pmatrix} & \begin{array}{c} (c_{p_2};r_{p_2}) \\ \\ (d_{q_1},\delta_{q_2}) \end{array} & \begin{array}{c} x \\ \\ \\ y \end{array} \\ \begin{pmatrix} m_3, n_3 \\ \\ p_3, q_3 \end{pmatrix} & \begin{array}{c} (e_{p_3},E_{p_3}) \\ \\ (f_{q_3},F_{q_3}) \end{array} & \end{array}\right] = \frac{1}{(2\pi i)^2}\int_{L_1}\int_{L_2} \phi_1(s,t)\,\phi_2(s)\,\phi_3(t)\,x^s\,y^t\,ds\,dt. \tag{A.10}$$

where $\phi_1(s,t)$, $\phi_2(s)$ and $\phi_3(t)$ are defined as follows:

$$\phi_1(s,t) = \frac{\prod_{j=1}^{n_1}\Gamma(1-a_j+\alpha_j s+A_j t)}{\prod_{j=m_1+1}^{p_1}\Gamma(a_j-\alpha_j s-A_j t)\prod_{j=1}^{q_1}\Gamma(1-b_j+\beta_j s+B_j t)}, \tag{A.11}$$

$$\phi_2(s) = \frac{\prod_{j=1}^{n_2}\Gamma(1-c_j+r_j s)\prod_{j=1}^{m_2}\Gamma(d_j-\delta_j s)}{\prod_{j=m_2+1}^{p_2}\Gamma(c_j-r_j s)\prod_{j=n_2+1}^{q_2}\Gamma(1-d_j+\delta_j s)}, \tag{A.12}$$

$$\phi_3(t) = \frac{\prod_{j=1}^{n_3}\Gamma(1-e_j+E_j t)\prod_{j=1}^{m_3}\Gamma(f_j-F_j t)}{\prod_{j=n_3+2}^{p_3}\Gamma(e_j-E_j t)\prod_{j=m_3+1}^{q_3}\Gamma(1-f_j+F_j t)}. \tag{A.13}$$

Such that x and y are not equal to zero and the set of variables $\{p_1, p_2, p_3, q_1, q_2, q_3, n_1, n_2, n_3, m_1, m_2, m_3\}$ are non-negative integers satisfying the following conditions $p_1 \geq n_1 \geq 0$; $p_2 \geq n_2 \geq 0$; $p_3 \geq n_3 \geq 0$; $q_1 \geq 0$; $q_2 \geq m_2 \geq 0$ and $q_3 \geq m_3 \geq 0$. The function can be evaluated efficiently using the MATHEMATICA® implementation in [59] or the MATLAB® implementation in [113]. In this work, the bivariate H-function was implemented and easily evaluated in MATHEMATICA®.

B The relationship between the extended generalized-K and double generalized Gamma distributions

Statistically, the extended Generalized-K (EGK) [47] and double Generalized Gamma (DGG) developed by [46] models are equivalent. The EGK is originated from the Generalized Nakagami-m (GNM) random variable (RV) i.e. $\mathcal{R}_i \sim \text{GNM}(m_i, \xi_i, \omega_i)$ where m_i, ξ_i, and ω_i are the fading, shaping parameters, and the average power, respectively. On the other hand, the double Generalized Gamma RV I is based on the generalized Gamma RVs $I_i \sim GG(\alpha_i, \beta_i, \Omega_i)$ where β_i is the fading parameter, α_i is the shaping parameter that can be derived from variance of the small and large scale fluctuations [17, Eq. (18)-(20)] inserted in [46, Eq. (8a), (8b)] and Ω_i given as [46, Eq. (9)]

$$\Omega_i = \left(\frac{\Gamma(m_i)}{\Gamma(\beta_i + 1/\alpha_i)} \right)^{\alpha_i} \beta_i. \tag{B.1}$$

It is well known that the square of GNM, $\mathcal{R}_i^2$, is Generalized Gamma RV, I_i [91]. The probability density function (PDF) of $\mathcal{R}_i^2$ given in [91, Eq. (7)] after some mathematical manipulation can be equal to

$$f_{\mathcal{R}_i^2}(z) = \frac{\xi_i z^{m_i \xi_i - 1}}{\Gamma(m_i)} \left(\frac{B_i}{\omega_i} \right)^{m_i \xi_i} \exp\left\{ - \left(\frac{B_i z}{\omega_i} \right)^{\xi_i} \right\}, \tag{B.2}$$

where $\Gamma(.)$ is the Gamma function as defined in [43, Eq.(8.310)] and $B_i = \frac{\Gamma(m_i + 1/\xi_i)}{\Gamma(m_i)}$. Comparing (B.2) to the Generalized Gamma PDF in [45, Eq. (2)]

$$f_x(x) = \frac{p x^{d-1}}{\Gamma(d/p) a^d} \exp\left\{ \left(\frac{x}{a} \right)^p \right\}, \tag{B.3}$$

we can reach to the following

$$p_i = \xi_i, \qquad d_i = m_i\xi_i, \qquad \text{and} \qquad a_i = \frac{\omega_i}{B_i}. \tag{B.4}$$

In addition, the PDF of I_i can be found in [46, Eq. (1) or (2)]

$$f_{I_i}(I) = \frac{\alpha_i I^{\beta_i\alpha_i - 1}}{\Gamma(\beta_i)} \left(\frac{\beta_i}{\Omega_i}\right)^{\beta_i} \exp\left\{-\frac{\beta_i}{\Omega_i} I^{\alpha_i}\right\} \tag{B.5}$$

Comparing it to (B.3), we reach to the following

$$p_i = \alpha_i, \qquad d_i = \beta_i\alpha_i, \qquad \text{and} \qquad a_i = \left(\frac{\Omega_i}{\beta_i}\right)^{1/\alpha_i}. \tag{B.6}$$

Then, given that $\omega_i = \mathbb{E}[\mathcal{R}_i^2] = \mathbb{E}[I_i] = 1$ we can relate the parameters as

$$\xi_i = \alpha_i, \qquad m_i = \beta_i, \qquad B_i = \left(\frac{\beta_i}{\Omega_i}\right)^{1/\alpha_i}. \tag{B.7}$$

Next, let

$$\mathcal{R} = \mathcal{R}_1^2\mathcal{R}_2^2, \tag{B.8}$$

where $\mathcal{R}_1$ and $\mathcal{R}_2$ are a pair of independent Generalized Nakagami-m RVs representing the shadowing (large-scale) and multi-path-fading (small-scale) with normalized average powers (i.e. $\mathbb{E}[\mathcal{R}_1^2] = \omega_1 = 1$ and $\mathbb{E}[\mathcal{R}_2^2] = \omega_2 = 1$) leading to $\mathcal{R}$ being an extended Generalized-k random variable [47] i.e. $\mathcal{R} \sim \mathcal{K}_G(m_1, \xi_1, m_2, \xi_2, \omega_1, \omega_2)$ with PDF equals to [47, Eq. (3)] [48, Eq. (26)].

$$f_R(z) = \frac{2}{z\Gamma(m_1)\Gamma(m_2)} \mathrm{H}_{0,2}^{2,0}\left(z^2 B_1^2 B_2^2 \middle| \begin{matrix} - \\ (m_1, \frac{2}{\xi_1}), (m_2, \frac{2}{\xi_2}) \end{matrix}\right), \tag{B.9}$$

where $\mathrm{H}_{p,q}^{m,n}[.]$ is the Fox's H-function that can be evaluated efficiently using MATHEMATICA® code listed in [91]. Now, let

$$I = I_1 I_2, \tag{B.10}$$

where I_1 and I_2 are independent RVs representing the large-scale and small-scale fluctuations, respectively. I is identified as a double GG RV whose PDF is given in [46, Eq. (4)] as

$$f_I(I) = \frac{\alpha_2 \lambda \sigma^{\beta_1 - \frac{1}{2}} \lambda^{\beta_2 - \frac{1}{2}} (2\pi)^{1-\frac{\sigma+\lambda}{2}}}{\Gamma(\beta_1)\Gamma(\beta_2) I} \mathrm{G}_{\lambda+\sigma,0}^{0,\lambda+\sigma}\left(\left(\frac{\Omega_2}{I^{\alpha_2}}\right)^{\lambda} \frac{\lambda^{\lambda}\sigma^{\sigma}\Omega_1^{\sigma}}{\beta_1^{\sigma}\beta_2^{\lambda}} \middle| \begin{matrix} \Delta(\sigma : 1-\beta_1), \Delta(\lambda : 1-\beta_2) \\ - \end{matrix} \right), \tag{B.11}$$

where $\mathrm{G}_{p,q}^{m,n}[.]$ is the Meijer's G-function as defined in [43, Eq.(9.301)], λ and σ are positive integers such as $\frac{\lambda}{\sigma} = \frac{\alpha_1}{\alpha_2}$ and $\Delta(x : y) \triangleq \frac{y}{x}, \frac{y+1}{x} \ldots, \frac{y+x-1}{x}$. Numerically (B.9) coincides with (B.11) as shown in Fig. B.1.

Although they are equal, the EGK distribution was mentioned in the literature to describe the fading model in radio frequency (RF) communications. To our best knowledge, double generalized Gamma was first mentioned to model the optical irradiance in [46]. The PDF in (B.11) is in terms of the Meijer's G-function that can be easily evaluated by MATHEMATICA® built-in function compared to the Fox H-function.

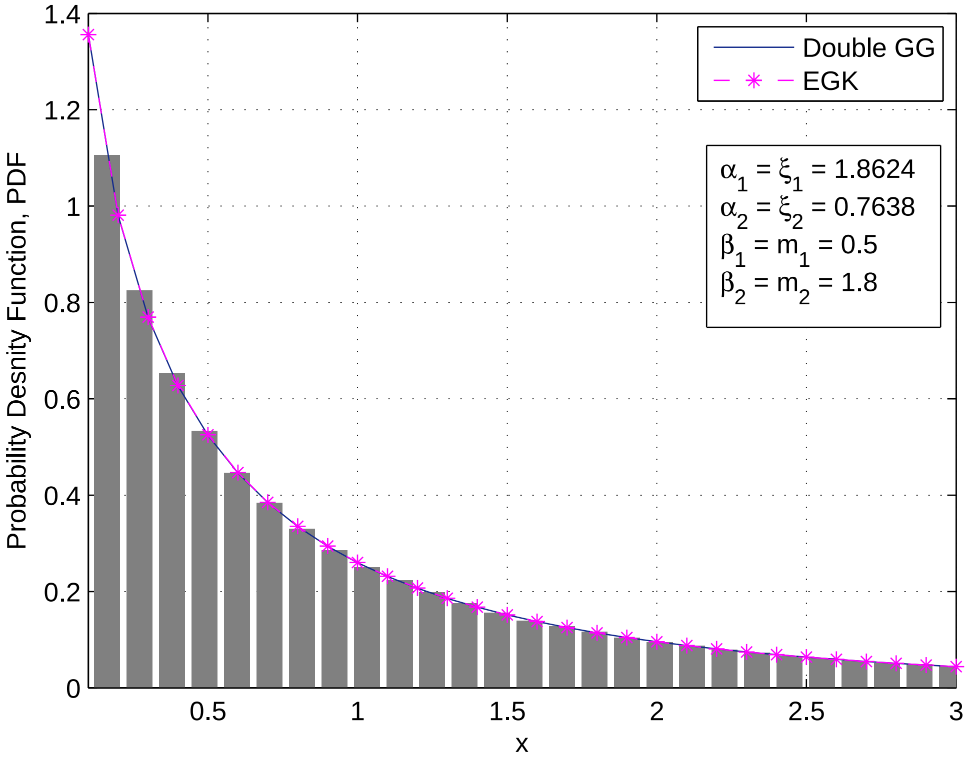

Figure B.1: Comparison between PDFs obtained analytically and via Monte Carlo simulations for EGK and double GG distributions.

C The relationship between the Málaga and double generalized Gamma distributions

The Málaga distribution (i.e. $I_{\mathcal{M}}(\hat{\alpha}, \hat{\beta}, \gamma, \hat{\Omega})$) and double generalized Gamma distribution (i.e. $I_{GG}(\alpha_1, \beta_1,\ \alpha_2, \beta_2, \Omega_1, \Omega_2)$ where $\Omega_i = \left(\frac{\Gamma(m_i)}{\Gamma(\beta_i + 1/\alpha_i)}\right)^{\alpha_i} \beta_i$) are statistically different. In other words, the DGG distribution is based on a doubly stochastic theory of scintillation and assumes that small-scale irradiance fluctuations I_x are coupled with large-scale irradiance fluctuations of the propagating wave I_y [49]

$$I_{GG} = I_x I_y. \tag{C.1}$$

However, the Málaga distribution models the small-scale into three parts: the first one is the LOS component U_L, the second one is coupled to the LOS contribution and is quasi-forward scattered by the eddies on the propagation axis U_S^C, and the third one is the energy which is scattered to the receiver by off-axis eddies U_S^G [49]. Thus, the irradiance can be written as

$$\begin{aligned} I_{\mathcal{M}} &= |U_L + U_S^C + U_S^G|^2 \exp(2X) && \text{(C.2)} \\ &= I_x I_y. && \text{(C.3)} \end{aligned}$$

Interestingly, the $\Gamma\Gamma$ model (i.e. $I_{\Gamma\Gamma}(\alpha, \beta)$) is a special case of both. Hence, both distributions can be linked to each other through the Gamma-Gamma model. First, the DGG model is a four-parameter distribution, we can map these parameters into the Gamma-Gamma using the higher-order amount of fading given as

$$AF_I^{(n)} = \frac{\mathbb{E}[I^n]}{\mathbb{E}[I]^n} - 1\,, \tag{C.4}$$

where the moments of the DGG and the Gamma-Gamma distributions can be written as

$$\mathbb{E}[I_{GG}^n] = \frac{\left(\frac{\Omega_1}{\beta_1}\right)^{\frac{n}{\alpha_1}} \Gamma\left(\frac{n+\alpha_1\beta_1}{\alpha_1}\right) \left(\frac{\Omega_2}{\beta_2}\right)^{\frac{n}{\alpha_2}} \Gamma\left(\frac{n+\alpha_2\beta_2}{\alpha_2}\right)}{\Gamma(\beta_2)\Gamma(\beta_2)}, \tag{C.5}$$

$$\mathbb{E}[I_{\Gamma\Gamma}^n] = \frac{\Gamma(n+\alpha)\Gamma(n+\beta)}{\alpha^n\beta^n\Gamma(\alpha)\Gamma(\beta)}. \tag{C.6}$$

By solving the following system

$$\begin{aligned} AF_{I_{\Gamma\Gamma}}^{(2)} &= AF_{I_{GG}}^{(2)}, \\ AF_{I_{\Gamma\Gamma}}^{(3)} &= AF_{I_{GG}}^{(3)}, \end{aligned} \tag{C.7}$$

we can get α and β equal to

$$\alpha = \frac{X - \sqrt{X^2 - 4Y}}{2Y}, \tag{C.8}$$

$$\beta = \frac{\sqrt{X^2 - 4Y} + X}{2Y}, \tag{C.9}$$

where

$$X = \frac{4(AF_{I_{GG}}^{(2)})^2 - AF_{I_{GG}}^{(3)} + 5AF_{I_{GG}}^{(2)}}{2AF_{I_{GG}}^{(2)} + 2}, \tag{C.10}$$

$$Y = \frac{AF_{I_{GG}}^{(3)} - 2(AF_{I_{GG}}^{(2)})^2 - 3AF_{I_{GG}}^{(2)}}{2AF_{I_{GG}}^{(2)} + 2}. \tag{C.11}$$

In addition, if we set the following parameters into the Málaga distribution: $\hat{\alpha} = \alpha$ obtained in (C.8), $\hat{\beta} = \beta$ obtained in (C.9), $\gamma = 0$ and $\hat{\Omega} = 1$, the Málaga distribution reduces to double GG.

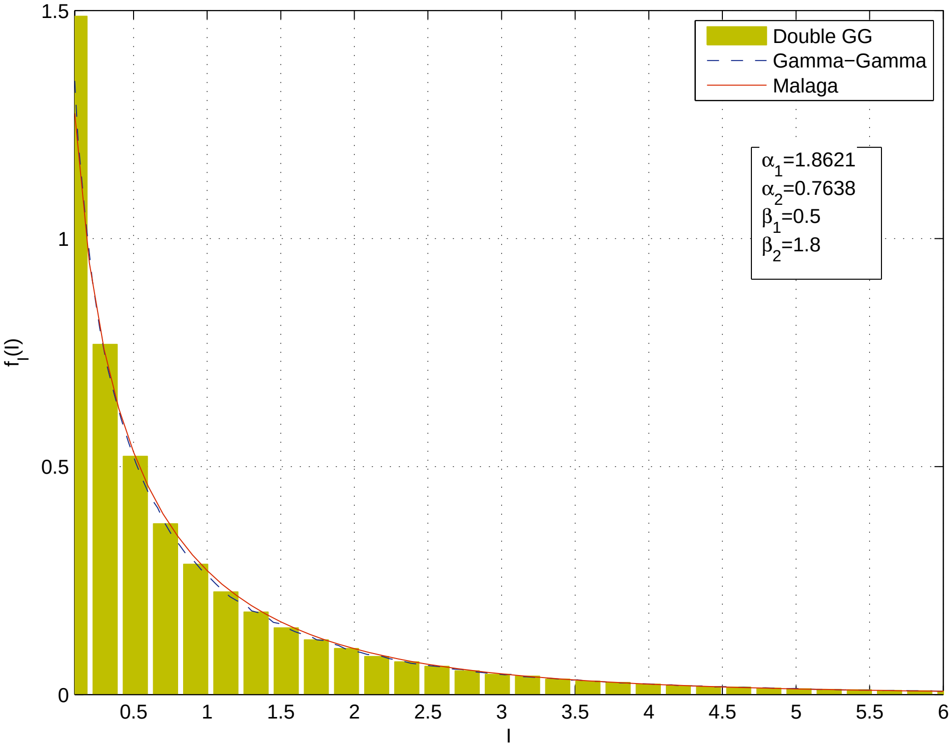

Figure C.1: Comparison between PDFs obtained analytically and via Monte Carlo simulations for Gamma-Gamma, the Málaga and double GG distributions under strong turbulence conditions.

For example, in Fig. C.1 we show the Monte-Carlo simulation of double generalized Gamma distributed irradiance in strong turbulence conditions. Then, we numerically evaluated the Gamma-Gamma irradiance PDF (2.9) with α and β obtained in (C.8) and (C.9), respectively. After that we set the appropriate parameters for the Málaga PDF [49, Eq. 24] to reduce to double generalized Gamma. The small difference between the PDFs in Fig. C.1 can be due to the approximation of β to be a natural number. Overall, the mapping is simple and accurate. Furthermore, the same methodology is performed for moderate turbulence as shown in Fig. C.2. Com-

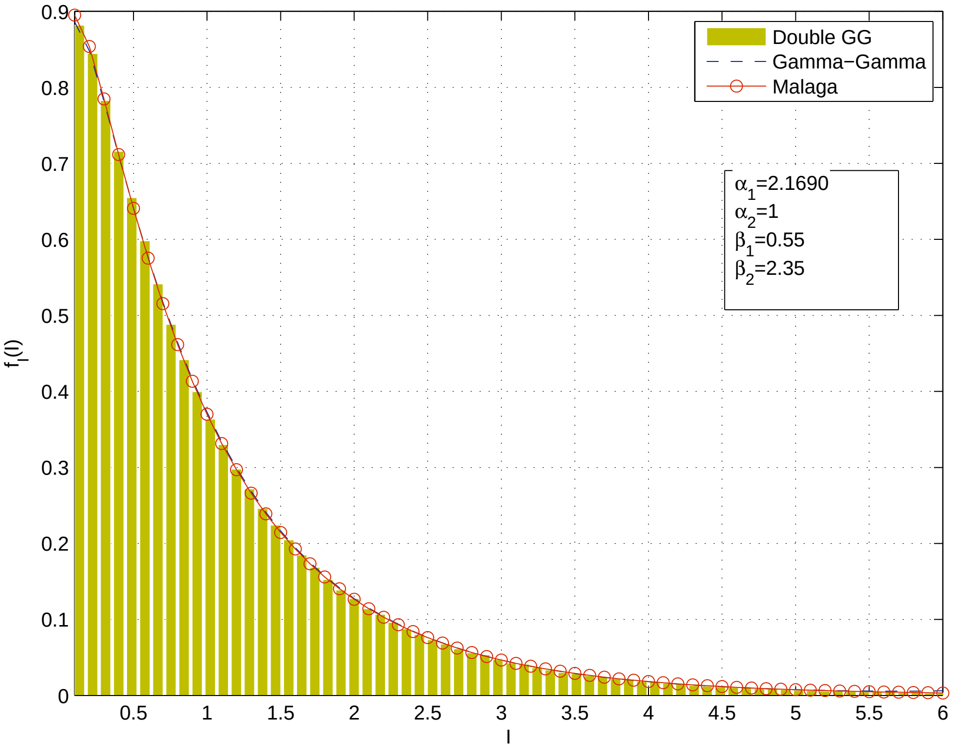

Figure C.2: Comparison between PDFs obtained analytically and via Monte Carlo simulations for Gamma-Gamma, the Málaga and double GG distributions under moderate turbulence conditions

paring the two figures, it can be concluded that the approximation is more accurate for moderate conditions.

D Papers Accepted

- [J3] H. AlQuwaiee, H.-C. Yang and M.-S. Alouini, ”The asymptotic capacity of dual-aperture FSO systems with a generalized pointing error model,” *in IEEE Transactions on Wireless Communications*, vol. 15, no. 1, pp. 6502-6512, Jan. 2016.
- [J2] H. AlQuwaiee, I. S. Ansari, and M.-S. Alouini, ”On the maximum and minimum of double generalized Gamma variates with applications to the performance of free-space optical communication systems,” *in IEEE Transactions on Vehicular Technology* , vol. 65, no. 1, pp. 8822-8831, Jan. 2016.
- [J3] H. AlQuwaiee, I. S. Ansari, and M.-S. Alouini, ”On the performance of free-space optical communication systems over double generalized Gamma channel,” *in IEEE Journal on Selected Areas in Communications*, vol. 33, no. 1, pp. 1829-1840, Jan. 2015.
- [C5] H. Al-Quwaiee, H.-C. Yang and M.-S. Alouini, ”On the asymptotic ergodic capacity of FSO links with generalized pointing error model,” *in Proceedings of IEEE International Conference on Communications (ICC'15)*, London, United Kingdom, June 2015.
- [C4] H. Al-Quwaiee and M.-S. Alouini, ”New exact and asymptotic results of dual-branch MRC over correlated Nakagami-m fading channels,” *in Proceedings of IEEE 81st Vehicular Technology Conference (VTC Spring' 2015)*, Glasgow, Scotland, May 2015.
- [C3] H. Al-Quwaiee and M.-S. Alouini, ”On the ergodic capacity of dual-branch correlated Log-Normal fading channels with Applications,” *in Proceedings of IEEE 81st Vehicular Technology Conference (VTC Spring' 2015)*, Glasgow, Scotland, May 2015.

- [C2] H. AlQuwaiee, I. S. Ansari, and M.-S. Alouini, "On the maximum and minimum of two modified Gamma-Gamma variates with applications," *in Proceedings of IEEE Wireless Communications and Networking Conference (WCNC' 2014)*, Istanbul, Turkey, Apr. 2014, pp. 269-274.
- [C1] H. AlQuwaiee, I. S. Ansari, and M.-S. Alouini, "On the performance of free space optical wireless communication systems over double generalized Gamma fading channel," *in Proceedings of the 4th International Conference on Communications and Networking (COMNET' 2014)*, Hammamet, Tunisia, 19-22 Mar. 2014.